14th International Scientific Conference

Intelligent Technologies in Logistics and Mechatronics Systems

ITELMS'2022

September 15th, 2022
Panevėžys, Lithuania

Editors

László T. Kóczy
Daiva Žostautienė
Olga Strikulienė

EDlearning

International Scientific Committee

Assoc. Prof. **Lütfi ATAY** (Çanakale Onsekiz Mart University, TURKEY)
Assoc. Prof. **Jonas BALTRUŠAITIS** (Lehigh University, USA)
Prof. **Remigijus BUBNYS** (Kaunas University of Technology, LITHUANIA)
Prof. **Vytautas BUČINSKAS** (Vilnius Gediminas Technical University, LITHUANIA)
Prof. **Jordi COLOMER FELIU** (University of Girona, SPAIN)
Assoc. Prof. **Asta DAUNORIENĖ** (Kaunas University of Technology, LITHUANIA)
Prof. **Atul GONSAI** (Saurashtra University, INDIA)
Assoc. Prof. **Volodymyr HUTSAYLYUK** (Military University of Technology, POLAND)
Prof. **Volodymyr IASNII** (Ternopil Ivan Puluj National Technical University, UKRAINE)
Prof. **Jacek JANISZEWSKI** (Military University of Technology, POLAND)
Prof. **Hilal Yıldırır KESER** (Bursa Technical University, TURKEY)
Prof. **Laszlo T. KOCZY** (Chair, Széchenyi István University and Budapest University of Technology and Economics, HUNGARY)
Assoc. Prof. **Radosław KORNEĆ** (Siedlce University of Natural Sciences and Humanities, POLAND)
Assoc. Prof. **Demetris KOURSAROS** (Cyprus University of Technology, CYPRUS)
Assoc. Prof. **Nida KVEDARAITĖ** (Kaunas University of Technology, LITHUANIA)
Assoc. Prof. **Diana LIPINSKIENĖ** (Kaunas University of Technology, LITHUANIA)
Assoc. Prof. **Evelina MEILIENĖ** (Kaunas University of Technology, LITHUANIA)
Prof. **Shahid MUMTAZ** (University of Aveiro, PORTUGAL)
Prof. **Iwona PRZYCHOCKA** (Helena Chodkowska University of Technology and Economics, POLAND)
Assoc. Prof. **Aušra REPEČKIENĖ** (Kaunas University of Technology, LITHUANIA)
Assoc. Prof. **Rafael ROBINA-RAMIREZ** (University of Extremadura, SPAIN)
Assoc. Prof. **Doga Basar SARIIPEK** (Kocaeli University, TURKEY)
Prof. **Lucjan SNIEZEK** (Military University of Technology, POLAND)
Assoc. Prof. **Brigita STANIKŪNIENĖ** (Kaunas University of Technology, LITHUANIA)
Prof. **Eglė STANIŠKIENĖ** (Kaunas University of Technology, LITHUANIA)
Assoc. Prof. Živilė STANKEVIČIŪTĖ (Kaunas University of Technology, LITHUANIA)
Dr. **Olga STRIKULIENĖ** (Kaunas University of Technology, LITHUANIA)
Assoc. Prof. **Dalia SUSNIENĖ** (Kaunas University of Technology, LITHUANIA)
Assoc. Prof. **Dainius VAIČIULIS** (Kaunas University of Technology, LITHUANIA)
Prof. **Darius VIRŽONIS** (Kaunas University of Technology, LITHUANIA)
Assoc. Prof. **Marcin WACHOWSKI** (Military University of Technology, POLAND)
Assoc. Prof. **Wioletta WEREDA** (Military University of Technology, POLAND)
Dr. Eng. **Tomasz WIERZBICKI** (Helena Chodkowska University of Technology and Economics, POLAND)
Assoc. Prof. **Jacek WOŹNIAK** (Military University of Technology, POLAND)
Prof. **Daiva ŽOSTAUTIENĖ** (Co-chair, Kaunas University of Technology, LITHUANIA)
Dr. **Justyna ZYLINSKA** (Helena Chodkowska University of Technology and Economics, POLAND)

All papers were reviewed.

© Copyright 2022 by EDITOGRAFICA s.r.l.
www.edlearning.it • congressi@editografica.com

All rights reserved. No part of this publication may be reproduced, stored in a retrieval system, or transmitted, in any form, or by any means, electronic, mechanical, photocopying, recording or otherwise, without the prior permission, in writing, from the publisher.

Printed in January 2022 by Editografica • Bologna (Italy)

ISBN 978-88-87729-77-1

ISSN 2345-0088 (print) ISSN 2345-0096 (online)

Foreword

The 14th International Scientific Conference Intelligent Technologies in Logistics and Mechatronics Systems – ITELMS'2022 was organized as an integral part of the 4rd Forum on Innovative Technologies and Management for Sustainability (ITMS'2022) that hosted two conferences: 9th International Scientific Conference Changes in Social and Business Environment – CISABE'2022 and 14th International Scientific Conference Intelligent Technologies in Logistics and Mechatronics Systems – ITELMS'2022.

The aim of this 4rd Forum on Innovative Technologies and Management for Sustainability is to provide a worldwide Forum, where the international participants can share their research knowledge and ideas on the latest research findings and map out the directions for future researchers and collaborations.

The main idea of this joint event was to stimulate interdisciplinary approach on sustainability issues since the most advanced, innovative solutions are created by close cooperation between social and technological sciences.

The importance of sustainable development is undeniable, but its implementation into corporate activities is often faced with the problems. Everybody strives for better quality of life and innovations. Innovations do not emerge out of nothing or nowhere, new ideas and the latest inventions result from old and living truths, so the main engine of innovation is knowledge that must be constantly updated, newly interpreted, and sometimes non-traditionally applied in practice.

The focus of the Forum is on various aspects of contemporary economic, social and technological environments for international business practice(s) and their target market(s). This Forum emerged as the result of collective efforts and here, we take the opportunity to express our recognition of all the people who have made ITMS'2022 possible, who have done the hard work in preparation and organization. This event is significant and exceptional because:

- We are proud to point out that Kaunas University of Technology, Panevėžys Faculty of Technologies and Business celebrated 60 years anniversary last year.
- The forum is organized in the spirit of the anniversary of the University of Lithuania. This year we celebrate our centenary.
- The forum is responsive to the global situation. This year we did not receive researchers from Russia and did not have their presentations as well as the researchers from the Ukraine because of the well-known war conflict situation. This situation confirms how unstable world is as well as how important the sustainability is.

Through these lines of welcome, we would like to especially pay tribute to the Scientific Committee which has assured the quality of the pool of accepted papers, and to the members of the Organizing Committee for their strong motivation and volunteer work, and eventually, to all the people who have directly or indirectly influenced the smooth progress towards the Forum. We are very thankful and express our gratitude to all the authors for contributing their papers to this volume.

Daiva ŽOSTAUTIENĖ

Contents

Multi-Objective Evaluation of the Effectiveness of the Materials of the Thermal Insulation Layer of the External Wall in A++ Class Public Building by MOORA Method
Donatas Aviža, Elvyra Zacharovienė 3

Mechanical Properties of Additive Manufactured PC / PTFE Parts
Krzysztof Grzelak 9

A New Concept of Electronic Devices Based on Type II Superconductor YBCO Films with Channel for Motion of Magnetic Vortices
Artūras Jukna 19

Multi-Criteria Evaluation of the Girder Bridge Beams
Jovita Kaupienė, Aurimas Česnulevičius 27

Additive Manufacturing in Hydraulic Systems – The Review
Agnieszka Klimek, Adam Bartnicki 35

Additive Manufacturing of Polyphenylene Sulfide: Material's Behavior During Tensile Testing
Janusz Kluczyński 43

Mechanical Properties Comparison of the Additively Manufactured Gears Made of Polymeric Materials with Improved Wear Resistance
Jakub Łuszczek, Lucjan Śnieżek, Krzysztof Grzelak 51

Selecting Military Transport Options, Taking Into Account Cost Analysis, Part 1 – Theoretical Basis
Jarosław Ziółkowski, Volodymyr Hutsaylyuk, Daniel Łukasiak 61

Selecting Military Transport Options, Taking Into Account Cost Analysis, Part 2 – Numerical Example
Jarosław Ziółkowski, Volodymyr Hutsaylyuk, Daniel Łukasiak 69

The Influence of Aramide Fibers Addition on the Tensile Properties of the Acrylonitrile Butadiene Styrene Dedicated for the FFF Technology
Ireneusz Szachogluchowicz 79

Glass Hollow Spheres Reinforced Polyamide for Additive Manufacturing: Strength Analysis
Janusz Torzewski 87

International Forum on Innovative Technologies and Management for Sustainability – ITMS'2022

International Scientific Conference Intelligent Technologies in Logistics and Mechatronics Systems – ITELMS'2022, 15th September, 2022, Panevėžys, Lithuania

Multi-Objective Evaluation of the Effectiveness of the Materials of the Thermal Insulation Layer of the External Wall in A++ Class Public Building by MOORA Method

Donatas Aviža[a,b]*, Elvyra Zacharovienė[a]

[a]*Kaunas University of Technology, Panevėžys Faculty of Technologies and Business, 33 Nemuno St., Panevėžys LT-37164, Lithuania*
[b]*Panevėžys University of Applied Sciences, 23 Laisvės Sq., Panevėžys LT-35200, Lithuania*

Abstract

This study aims to provide an evaluation of the effectiveness of the materials of the thermal insulation layer of the external wall in A++ class public building. MOORA method was selected for the multi-objective evaluation of the effectiveness of the thermal insulation materials alternatives. Four indicators were evaluated: The thickness of the thermal insulation layer, the thermal conductivity coefficient, the density and the price of thermal insulation material. Findings of the performed empirical research suggest that the polystyrene foam EPS70N is the most effective thermal insulation material for the external wall of the nearly zero-energy public building. This alternative scored the highest number of points (-0,187). The least effective option (from the researched alternatives) is the rock wool – *Paroc Linio* 80 (-0,331 points). The study findings are relevant to architects, structural designers and experts.

© 2022 Donatas Aviža, Elvyra Zacharovienė.
Peer-review under responsibility of the Kaunas University of Technology and the Panevėžys Faculty of Technologies and Business.

Keywords: MOORA method; Wall; Thermal insulation material; Multi-objective evaluation.

* Corresponding author. Tel.: +370 623 75003.
E-mail address: donatas.aviza@ktu.lt

© 2022 Aviža Donatas, Zacharovienė Elvyra.
F916G0001
Peer-review under responsibility of the Kaunas University of Technology, Panevėžys Faculty of Technologies and Business.

1. Introduction

Buildings and housing collectively account for more than one-third (1/3) of global final energy demand [1] and nearly 40 % of both indirect and direct CO_2 emissions. Energy-efficient building design consists of building upgrades that will maximize energy efficiency by minimizing energy losses and reducing heat losses across the building envelope [2]. There is a number of studies in the scientific literature about zero-energy or A++ class buildings (Omrany et al. [3]; Wu et al. [4]; Taherahmadi et al. [5]; Mata et al. [6]; Aviža et al. [7] and other).

The nearly zero-energy buildings are the buildings, which comply with the requirements set out for A++ energy efficiency class buildings in the Lithuanian Construction Technical Regulation STR 2.01.02:2016 "*Design and Certification of Energy Performance of Buildings*". These are highly energy efficient buildings, which consume almost zero or very low amount of energy. The renewable energy, which is mostly produced locally or come from nearby sources, accounts for the majority of energy consumption in these buildings [8].

Objectives of the research:

1. To perform the analysis of scientific resources revealing the requirements for the walls of zero-energy public buildings.
2. To analyse the MOORA method.
3. To perform a multi-objective evaluation study of the effectiveness of the wall thermal insulation materials.

Research methods: the review of scientific and technical sources, the MOORA method and the empirical study.

2. The MOORA method

A new method is proposed for multi-objective optimization with discrete alternatives: MOORA (Multi-Objective Optimization on the basis of Ratio Analysis) [9]. This method refers to a matrix of responses of alternatives to objectives, to which ratios are applied. A well-established other method for multi-objective optimization is used for comparison, namely the reference point method. Later on, it is demonstrated that this is the best choice among the different competing methods. In MOORA the set of ratios has the square roots of the sum of squared responses as denominators. These ratios, as dimensionless, seem to be the best choice among different ratios. These dimensionless ratios, situated between zero and one, are added in the case of maximization or subtracted in case of minimization. Finally, all alternatives are ranked, according to the obtained ratios. Eventually, to give more importance to an objective, an objective can be replaced by different sub-objectives or a coefficient of importance can be specified. An example on privatization in a transition economy illustrates the application of the method. If application is situated originally in a "welfare" economy, centred on production, MOORA becomes even more significant in a "wellbeing economy", where consumer sovereignty is assumed.

Multi-objective optimization (or programming), also known as multi-criteria or multi attribute optimization, is the process of simultaneously optimizing two or more conflicting attributes (objectives) subject to certain constraints. The MOORA method, first introduced by Brauers [10] is such a multi-objective optimization technique that can be successfully applied to solve various types of complex decision making problems in the manufacturing environment. The MOORA method [9–17] starts with a decision matrix showing the performance of different alternatives with respect to various attributes (objectives).

Step 1. The first step is to determine the objective, and to identify the pertinent evaluation attributes.

Step 2. The next step is to represent all the information available for the attributes in the form of a decision matrix. The data given in eq. (1) are represented as matrix X_{mxn}. Where i_{ij} is the performance measure of i^{th} alternative on j^{th} attribute, m is the number of alternatives, and n is the number of attributes. Then a ratio system is developed in which each performance of an alternative on an attribute is compared to a denominator, which is a representative for all the alternatives concerning that attribute.

$$X = \begin{bmatrix} x_{11} & x_{12} & \cdot & x_{1n} \\ x_{21} & x_{22} & \cdot & x_{2n} \\ \cdot & \cdot & \cdot & \cdot \\ x_{m1} & x_{m2} & \cdot & x_{mn} \end{bmatrix}. \quad (1)$$

Step 3. Brauers et al. [10] concluded that for this denominator, the best choice is the square root of the sum of squares of each alternative per attribute. This ratio can be expressed as below:

$$x_y^* = \frac{x_{ij}}{\sqrt{\left[\sum_{i=1}^{m} x_{ij}^2\right]}}; \qquad (j = 1, 2, \ldots, n); \tag{2}$$

where x_{ij} is a dimensionless number which belongs to the interval [0, 1] representing the normalized performance of i^{th} alternative on j^{th} attribute.

Step 4. For multi-objective optimization, these normalized performances are added in case of maximization (for beneficial attributes) and subtracted in case of minimization (for non-beneficial attributes). Then the optimization problem becomes:

$$y_i = \sum_{j=1}^{g} x_{ij}^* - \sum_{j=g+1}^{n} x_{ij}^*; \tag{3}$$

where g is the number of attributes to be maximized, $(n-g)$ is the number of attributes to be minimized, and y_i is the normalized assessment value of i^{th} alternative with respect to all the attributes.

In some cases, it is often observed that some attributes are more important than the others. In order to give more importance to an attribute, it could be multiplied with its corresponding weight (significance coefficient) [12]. When these attribute weights are taken into consideration, Eq. 3 becomes as follows:

$$y_i = \sum_{j=1}^{g} w_j x_{ij}^* - \sum_{j=g+1}^{n} w_j x_{ij}^*; \qquad (j = 1, 2, \ldots, n); \tag{4}$$

where w_j is the weight of j^{th} attribute, which can be determined applying analytic hierarchy process (AHP) or entropy method.

Step 5. The y_j value can be positive or negative depending of the totals of its maxima (beneficial attributes) and minima (nonbeneficial attributes) in the decision matrix. An ordinal ranking of y_j shows the final preference. Thus, the best alternative has the highest y_j value, while the worst alternative has the lowest y_j value.

3. Research

The research assessed the efficiency of thermal insulation layer of the external wall in A++ class public building. Heat transfer coefficient – U = 0.12 W/m²K. The research model is presented in Figure 1.

The MOORA (Multi-Objective Optimization on the basis of Ratio Analysis) method was chosen for the multi-objective evaluation of the effectiveness of the thermal insulation material alternatives.

In the first stage, a decision-making matrix (see Table 1) is compiled and 5 different thermal insulation materials are assessed according to four indicators: the thickness of the thermal insulation layer; the thermal conductivity coefficient; the density and the price (the first quarter of 2022) of thermal insulation material. The significance of all indicators is assumed to be proportionate and equal.

In the second stage, the decision matrix is normalized (see Table 2).

Table 1. Decision-making matrix

Alternatives (different thermal insulation materials) / Significance	Indicators			
	The layer thickness, mm	The thermal conductivity coefficient, W/mK	The density, kg/m^3	The price of the thermal insulation, €/m^2
Paroc Linio 80	300	0.040	85.00	26.72
EPS70	290	0.039	14.50	22.00
EPS70N	240	0.032	14.50	21.24

Alternatives (different thermal insulation materials) / Significance	Indicators			
	The layer thickness, mm	The thermal conductivity coefficient, W/mK	The density, kg/m^3	The price of the thermal insulation, €/m^2
XPS	250	0.035	32.00	36.60
FF-PIR	180	0.022	34.00	36.00
Significance	0.25	0.25	0.25	0.25

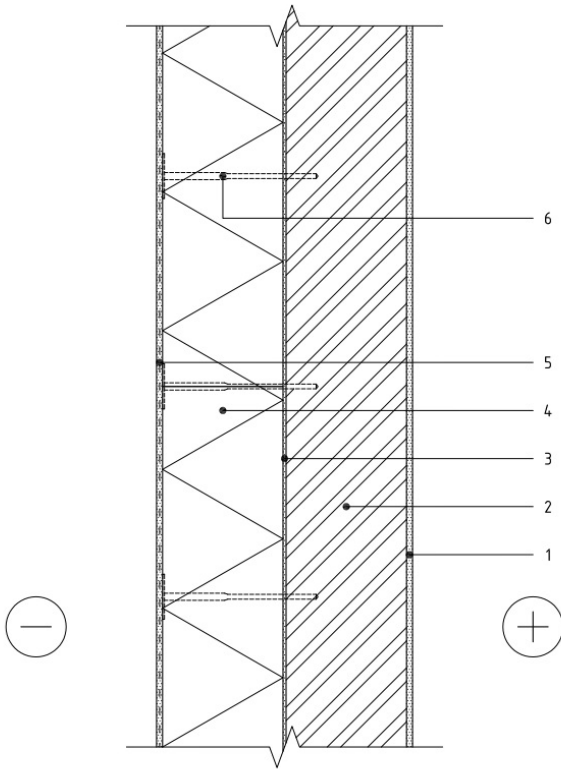


Fig. 1. Research model [18]: 1 – Internal surface (10 mm); 2 – Block masonry (autoclaved aerated concrete) (240 mm); 3 – Adhesive mortar (5 mm); 4 – Tested layer (5 materials); 5 – Adhesive mortar coated with masonry sealer / Reinforcing mesh / Decorative coat; 6 – Mechanical fasteners

Table 2. Normalized matrix

Alternatives (different thermal insulation materials)	Indicators			
	The layer thickness, mm	The thermal conductivity coefficient, W/mK	The density, kg/m^3	The price of the thermal insulation, €/m^2
Paroc Linio 80	0.52	0.52	0.86	0.41
EPS70	0.51	0.51	0.15	0.34
EPS70N	0.42	0.42	0.15	0.32
XPS	0.44	0.46	0.32	0.56
FF-PIR	0.31	0.29	0.34	0.55

In the third stage, the weighted alternative values are calculated (see Table 3).

Table 3. Weighted normalized matrix

Alternatives (different thermal insulation materials)	**Indicators**			
	The layer thickness, mm	**The thermal conductivity coefficient, W/mK**	**The density, kg/m^3**	**The price of the thermal insulation, €/m^2**
Paroc Linio 80	0.13	0.13	0.21	0.10
EPS70	0.13	0.13	0.04	0.08
EPS70N	0.10	0.10	0.04	0.08
XPS	0.11	0.11	0.08	0.14
FF-PIR	0.08	0.07	0.09	0.14

In the fourth stage, the contribution index is calculated and then the alternative priority row is determined (see Table 4).

Table 4. Ranking alternatives

Alternatives (different thermal insulation materials)	**Contribution index**	**Ranking**
Paroc Linio 80	-0.578	5
EPS70	-0.375	3
EPS70N	-0.327	1
XPS	-0.444	4
FF-PIR	-0.374	2

Upon completion of the multi-objective evaluation, effectiveness alternatives were calculated for each thermal insulation materials (see Fig. 2).

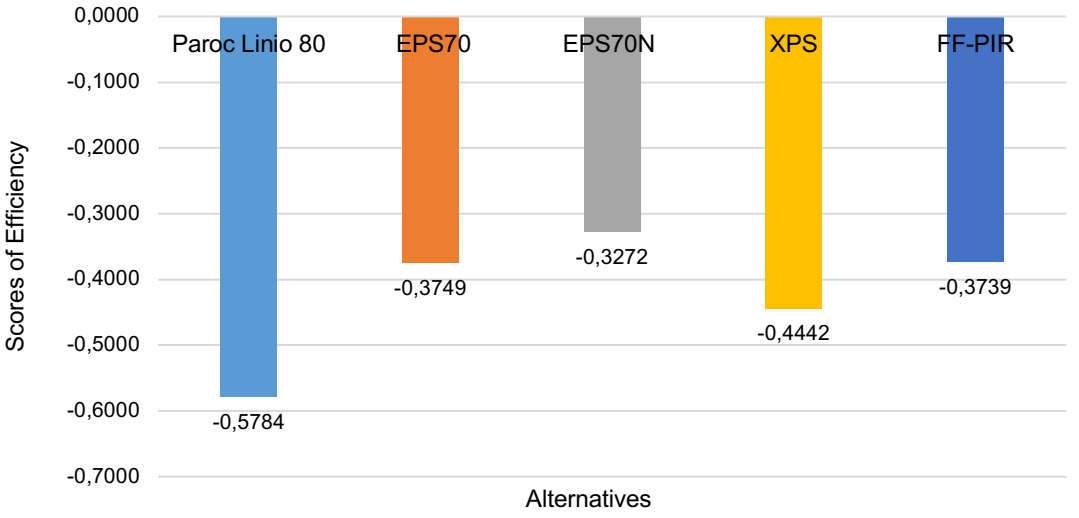


Fig. 2. Evaluation of the efficiency of the wall thermal insulation layer

An empirical study shows that the most effective thermal insulation layer for a public A++ class building wall is the polystyrene foam EPS70N, the least effective is rock wool *Paroc Linio* 80 (-0,5784 points).

4. Conclusions

1. Having evaluated the thickness of the thermal insulation layer, the thermal conductivity coefficient, the density and the price of thermal insulation material by the MOORA method, it was revealed that the most effective thermal insulation of a wall of A++ class public building (taking into account five alternatives and four proportional indicators) is the polystyrene foam – EPS70N. This alternative scored the highest number of points (-0.327).
2. The least effective option (from the five tested alternatives) is the rock wool – *Paroc Linio* 80 (-0.578 points). The difference between the best and worst alternatives is 56.57 %.

References

[1] International energy agency. *Buildings: A Source of Enormous Untapped Efficiency Potential* [Internet]. 2022. Available from: https://www.iea.org/topics/buildings (accessed on 01-03-2022).
[2] Ahmad, T., Zhang, D., AlGhamdi, A. S., Ullah, F. Alshamrani, S. S. Design parametric analysis of low-energy residential buildings on the way to a defined cost-optimal capacity point. *Alexandria Engineering Journal*, 2022, 1110–1168.
[3] Omrany, H. et al. A bibliometric review of net zero energy building research 1995–2022. *Energy & Buildings*, 2022, 111996.
[4] Wu, W., Skye, H. M. Residential net-zero energy buildings: Review and perspective. *Renewable and Sustainable Energy Reviews*, 2021, 142, 110859.
[5] Taherahmadi, J., Noorollahi, J., Panahi, M Toward comprehensive zero energy-building definitions: A literature review and recommendations. *International Journal of Sustainable Energy*, 2021, 40, 2, 120–148.
[6] Mata, E. et al. A map of roadmaps for zero and low energy and carbon buildings worldwide. *Environmental Research Letters*, 2020, 15, 113003.
[7] Aviža, D. et al. Multi-objective assessment of the effectiveness of the thermal insulation layer of the flat roof by EDAS method. *Forum on Innovative Technologies and Management for Sustainability* (ITMS'2020), 2020, Panevėžys, Lithuania.
[8] Technical construction regulation STR 2.01.02:2016. *Design and Certification of Energy Performance of Buildings*. Vilnius: Ministry of Environment of the Republic of Lithuania, 2016.
[9] Brauers, W. K. M., Zavadskas, E. K. The MOORA method and its application to privatization in a transition economy. *Control and Cybernetics*, 2006, 35(2), 445–469.
[10] Brauers, W. K. M. *Optimization Methods for a Stakeholder Society. A Revolution in Economic Thinking by Multiobjective Optimization: Nonconvex Optimization and Its Applications*. Kluwer Academic Publishers, Boston, U.S.A., 2004.
[11] Brauers, W. K. M., Zavadskas, E. K., Peldschus, F., Turskis, Z. Multiobjective decision-making for road design. *Transport*, 2008, 23(3), 183–193.
[12] Brauers, W. K. M., Zavadskas, E. K. Robustness of the multiobjective MOORA method with a test for the facilities sector. *Technological and Economic Development of Economy: Baltic Journal on Sustainability*, 2009, 15(2), 352–375.
[13] Brauers, W. K. M. Multiobjective contractor's ranking by applying the MOORA method. *Journal of Business Economics and Management*, 2008, 4, 245–255.
[14] Brauers, W. K. M., Zavadskas, E. K., Peldschus, F., Turskis, Z. Multi objective optimization of road design alternatives with an application of the MOORA method. *Proceedings of the 25th International Symposium on Automation and Robotics in Construction*, Vilnius Gediminas Technical University, Lithuania, 2008, June 26–29, 541–548.
[15] Kalibatas, D., Turskis, Z. Multi-criteria evaluation of inner climate by using MOORA method. *Information Technology and Control*, 2008, 37, 79–83.
[16] Rao, R. V. *Decision Making in the Manufacturing Environment: Using Graph Theory and Fuzzy Multiple Attribute Decision-Making Methods*. London, Springer Verlag, 2007. ISBN: 9781846288180.
[17] Chakraborty, S. Applications of the MOORA method for decision making in manufacturing environment [Internet]. *International Journal of Advanced Manufacturing Technology*, 2010, 54(9–12), 1155–1166. Available from: doi:10.1007/s0017001029720 (accessed on 07-05-2022).
[18] Rook wool [Internet]. *Catalog*. Available from: www.paroc.lt (accessed on 01-03-2022).

International Forum on Innovative Technologies and Management for Sustainability – ITMS'2022

International Scientific Conference Intelligent Technologies in Logistics and Mechatronics Systems – ITELMS'2022, 15th September, 2022, Panevėžys, Lithuania

Mechanical Properties of Additive Manufactured PC / PTFE Parts

Krzysztof Grzelak[a]*

[a]*Institute of Robots & Machine Design, Faculty of Mechanical Engineering, Military University of Technology, 2 Gen. S. Kaliskiego St., Warsaw 00-908, Poland*

Abstract

The research involved determining the strength properties of a PTFE-doped polycarbonate (PC) based composite material in incremental technology (AM) applications. The study showed the influence of the manufacturing direction of the PC / PTFE composite material on the basic strength parameters. Specimens were fabricated in three orientation directions relative to the working plane using the FFF process. Additional digital-image correlation studies were performed to extend the study. The results indicate a high dependence of fabrication directionality on strength properties.

© 2022 Krzysztof Grzelak.
Peer-review under responsibility of the Kaunas University of Technology, Panevėžys Faculty of Technologies and Business.

Keywords: Additive Manufacturing; Fused Filament Fabrication; PC / PTFE; Mechanical properties analysis.

1. Introduction

Composite materials in incremental technology applications occupy a growing area of research and development. Obtaining the desired material properties is possible through the use of composite materials [1–5]. Composite materials allow diverse properties to be obtained most often by doping the matrix material with an additional component.

The combination is chosen in such a way as to achieve a synergy of properties for a specific application need.

Additive Manufacturing (AM) technologies are still of significant interest to many researchers, but the development of AM technologies in various industries is also evident [6–9]. One of the most common AM techniques, is the

* Corresponding author.
E-mail address: krzysztof.grzelak@wat.edu.pl

© 2022 Krzysztof Grzelak.

Peer-review under responsibility of the Kaunas University of Technology, Panevėžys Faculty of Technologies and Business.

thermoplastic extrusion of materials (ME) mainly known as Fused Deposition Modelling (FDM), or Fused Filament Fabrication (FFF), which are very common and widely used.

FFF / FDM fabrication is based directly on a computer model of the geometry in the form of 3D CAD files without the need for 2D drawings to prepare the process. During the process, plastic wire, also known as filament, is plasticised in a heated nozzle. The filament, which is plasticised and pressed through the nozzle, is arranged in the working plane of the machine in the desired shape of the respective layer of the manufactured part geometry. Subsequent layers are produced one after the other until the entire product geometry is achieved.

The most commonly used material in FFF technology is polylactic acid biopolymer (PLA). Its main advantages relate to its very low shrinkage, and relatively good tensile properties [10–14]. However, this material has disadvantages, the most important of which are low plasticisation temperature, lack of UV resistance and brittleness. These problems represent a strong limitation to the use of these materials in some specific industrial applications. For this reason, manufacturers of materials for FFF technology are introducing various innovations based on a combination of common and innovative materials [15–17] and fibres [19–21]. Interesting results were shown by the work of Xiaowei Mu et al [22], in which the authors compared an improved PC polymer with a PC / PPFBS and PC / PSR composite by analysing fire resistance properties. Kaur et al [18] analysed the use of ABS modification with additives to enhance tribological properties. The ever-increasing interest in the use of AM technology [23–30] and layered materials [31–33] in research and industry was the motivation to analyse the impact of using polycarbonate, which has high strength with PTFE additives to enhance tribological properties.

2. Materials and methods

For the test, it was used the *XYZ* – PC / PTFE material provided by the "Spectrum Filaments Ltd. Company". The *XYZ* – PC / PTFE is advanced composite filament based on polycarbonate (PC) with the addition of PTFE commonly known as Teflon. The high demand and limited availability of Additive Manufacturing materials with very good mechanical properties, with particular emphasis on high abrasion resistance, has initiated efforts to combine the very good properties of PC and PTFE. Polycarbonate provides high mechanical resistance and PTFE complements it by reducing wear and friction.

Basic properties of PC / PTFE:

- low processing shrinkage (linear) of approx. – 0.6 %;
- heat distortion temperature (HDT) – 140 °C;
- Vicat softening point – 145 °C;
- flammability class UL 94 (3.0 mm) – V1;
- electrical resistance – 1E12 Ohm;
- static coefficient of friction – 0.18;
- dynamic coefficient of friction – 0.14;
- high abrasion resistance;
- high mechanical strength;
- very strong layer lamination.

Application possibilities:

- manufacture of parts with a low coefficient of friction;
- manufacture of thermally, electrically and thermally insulating parts;
- manufacture of low-load gears and drive components;
- manufacture of tools used in the assembly of components during production;
- parts for end use;
- functional prototyping.

To reach desirable elements properties it had been designed the following process parameters:

- hotend temperature – 315 °C;
- heatbed temperature – 120 °C;
- chamber temperature – 80 °C;
- layer thickness – 0.2 mm;
- outline shell thickness – 2 mm;
- infill – 100 %;
- part cooling intensity – 40 %;
- printing speed – 50 mm/s;
- nozzle diameter – 0.4 mm.

Producing suitable samples from PC / PTFE plastic required the use of a suitable device, the "Intamsys Funmat HT" 3D printer. This device has a heating chamber, a high-temperature hotend and a heated workbench plate up to 160 °C to ensure that the samples are properly produced without thermal stress. Sample parts were oriented along each of the three axes (see Fig. 1) to allow the determination of how layer deposition of the FFF parts affects tensile properties.

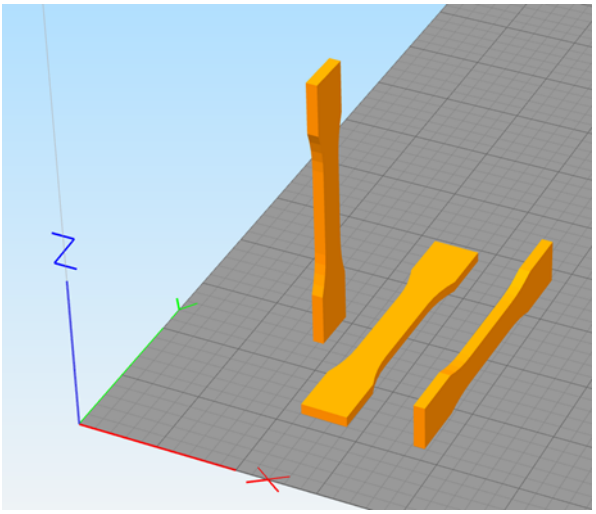


Fig. 1. Samples' orientation in the substrate plate

To evaluate the mechanical properties, dog-bone shaped parts were fabricated by the FFF additive technology printer according to ASTM D638 "*Standard Test Method for Tensile Properties of Plastics*". For each test, five same samples were prepared to make sure the obtained values of designed joints mechanical properties reliable. The geometry of designed sample is shown in Figure 2.

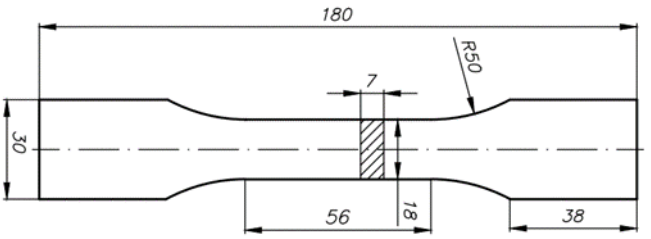


Fig. 2. Geometry of plain flat specimen tested under tensile loading (dimensions in mm)

Tensile tests and low cycle fatigue tests have been performed at room temperature by adopting an "Instron" 8802 axial servo-hydraulic testing machine ("Instron", Norwood, MA, USA), with a load capacity of 250 kN and equipped with an "Instron" 8800 controller. The uniaxial extensometer "Instron" 2630-112 with a gauge length of 50 mm (axial travel +50 %) has been adopted to measure the axial strain during tensile tests. The dynamic extensometer "Instron" 2620-602 with a gauge length of 25 mm (axial travel ±5 %) was used for strain-controlled tests. DIC – non-contact, optical method from "Dantec Dynamics" (Ulm, Germany).

3. Tensile test – results, and discussion

All tensile tests were performed under room temperature conditions using a universal testing machine "Instron" 8802 with a quasi-static loading condition (5 mm/min.). The obtained material properties included tensile strength and elongation at break of the samples are presented in Table 1.

Table 1. Mechanical properties of samples tested

Type of property	Value for *X*-orientation	Value for *Y*-orientation	Value for *Z*-orientation
Ultimate tensile strength (MPa)	35.79	34.1	7.15
Yield strength (MPa)	25.5		
Strain at break (%)	10.3	8	0.8

To better illustrate the behaviour of the PC / PTFE material, the course of the static tensile test of the specimens is shown in the diagrams (see Figs. 3–5).

The static tensile test results obtained show a high dependence of the specimen orientation in the fabrication process.

As can be seen from the summary in Table 1, the basic quantities vary strongly depending on the specimen orientation. The highest strength values were observed for specimens manufactured in the *X*-orientation. The *YS* value can also be determined for these samples. For the remaining samples in *Y*- and *Z*-orientation, the *YS* value cannot be determined unambiguously.

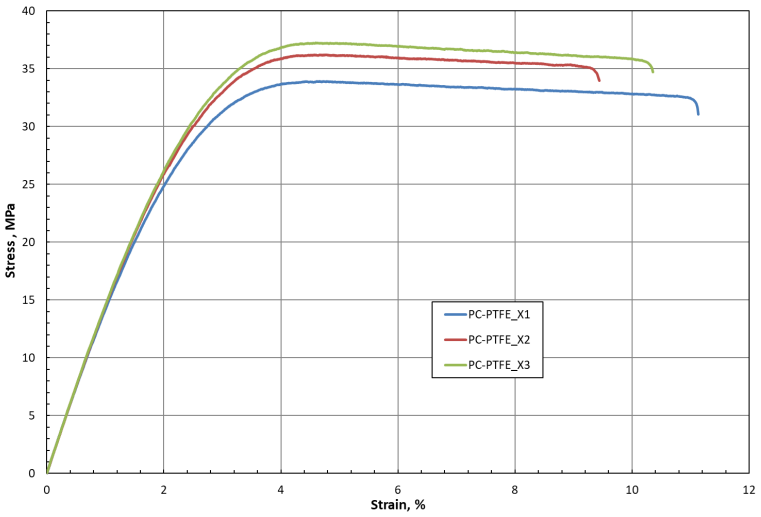


Fig. 3. Strain-stress chart for *X*-oriented samples made of the PC / TFE material

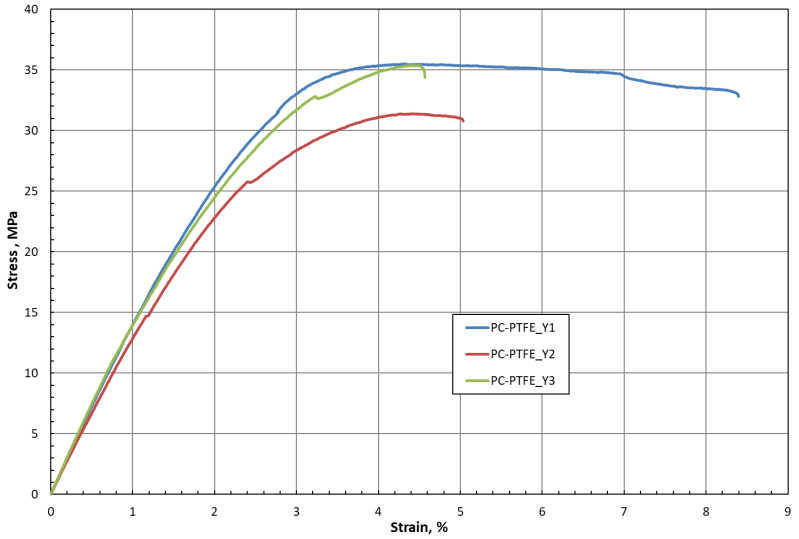


Fig. 4. Strain-stress chart for *Y*-oriented samples made of the PC / PTFE material

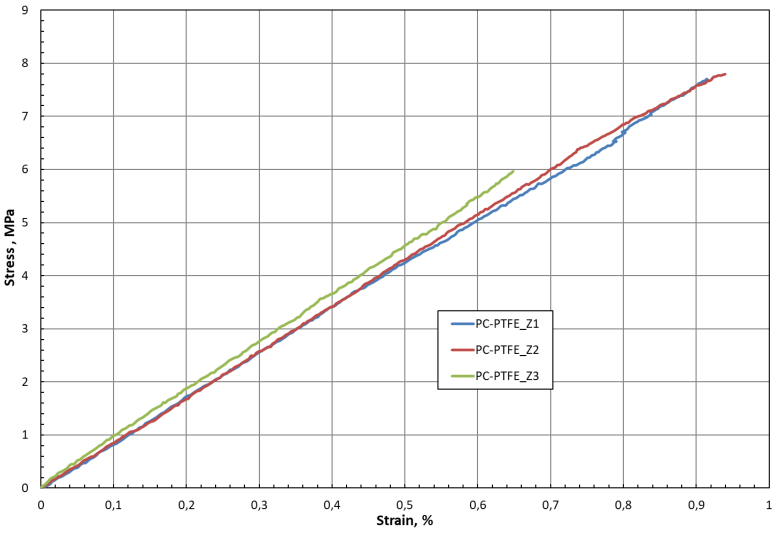


Fig. 5. Strain-stress chart for *Z*-oriented samples made of the PC / PTFE material

Samples in the *X* orientation are also characterized by the largest strain range. Samples in the *Z*-orientation show lower values, which is consistent with the typical nature of the interaction of FFF fabricated components in this layer growth pattern.

4. Digital image correlation – results, and discussion

The deformation behaviour of the PC / PTFE specimens during the tensile test was monitored using the DIC method. The strain maps obtained for the three fabrication directions are shown in Figures 6–8 for the *X*, *Y* and *Z* directions, respectively.

The figures (see Figs. 6–8) in the form of maps illustrate the four phases of deformation.

Initial phase – unloaded specimen (“Reference”).

Second phase – loading of the specimen resulting in a deformation corresponding to the yield stress (0.2 % deformation).

Third phase – loading of the specimen corresponding to the ultimate tensile strength ("UTS").

Final stage – damaged specimen ("After").

This combination of strain maps allows a comparative analysis of the deformation of specimens produced in different orientations under tensile testing.

The results clearly showed that the nature of the deformation is almost uniform in terms of tensile area in specimens with fabrication orientations *X* and *Y*. This demonstrates the uniform distribution of doped PTFE in the PC matrix of the test material. In the case of the *Z* direction, the layered direction of the maximum deformation on the specimen surface can be clearly seen (see Fig. 8). This layering is due to the realization of the layering process of the FFF technique and is a direct factor in the high anisotropy of the properties of this material.

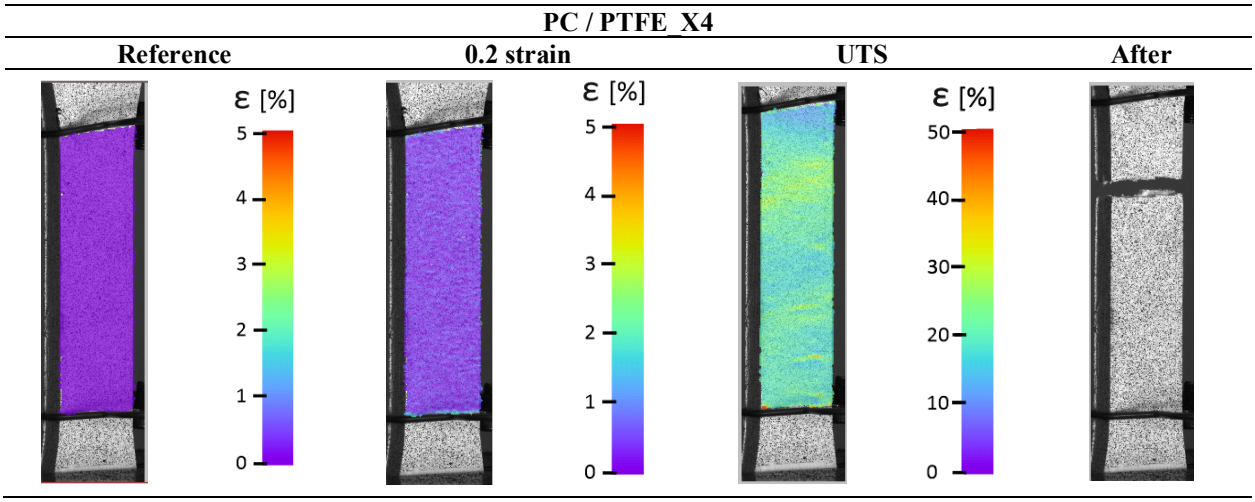


Fig. 6. Representative DIC results for specimens made in the *X* direction

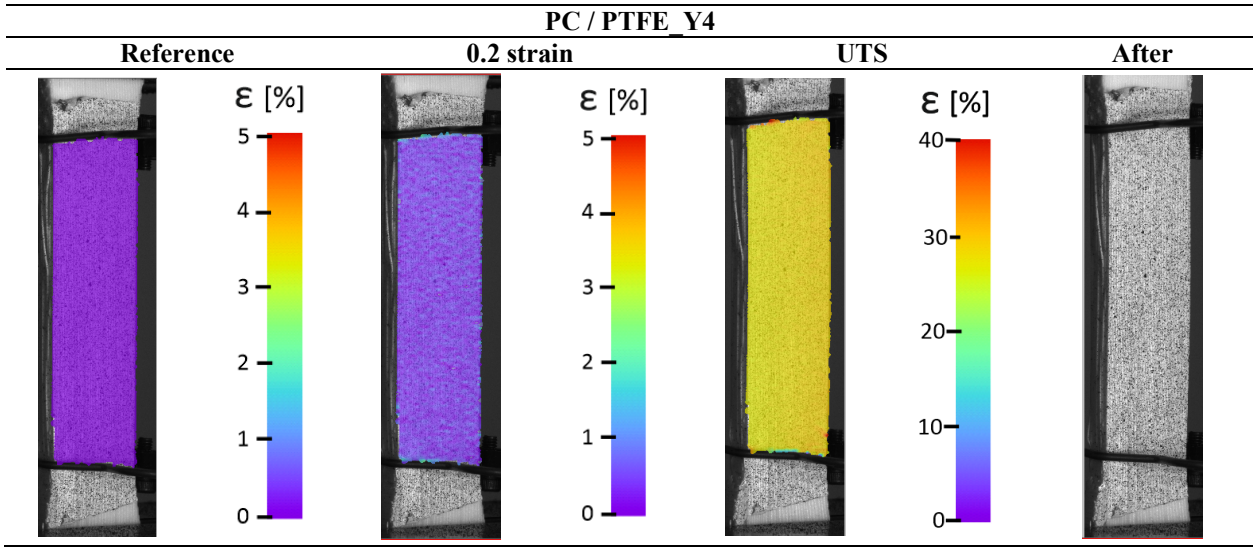


Fig. 7. Representative DIC results for specimens made in the *Y* direction

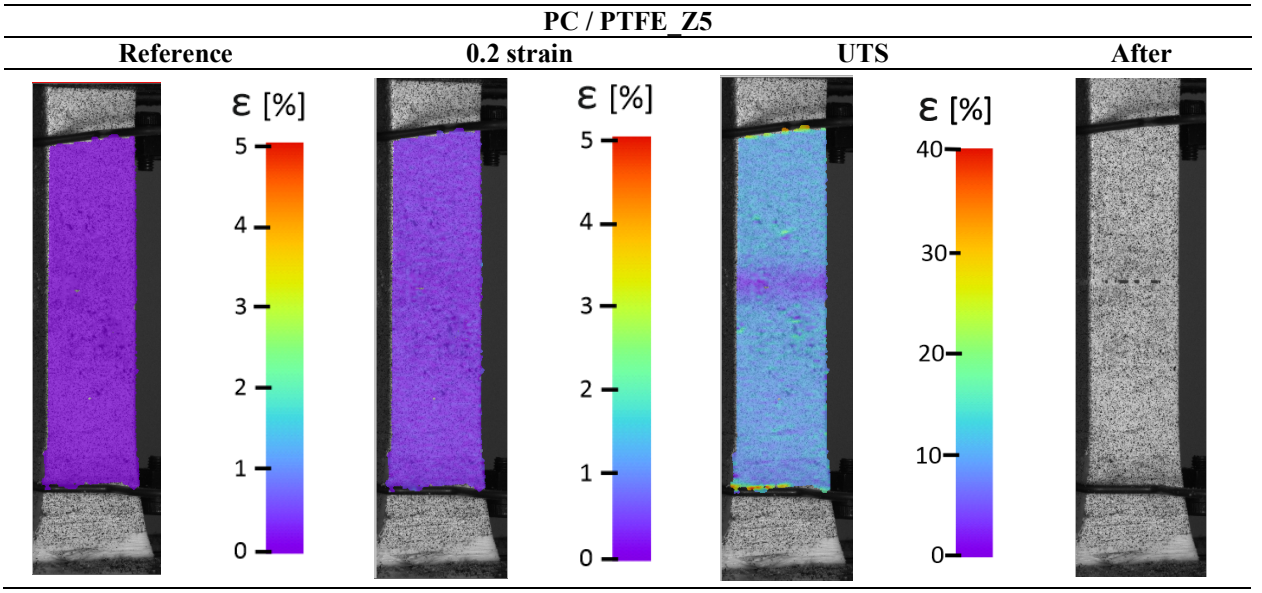


Fig. 8. Representative DIC results for specimens made in the *Z* direction

During the initial loading period (0.2 % strain), all the specimens showed a similar level of strain across the entire surfaces of the analysed measurement area. The highest deformations were observed for the PC / PTFE Y4 and PC / PTFE X4 specimens, which is consistent with the results shown in the graphs (see Figs. 3–5) and the dnas in Table 1. Similar levels of maximum deformations were observed for the *X*- and *Y*-direction specimens. Nevertheless, it is worth noting that the maximum deformation of the PC / PTFE Y4 specimen was obtained at a slightly lower loading level.

5. Conclusions

On the basis of the research carried out and the analysis of the results obtained, the following conclusions can be drawn:

1. Components manufactured by FFF technology from PC / PTFE material are characterized by high anisotropy of strength properties depending on the orientation of their manufacturing direction with respect to the load direction.
2. The highest strength properties are demonstrated for components manufactured in the *X*-orientation and slightly lower (about 1–2 %) for the *Y*-orientation.
3. Measurements made using the DIC method showed that the most heterogeneous nature of the deformation occurred for specimens made in the *Z* direction.

References

[1] Małek, M., Grzelak, K., Łasica, W., Jackowski, M., Kluczyński, J., Szachogłuchowicz, I., Torzewski, J., Łuszczek, J. Cement-glass composite bricks (CGCB) with interior 3D printed PET-G scaffolding [Internet]. *Journal of Building Engineering*, 2022, 52, 104429. Available from: https://doi.org/https://doi.org/10.1016/j.jobe.2022.104429 (accessed on 18-09-2022).

[2] Sniezek, L., Szachogluchowicz, I., Wachowski, M., Torzewski, J., Mierzynski, J. High cycle fatigue properties of explosively welded laminate AA2519/AA1050/Ti6Al4V [Internet]. *Procedia Structural Integrity*, 2017, 5, 422–429. Available from: doi:10.1016/j.prostr.2017.07.191 (accessed on 18-09-2022).

[3] Szachogluchowicz, I., Sniezek, L., Sulym, H., Gloc, M. Testing and verification modeling of wave-shape formation under explosion welding to laminate AA 2519-Ti6Al4V [Internet]. *Procedia Structural Integrity*, 2016, 2, 2375–2380. Available from: doi:10.1016/j.prostr.2016.06.297 (accessed on 18-09-2022).

[4] Sniezek, L., Szachogluchowicz, I., Gocman, K. The mechanical properties of composites AA.2519-Ti6Al4V obtained by detonation method. *Intelligent Technologies in Logistics and Mechatronics Systems*, 2013, 214–219.

[5] Fras, T., Szachogluchowicz, I., Sniezek, L. Ti6Al4V-AA1050-AA2519 explosively-cladded plates under impact loading. *European Physical Journal-Special Topics* [Internet]. 2018, 1–2, 17–27. Available from: doi:10.1140/epjst/e2018-00114-9 (accessed on 18-09-2022).
[6] Günther, D., Heymel, B., Günther, J. F., Ederer, I. Continuous 3D-printing for Additive Manufacturing [Internet]. *Rapid Prototyping Journal*, 2014, 20, 320–327. Available from: doi:10.1108/RPJ-08-2012-0068 (accessed on 21-09-2022).
[7] Campbell, I., Bourell, D., Gibson, I. Additive Manufacturing: Rapid prototyping comes of age [Internet]. *Rapid Prototyping Journal*, 2012, 18, 255–258. Available from: doi:10.1108/13552541211231563 (accessed on 21-09-2022).
[8] Ivanova, O. S., Williams, C. B., Campbell, T. A. Additive Manufacturing (AM) and nanotechnology: Promises and challenges [Internet]. *International Solid Freeform Fabrication Symposium / 2011 International Solid Freeform Fabrication Symposium*, 2011, 733–749. Available from: doi:10.1108/RPJ-12-2011-0127 (accessed on 21-09-2022).
[9] Glardon, R. Direct rapid tooling: Research. *Rapid Prototyping Journal*, 1998, 4, 77–89.
[10] Kluczyński, J., Śnieżek, L., Kravcov, A., Grzelak, K., Svoboda, P., Szachogłuchowicz, I., Franek, O., Morozov, N., Torzewski, J., Kubeček, P. The examination of restrained joints created in the process of multi-material FFF Additive Manufacturing technology [Internet]. *Materials* (Basel), 2020, 13, 903. Available from: doi:10.3390/ma13040903 (accessed on 21-09-2022).
[11] Lifton, V. A., Lifton, G., Simon, S. Options for additive rapid prototyping methods (3D printing) in MEMS technology [Internet]. *Rapid Prototyping Journal*, 2014, 20, 403–412. Available from: doi:10.1108/RPJ-04-2013-0038 (accessed on 21-09-2022).
[12] du Plessis, A., Broeckhoven, C., Yadroitsava, I., Yadroitsev, I., Hands, C. H., Kunju, R., Bhate, D. Beautiful and functional: A review of biomimetic design in Additive Manufacturing [Internet]. *Additive Manufacturing*, 2019, 27, 408–427. Available from: doi:10.1016/j.addma.2019.03.033 (accessed on 21-09-2022).
[13] Pawlak, W., Wieleba, W., Kluczyński, J., Śnieżek, L. The influence of the addition of graphite on the tribological properties of polylactic (PLA) applied in 3D printing technology. *Tribologia*, 2018, 277(1), 89–93 Available from: doi:10.5604/01.3001.0011.9970.
[14] Rajakaruna, R. A. D. N. V., Subeshan, B., Asmatulu, E. Fabrication of hydrophobic PLA filaments for Additive Manufacturing [Internet]. *Journal of Materials Science*, 2022, 57, 8987–9001. Available from: doi:10.1007/s10853-022-07217-5 (accessed on 21-09-2022).
[15] Alam, P., Mamalis, D., Robert, C., Floreani, C., Ó Brádaigh, C. M. The fatigue of carbon fibre reinforced plastics – A review [Internet]. *Composites Part B: Engineering*, 2019, 166, 555–579. Available from: doi:10.1016/j.compositesb.2019.02.016 (accessed on 21-09-2022).
[16] Frascio, M., Avalle, M., Monti, M. Fatigue strength of plastics components made in Additive Manufacturing: First experimental results [Internet]. *Procedia Structural Integrity*, 2018, 12, 32–43. Available from: doi:10.1016/j.prostr.2018.11.109 (accessed on 21-09-2022).
[17] Wen, Y., Xu, C., Wang, H., Chen, A., Batra, R. C. Impact of steel spheres on ballistic gelatin at moderate velocities [Internet]. *International Journal of Impact Engineering*, 2013, 62, 142–151. Available from: doi:10.1016/j.ijimpeng.2013.07.002 (accessed on 21-09-2022).
[18] Heidari-Rarani, M., Rafiee-Afarani, M., Zahedi, A. M. Mechanical characterization of FDM 3D Printing of continuous carbon fiber reinforced PLA composites [Internet]. *Composites Part B: Engineering*, 2019, 175. Available from: doi:10.1016/j.compositesb.2019.107147 (accessed on 21-09-2022).
[19] Chacón, J. M., Caminero, M. A., García-Plaza, E., Núñez, P. J. Additive Manufacturing of PLA structures using fused deposition modelling: Effect of process parameters on mechanical properties and their optimal selection [Internet]. *Materials & Design*, 2017, 124, 143–157. Available from: doi:10.1016/j.matdes.2017.03.065 (accessed on 21-09-2022).
[20] Gao, X., Zhang, D., Qi, S., Wen, X., Su, Y. Mechanical properties of 3D parts fabricated by fused deposition modeling: Effect of various fillers in polylactide [Internet]. *Journal of Applied Polymer Science*, 2019, 136, 1–10. Available from: doi:10.1002/app.47824 (accessed on 21-09-2022).
[21] Yao, Y., Li, M., Lackner, M., Herfried, L. A continuous fiber-reinforced Additive Manufacturing processing based on PET fiber and PLA [Internet]. *Materials* (Basel). 2020, 13. Available from: doi:10.3390/ma13143044 (accessed on 21-09-2022).
[22] Mu, X., Jin, Z., Chu, F., Cai, W., Zhu, Y., Yu, B., Song, L., Hu, Y. High-performance flame-retardant polycarbonate composites: Mechanisms investigation and fire-safety evaluation systems establishment. *Composites Part B: Engineering*, 2022, 238, 109873.
[23] Kluczyński, J., Śniezek, L., Grzelak, K., Mierzyński, J. The influence of exposure energy density on porosity and microhardness of the SLM Additive Manufactured elements [Internet]. *Materials* (Basel), 2018, 11. Available from: doi:10.3390/ma11112304 (accessed on 21-09-2022).
[24] Śniezek, L., Grzelak, K., Torzewski, J., Kluczyński, J. Study of the mechanical properties components made by SLM additive technology. *Proceedings of the 11th International Conference on Intelligent Technologies in Logistics and Mechatronics Systems* (ITELMS 2016), 2016, 145–153.
[25] Kluczyński, J., Śniezek, L., Grzelak, K., Torzewski, J., Szachogłuchowicz, I., Wachowski, M., Łuszczek, J. Crack growth behavior of Additively Manufactured 316L steel-influence of build orientation and heat treatment [Internet]. *Materials* (Basel), 2020, 13. Available from: doi:10.3390/MA13153259 (accessed on 21-09-2022).
[26] Kluczyński, J., Śniezek, L., Grzelak, K., Oziebło, A., Perkowski, K., Torzewski, J., Szachogłuchowicz, I., Gocman, K., Wachowski, M., Kania, B. Comparison of different heat treatment processes of selective laser melted 316L steel based on analysis of mechanical properties [Internet]. *Materials* (Basel), 2020, 13. Available from: doi:10.3390/ma13173805 (accessed on 21-09-2022).
[27] Kluczyński, J., Śnieżek, L., Grzelak, K., Janiszewski, J., Płatek, P., Torzewski, J., Szachogłuchowicz, I., Gocman, K. Influence of selective laser melting technological parameters on the mechanical properties of Additively Manufactured elements using 316L austenitic steel [Internet]. *Materials* (Basel), 2020, 13, 1449. Available from: doi:10.3390/ma13061449 (accessed on 21-09-2022).
[28] Kluczyński, J., Śnieżek, L., Grzelak, K., Oziębło, A., Perkowski, K. Hot Isostatic pressing influence on the mechanical properties of selectively laser-melted 316L steel [Internet]. *Bulletin of the Polish Academy of Sciences / Technical Sciences*, 2020, 68, 1413–1424. Available from: doi:10.24425/bpasts.2020.135396 (accessed on 18-09-2022).
[29] Grzelak, K., Kluczyński, J., Szachogłuchowicz, I., Łuszczek, J., Śnieżek, L., Torzewski, J. Modification of structural properties using process parameters and surface treatment of monolithic and thin-walled parts obtained by selective laser melting [Internet]. *Materials* (Basel), 2020, 13, 1–12. Available from: doi:10.3390/ma13245662 (accessed on 18-09-2022).

[30] Małek, M., Łasica, W., Kadela, M., Kluczyński, J., Dudek, D. Physical and mechanical properties of polypropylene fibre-reinforced cement – glass composite [Internet]. *Materials* (Basel), 2021, 14, 1–19. Available from: doi:10.3390/ma14030637 (accessed on 18-09-2022).

[31] Szachogluchowicz, I., Sniezek, L., Slezak, T., Kluczyński, J., Grzelak, K., Torzewski, J., Fras, T. Mechanical properties analysis of the AA2519-AA1050-Ti6Al4V explosive welded laminate [Internet]. *Materials* (Basel), 2020, 13, 4348. Available from: doi:10.3390/ma13194348 (accessed on 18-09-2022).

[32] Szachogluchowicz, I., Sniezek, L., Hutsaylyuk, V. Low cycle fatigue properties laminate AA2519-TI6AL4V [Internet]. *Procedia Engineering*, 2015, 114, 26–33. Available from: doi:10.1016/j.proeng.2015.08.022 (accessed on 18-09-2022).

[33] Wachowski, M., Śnieżek, L., Szachogłuchowicz, I., Kosturek, R., Płociński, T. Microstructure and fatigue life of Cp-Ti/316L bimetallic joints obtained by means of explosive welding [Internet]. *Bulletin of the Polish Academy of Sciences / Technical Sciences*, 2018, 66, 925–933. Available from: doi:10.24425/bpas.2018.125940 (accessed on 18-09-2022).

International Forum on Innovative Technologies and Management for Sustainability – ITMS'2022

ktu 1922 panevėžys faculty of technologies and business

International Scientific Conference Intelligent Technologies in Logistics and Mechatronics Systems – ITELMS'2022, 15th September, 2022, Panevėžys, Lithuania

A New Concept of Electronic Devices Based on Type II Superconductor YBCO Films with Channel for Motion of Magnetic Vortices

Artūras Jukna[a]*

[a]*Photovoltaic Technologies Laboratory, Faculty of Fundamental Sciences, Vilnius Gediminas Technical University (VILNIUS TECH), 11 Saulėtekio Av., Vilnius LT-10223, Lithuania*

Abstract

The critical superconducting current is one of the most important characteristics of superconducting films if films are applied in low- and high-power superconducting electronic and / or optoelectronic devices. If the superconductor is under supercritical current, then its diamagnetic properties depend on the amplitude of the current self-produced magnetic field, which results in the first flux penetration into a mixed-state superconductor in the form of Abrikosov magnetic vortices, and on a balance between the pinning F_p and the Lorentz F_L forces acting on these magnetic vortices. (Here, the mixed state is the state in which the superconducting and normal phases of the superconductor material can coexist together.) The increase in F_L results in the onset of the critical current density J_c in the superconducting devices and the onset of an energy dissipative state in the superconductor caused by the nucleation and motion of Abrikosov magnetic vortices. The superconducting properties of type II superconductor cuprates are a function of the ambient temperature, the amplitude and direction of an external magnetic field, and the level of doping by oxygen. Current work demonstrates the potential to control the balance between F_p and F_L through the artificial introduction of partially decomposed by oxygen 5-μm-wide and 50-μm-long line (channel for a motion of Abrikosov magnetic vortices) in $50 \times 100 \times 0.3$ μm^3 (width × length × thickness) $YBa_2Cu_3O_{7-\delta}$ (YBCO) devices. Due to the inhomogeneous distribution of oxygen concentration in the channel, our devices exhibit nonlinear stepped-like current-voltage (*I-V*) characteristics resulting from a periodic on / off of vortex motion in the channel at temperatures below the T_c^{on} of the superconductor, which is optimally doped by oxygen. The technology of nonuniform oxygen concentration profiles in the YBCO superconducting film and the origin of the stepped-like *I-V* characteristic of the YBCO devices biased with supercritical current at temperatures below T_c^{on} are presented and discussed. Our results can be applied for developing advanced superconducting electronic and optoelectronic devices with superconducting properties of the device driven by precisely controlled internal (*i.e.*, self-produced by the current) and / or external magnetic fields.

* Corresponding author. Tel.: +370 5 251 2462.
E-mail address: arturas.jukna@vilniustech.lt

© 2022 Arturas Jukna.
F916G0003

Peer-review under responsibility of the Kaunas University of Technology, Panevėžys Faculty of Technologies and Business.

© 2022 Artūras Jukna.
Peer-review under responsibility of the Kaunas University of Technology, Panevėžys Faculty of Technologies and Business.

Keywords: Type II superconductor; Abrikosov vortex; Mixed state; Current-voltage characteristic; Energy dissipation; Joules heat.

1. Introduction

The high critical current density [1] (*i.e.*, the maximal density of current that can flow lossless through the superconducting material), a specific dependence of the critical current density versus temperature, and the absolute diamagnetism [2] (*i.e.*, exclusion of magnetic field from the material interior) are the most important and preferable characteristics of superconductors for their applications in low- and high-power (*i.e.*, electromagnets, motors, current limiters, high-power optically triggered ultrafast switches [3], etc.) superconducting electronic and optoelectronic devices. When biased with a supercritical current, the magnetic field produced by the current (internal) can penetrate the bulk of the superconductor, creating a mixed state in it [4]. (Here, the mixed state is the state in which the superconducting phase and normal (*i.e.*, nonsuperconducting) phase of the material can coexist together). The same mixed state can be created by exposing the superconducting film to an external magnetic field, with a field amplitude greater than H_{c1}. When interacting with the type II superconductor, the internal (or external) magnetic field penetrates the bulk of material in a form of Abrikosov magnetic vortices and antivortices (see Fig. 1). The vortex (or antivortex) is the circular current flowing around the core of normal phase material that passes through the magnetic flux quantum $\Phi_0 = hc/2e = 2.07 \times 10^{-15}$ Wb and the strength of the current surrounding that core generates a magnetic flux $\Phi = \Phi_0$, but opposite in direction. Here, h is the Planck constant, c is the speed of light, and e is the elementary charge. The size of the vortex / antivortex is defined by the superconducting coherence length ξ [5] and magnetic field penetration in to the superconductor $\lambda \sim \Phi_0 / \pi H_{c1}$) [6] (see Fig. 1).

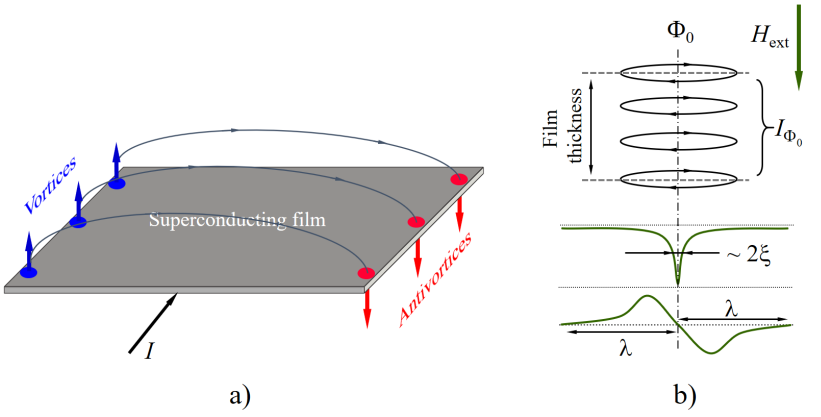


Fig. 1. (a) Scheme of the penetration of the magnetic field in a type II superconducting thin film in the form of magnetic vortices / antivortices if the film is biased with current I which creates the current density $J \sim J_c$; (b) Schematics of Abrikosov magnetic vortex with normal core limited by the coherence length ξ and magnetic field penetration length into the superconductor λ

When the superconducting device is biased with the supercritical current density, the current self-produced electric and magnetic fields create a Lorentz force (F_L), which forces Abrikosov magnetic vortices to nucleate at film edges and move toward the film center and annihilate meeting there the antivortex arriving from opposite edge of the film (see Fig. 1). Vortices / antivortices moving perpendicularly to the direction of a bias current experience a viscous drag, originating from energy dissipation in the vortex cores (the cylindrical core composed of dismantled Cooper pairs or quasiparticles) [7] that can pin to pinning centers (*i.e.*, crystal defects [8], impurities, etc.). If the pinning force F_p produced by the pinning centers is equal to the Lorentz force F_L, the motion of vortices / antivortices stops, the mixed-state resistivity originated from the motion of magnetic vortices disappears, and the superconducting current density in the material recovers.

Energy dissipation in the mixed state superconductor biased with supercritical current expresses itself during the experiment as mixed state resistance, which depends on the strength of the internal (created by the current) or external magnetic fields, temperature, and biasing conditions [9]. While traveling in the superconductor, the vortices / antivortices retain their cylindrical core and leave tailgating of quasiparticles (*i.e.*, form a region of suppressed superconductivity), creating favourable conditions for a subsequent vortex to follow the previous. This forces current-driven vortices and antivortices in thin films to wander between pinning centers along spontaneously created vortex channels maintained by the heat of the vortex motion [10]. When an external magnetic field exceeds H_{c1}, the vortices interact through a vortex current mediating repulsive forces and appear to be squeezed into a vortex channel by a magnetic pressure originating from the Meissner effect in a surrounding superconducting environment. The motion of vortices in $YBa_2Cu_3O_{7-\delta}$ (YBCO) type-II superconducting films could be controlled by temperature, magnetic field, and non-uniform doping by oxygen; however, these factors also affect variation in J_c, T_c^{on}, ξ, and λ of the superconductor therefore their effect is not unambiguous [11–12].

With increasing bias current, the number of Abrikosov magnetic vortices increases, and the vortices arrange themselves into arrays of vortices with the areal density n_a set by magnetic induction $n_a = B/\Phi_0$. Because of the strong interaction between magnetic vortices, the arrays of vortices increase or decrease depending on the strength of the vortex-vortex interaction, thermal fluctuations, and vortex interaction with various defects, which work as pining centers for vortices in the material. All the factors mentioned above modify the shape of the current density-voltage (*J-V*) dependence of superconducting devices and result in the appearance of different regimes of vortex motion depending on the ratio between F_p and F_L. At $J > J_c$, the energy dissipation due to the motion of vortices is observable up in the *J-V* dependence via vortex-matter different regimes, which can be split into three stages (see Fig. 2). The first stage that takes place at $J \geq J_c$ is the regime of the thermally activated flux flow (*i.e.*, random pinning / nucleation of single vortices at the film edges and pinning centers). At this stage, $F_p > F_L$, therefore, only thermally activated single vortices can be released from the weak pinning centers and again get pinned on the stronger pinning centers. With an increase in current density (internal magnetic field), vortices remain pinned only at the strongest pinning centers where still $F_p \sim F_L$. It affects a sudden increase in the mixed-state material resistance caused by the motion of unpinned vortices rearranged into vortex arrays. This is the so-called flux creep phase of vortex matter [13]. When $F_p < F_L$, the vortex arrays can nucleate at the edge of the film, move toward the center of the film, and annihilate there with antivortices arriving from an opposite edge of the film. This regime is called flux flow [9]. This regime can be recognized from the linear dependence of the mixed state resistance versus the bias current density seen in Figure 2.

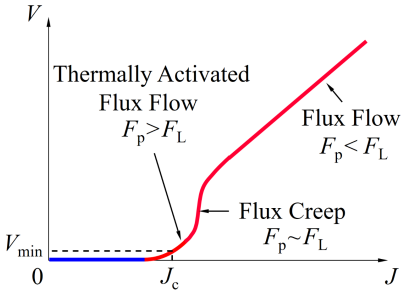


Fig. 2. A nonlinear direct current density-voltage (*J-V*) characteristic with four distinguishable regions in the type II superconductor film. At $J < J_c$ the material is in the superconducting state (the first region). At $J > J_c$, the remaining three regions are caused by a motion of Abrikosov magnetic vortices: a thermally activated flux flow at $F_p > F_L$, the flux creep at $F_p \sim F_L$, and the flux flow at $F_p < F_L$

This work reports on the results of the investigation of the vortex motion regimes in an YBCO superconducting thin-film device containing a channel for a motion of Abrikosov magnetic vortices. We manufactured the channel by utilizing a focused beam from a continuous-wave laser and a computer-controlled two-coordinate translational stage with our YBCO device fixed on it. Light absorption in the YBCO material initiated an increase in temperature and partial depletion by oxygen ($\delta \sim 0.2$) in its illuminated area. At temperatures $T < T_c^{on}$, the first magnetic field of current penetrates the channel in a form of magnetic flux, which under Lorentz force F_L can open the channel when $F_p > F_L$ or close it when $F_p \sim F_L$, however, due to heat generated by moving vortices, most of vortices are pinned to the pining

centers. We conclude that the onset of different regimes of vortex motion in YBCO devices with channel depends on the ratio between F_L and F_p, which in its way depends on the bias conditions, the temperature, and the oxygen profile in the channel area.

2. Technology of the tested sample

Epitaxial 0.3-μm-thick YBCO film with a crystalline *c*-axis oriented perpendicularly to the crystalline substrate of $LaAlO_3$ (100) was grown using the MOCVD technique [14]. The critical temperature in the superconducting film $T_c^{on} \sim 91.4$ K, with the width of the superconducting transition $\Delta T_c \sim 0.4$ K was estimated from resistivity versus temperature dependences measured using a direct current technique, and the critical current density $J_c \sim 1.5$ MA/cm^2 at temperature $T = 78$ K, estimated using $V_{min} \sim 10$ μV voltage criterion, from the current-voltage characteristic (*I-V*) measured with pulsed current technique [15]. The vortex channels in the film were implemented by continuous-wave Ar-ion laser light focused down to a Gaussian spot size diameter of ~5 μm (laser fluence on the surface of the YBCO film in a range of ~20 mW/μm^2) and scanned at a speed of 50 μm/s utilizing a computer-controlled two coordinate translation stage. Due to the conversion of optical energy to Joules heat, the temperature in the illuminated area increased to ~500 °C initiating the oxygen diffusion process there. Since in the *c*-axis direction the oxygen diffusion is on the order of magnitude higher than along the *a-b* basal planes in the YBCO superconductor [16], the highest level of oxygen depletion was expected to occur on the film surface but with a higher concentration in the vicinity of the YBCO/$LaAlO_3$ interface. Subsequently, using increased laser fluence (~130 mW/μm^2), we completed the patterning of six identical 50 × 100 μm^2 (width × length) microbridges each containing large contact pads and Cr/Ag contacts for electrical measurements (see Fig. 3). Now, the four microbridges had a 5-μm-wide vortex channel and the two rest were without the vortex channel. The latter were used for reference purposes.

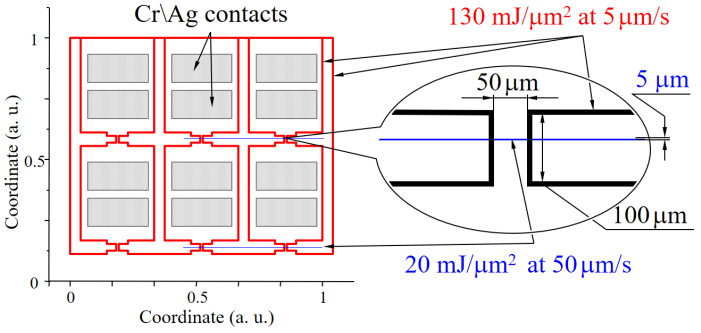


Fig. 3. Schematics of six 50 × 100 μm^2 dimensions YBCO/$LaAlO_3$ samples patterned by laser fluence 130 mW/μm^2. Each sample contains large contact pads with Cr/Ag contacts for measurements of electric properties. Four samples are supplied with the vortex channel using 20 mW/μm^2 laser fluence and 5 μm/s beam translational velocity and two devices that were left blank (without the channel) for reference purposes

The residual oxygen content in the vortex channel was investigated at room temperature using a scanning electron microscope and an *X*-ray energy dispersive system to measure the chemical composition. The electric transport properties we measured using a 4-probe technique at temperatures ranging between 78 and 300 K when the YBCO sample was held in a low vacuum in a cryostat cooled by liquid nitrogen.

3. Results and discussion

Our results of oxygen concentration measurements in a vortex channel let us predict that the Gaussian shape of the laser beam at laser fluence 20 mW/μm^2 at 50 μm/s scanning speed can noticeably change in oxygen concentration at the level of local deoxygenation $\delta \sim 0.2$. As we showed earlier [17], due to the uneven distribution of optical power in the Gaussian shape optical spot, the laser beam interacting with a YBCO thin film creates a channel with comparatively large slopes characterized by relatively higher oxygen concentration compared to the oxygen concentration in the center of the channel (see Fig. 4). Moreover, depending on laser fluence distribution in the spot, the width of the vortex

channel at the top of the film can be as much as twice that at the bottom. The optically initiated temperature gradient in the oxygen YBCO film can affect diffusion from illuminated areas mainly through the surface of the *c*-axis textured film [16]. At the same time, the YBCO/$LaAlO_3$ interface at the bottom of the channel blocks the oxygen diffusion process and helps to appear excess oxygen on the channel slopes.

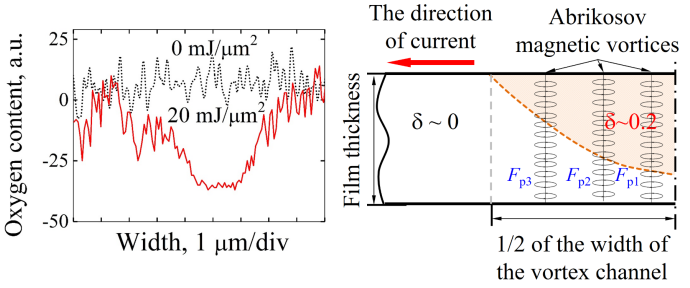


Fig. 4. (*On the left*) A dependence of relative oxygen content in the channel area versus its width measured on the surface of the YBCO device. (*On the right*) Schematic of one-half of the width of 5 μm wide vortex channel, which manufactured utilizing a laser beam of fluence of 20 mJ/μm^2 focused into a 5-μm diameter spot of Gaussian shape. The direction of a current and that of the Lorentz force acting on the vortices are pointed parallel and perpendicular to the plane of the figure, respectively. Three pinned magnetic vortices experience different pinning forces $F_{p1} < F_{p2} < F_{p3}$

Since the critical superconducting temperature [18], the critical magnetic field, and the critical current decrease with decreasing oxygen concentration in the YBCO superconductor [19], the first magnetic field of the current penetrates in a form of Abrikosov magnetic vortices the places of weakest superconductivity which are characterized by the lowest concentration of oxygen (*i.e.*, the channel area). Therefore, firstly, Abrikosov magnetic vortices will occupy the central part of the vortex channel, and with increasing the amplitude of bias current (*i.e.*, increasing current produced magnetic field), they will appear on the channel slopes. Since magnetic vortices repel each other, they arrange themselves in a triangle magnetic lattice [20] with lattice constant $a = \xi^{-1}\ (2\Phi_0/B\sqrt{3})^{1/2}$. Here $\Phi_0 = 2.07 \times 10^{-15}$ Wb is the magnetic flux quantum and B is the magnetic field induction induced by current in the channel area. With increasing B, the channel slopes will also be penetrated by Abrikosov magnetic vortices; however, due to the uneven distribution of the F_p force for vortices in the central part of the channel and on the slopes of the channel (see Fig. 4) the Lorentz force initiates the motion of the vortices only in the central part of the channel that is characterized by the lowest F_p [21]. Therefore, the vortices on the slopes of the channel remain pinned until F_L, in turn, exceeds the pining force for vortices No. 1, No. 2, and finally for vortices No. 3 (see Fig. 4).

A typical stepped-like *I-V* characteristic (see Fig. 5) of a YBCO device with a vortex channel confirms the presence of the oxygen profile in the vortex channel manufactured using an optical spot of Gaussian shape from the laser. Similar voltage steps in the *I-V* characteristic of YBCO devices were observed in a narrow temperature interval ranging between 84.75 K ($0.927 \cdot T_c^{on}$) > T > 87.43 K ($0.956 \cdot T_c^{on}$).

The onset of the vortex motion in the YBCO device micro bridge causes energy dissipation and nonlinear behaviour of the *I-V* characteristic. A nonlinear character of the *I-V* characteristic is determined by the ΔV_1 and ΔI_1 (*i.e.*, potentially it is the flux flow regime in the vortex channel at $F_p \sim F_L$) and by the ΔV_2 and ΔI_2 (potentially is the thermally activated flux flow regime in the vortex channel at $F_p \geq F_L$) is seen at temperature T = 87.10 K = $0.953 \cdot T_c$. Starting with the first voltage step in the *I-V* characteristic when for the first time the mode of the thermally activated flux flow is replaced by the flux-creep regime, it continues up to step number above one hundred (a detection limit of our measurement setup). The shape of each step in the *I-V* characteristic slightly varies with the biasing conditions (see Figs. 5b – 5e).

Starting with the first step in the *I-V* characteristic, a dynamic resistance calculated from the *I-V* characteristic (see Fig. 5a) varies in range from 3.27 Ω, measured while the dissipation is characterized by ΔV_1 and ΔI_1 till 0.05–0.5 Ω, which is measured when the vortex matter creates a dissipation characterized by the ΔV_2 and ΔI_2. This large variation in the dynamic resistance of the YBCO device with the channel [22] may be due to the flux-creep regime (*i.e.*, a large part of the vortices move (high level of energy dissipation) and suddenly stop (low level of dissipation) in the channel

due to heat released by the moving bundles of vortices [10]. An increase in the local temperature causes an increase in the overall F_p of the moving vortices and changes the relationship between F_p and F_L, which stops the vortex movement in the channel (the channel closes). When the vortices stop, the heat from the channel is extracted by the sample cooler, and the F_p in the channel gradually decreases, again making favourable conditions for the reopening of the vortex channel.

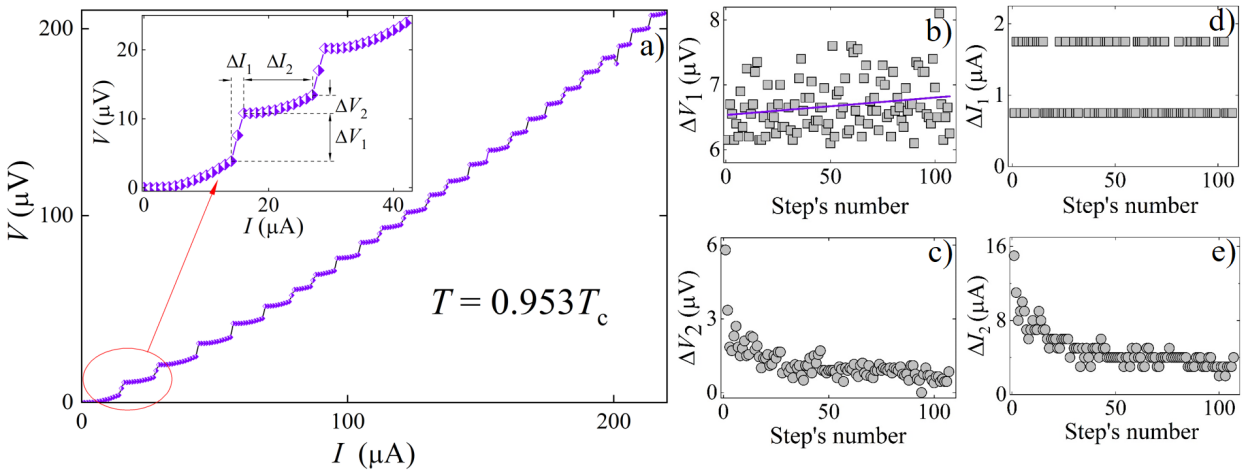


Fig. 5. (a) An example of the current-voltage characteristic of the 50 × 100 μm^2 YBCO device with vortex channel at temperatures $T = 0.953 \cdot T_c$. The inset represents the same dependence on an expanded scale, showing the interval voltages ΔV_1 and ΔV_2 and interval of currents ΔI_1 and ΔI_2 related to the different regimes of the vortex flow in the sample, respectively. (b) and (c) represents the voltages intervals ΔV_1 and ΔV_2, and (d) and (e) represent the interval of currents ΔI_1 and ΔI_2 variation with the step's number in the current-voltage characteristic at temperature $T = 0.953\ T_c$. The straight line in (b) demonstrates the linear fit of the experimental data

Figures 5b – 5d demonstrate the dynamics of the shape of the step with increasing bias current, *i.e.*, with increasing step number. Here, ΔV_1, ΔI_1 and ΔV_2, ΔI_2 are voltage and current intervals of a step when the vortex matter creates high-level dissipation and low-level dissipation in the channel, respectively. Although the ΔV_1 and ΔI_1 intervals remain almost constant with increasing current up to the 110th step in the *I-V* characteristic, the ΔV_2 and ΔI_2 intervals decease by the rate of the $\Delta V_2^{1st\ step}/\Delta V_2^{110th\ step} \sim 7$ times (see Fig. 5c) and $\Delta I_2^{1st\ step}/\Delta I_2^{110th\ step} \sim 8$ times (see Fig. 5e). This means that the amount of energy dissipated as a result of the motion of the vortex bundles in the channel does not change with increasing current. This means that the size of the moving / stopping bundles of vortices does not remarkably change with an increase in amplitude of the bias current self-produced magnetic field. Since the magnetic lattice constant a decreases with increasing magnetic induction induced by current [20] and F_L increases with increasing current, the balance between F_p and F_L can only be explained by the magnetic drag force for moving vortices produced by stationary vortices pinned on the slopes of the channel. When the current is increasing, a number of Abrikosov magnetic vortices in the channel constantly increase, and then stationary vortices No. 2 and No. 3 for which F_{p2}, $F_{p3} > F_L$ (see Fig. 4) act by a magnetic repulsion force (magnetic drag force F_{MD}) on vortices moving in the channel. When $F_p + F_{MD} > F_L$, the vortices stop moving, resulting in channel closure. With an increase in current, the F_L again exceeds the $F_p + F_{MD}$, and the vortices start to move. With an increasing number of Abrikosov magnetic vortices, they are forced to rearrange, getting penetrating also in the slopes of the channel, and in this way compressing the magnetic lattice and stopping the moving vortices in the channel. The increase in F_{MD} creates a new balance $F_p + F_{MD} > F_L$ and stops the vortex motion in the channel.

Current results let concluding that the height of the voltage individual step $\Delta V_1 + \Delta V_2$ in the *I-V* characteristic becomes almost current amplitude independent when step number is greater than No. 45. At this regime, the YBCO device with vortex channel can be used as analogue-to-digital converter (ADC) in the superconducting electronic circuit driven by motion of Abrikosov magnetic vortices in the vortex channel at temperatures below T_c. However, for the precise operation of such a superconducting device, the temperature stabilizer with a precision better than ±0.01 K has to be used together with an effective absorber of heat generated by the moving bundles of Abrikosov vortices in

the vortex channel. The latter can affect the voltage interval $\Delta V_1 + \Delta V_2$ and the current interval $\Delta I_1 + \Delta I_2$ of the steps in the *I-V* characteristic of the device and simultaneously the discretization level of the superconducting ADC device.

4. Conclusions

This work reports on a new concept of an electronic device based on the type II superconductor $YBa_2Cu_3O_{7-x}$ film with a channel for the motion of magnetic vortices. The device is based on $0.3 \times 50 \times 100\ \mu m^3$ (thickness × width × length) *c*-axis textured $YBa_2Cu_3O_{7-\delta}$ (YBCO) superconducting microbridge prepared on a crystalline $LaAlO_3$ substrate and provided with a 5-μm-wide and 50-μm-long channel of partially decomposed by oxygen ($\delta \sim 0.2$) YBCO material for motion of Abrikosov magnetic vortices. The uneven distribution of oxygen, which creates a focused laser beam in the channel area, results in the appearance of channel slopes, operating as centers of pinning that are comparatively stronger than the pinning in the channel center. The pinned vortices result in a magnetic drag force for moving vortices and are responsible for the appearance of the voltage steps in the current-voltage (*I-V*) characteristics of the YBCO devices with channel. Since the height of each individual step in the *I-V* characteristic is almost current-amplitude independent for the steps Nos. 45–110, the YBCO device with vortex channel shows potential to be used as an analog-to-digital converter (ADC) of electric current in superconducting electronic circuits driven by the motion of Abrikosov magnetic vortices in the vortex channel at temperatures below T_c. However, for the precise operation of such a superconducting device, the temperature stabilizer with a precision better than ±0.01 K has to be used together with an effective absorber of heat generated by the moving bundles of Abrikosov vortices in the vortex channel. The latter can affect the voltage interval and the current interval of the steps in the *I-V* characteristic of the device and simultaneously the level of current discretization by the superconducting ADC device.

References

[1] Bachtrögler, J., Hammer, C., Reuter, W. H., Schwendinger, F. Guide to the galaxy of EU regional funds recipients: evidence from new data. *Empirica*, 2019, 46, 103–150.

[2] Andersson, L. F., Danley, T., Eriksson, R., Henning, M. Workers' participation in regional economic change following establishment closure. *Small Business Economics*, 2018, 1–16.

[3] Balevičius, S., Balčiūnas, V., Deksnys, A., Jukna, A., Vengalis, B. Ultra-fast high-power protectors against EMP. *Proceedings of the 2nd Conference on the Electromagnetic Compatibility*, Firenze, Italy, Oct. 23–25, 1996, 10–13.

[4] Bednarz, M., Broekel, T. The relationship of policy induced R&D networks and inter-regional knowledge diffusion. *Journal of Evolutionary Economics*, 2019, 29, 1459–1481.

[5] Zalecki, R., Woch, W. M., Chrobak, M., Kołodziejczyk, A. Penetration depth of magnetic field into $YBa_2Cu_3O_x$ film on polycrystalline Ag substrate. *Acta Physica Polonica Series A*, 2015, 127, 272–274.

[6] Nguyen, P. P., Wang, Z. H., Rao, A. M., Dresselhaus, M. S., Moodera, J. S., Dresselhaus, G., Radousky, H. B., Glass, R. S., Liu, J. Z. Transport properties of $YBa_2Cu_3O_{7-\delta}Br_y$ single crystals. *Physical Review B*, 1993, 48, 1148–1155.

[7] Jacksony, D. J. C., Das, M. P. Melting of the flux line lattice. *Superconductor Science and Technology*, 1996, 9, 713–727.

[8] Vodolazov, D. Yu., Ilin, K., Merker, M., Siegel, M. Defect-controlled vortex generation in current-carrying narrow superconducting strips. *Superconductor Science and Technology*, 016, 29, 025002.

[9] Raissia, F., Hassani, F. Flux-flow behavior in high T_c superconductors. *Applied Physics Letters*, 2014, 104, 242602.

[10] Gross, R., Bosch, J., Wener, H. G., Fischer, J., Huebener, R. P. Temperature stabilized sample stage for the investigation of high *Tc* superconductors by scanning electron microscopy. *Cryogenics*, 1989, 29(7), 716–719.

[11] Brandt, E. H. The flux-line lattice in superconductors. *Reports on Progress in Physics*, 1995, 58, 1465–1594.

[12] Wai-Kwong Kwok, W-K., Welp, U., Glatz, A., Koshelev, A. E., Kihlstrom, K. J., Crabtree, G. W. Vortices in high-performance high-temperature superconductors. *Reports on Progress in Physics*, 2016, 79, 116501.

[13] Eley, S., Miura, M., Maiorov B., Civale, L. Universal lower limit on vortex creep in superconductors. *Nature Materials*, 2017, 16(4), 409–413.

[14] Abrutis, A, Sénateur, J. P., Weiss, F., Kubilius, V., Bigelytė, V., Šaltytė, Z., Vengalis, B., Jukna, A. Thin YBCO Films on $NdGaO_3$(001) substrates grown by injection MOCVD. *Superconductor Science and Technology*, 1997, 10(12), 959–965.

[15] Jukna, A., Yun, S.H., Balevicius, S., Karlsson, U. O. Electric properties of planar Ag/$HgBa_2CaCu_2O_{6+\delta}$ interface. *Physica C: Superconductivity*, 1999, 316(1–2), 83–88.

[16] Xie, X. M., Chen, T. G., Wu, Z. L. Oxygen diffusion in the superconducting oxide $YBa_2Cu_3O_{7-x}$. *Physical Review B*, 1989, 40, 4549–4556.

[17] Jukna, A., Steponaviciene, L., Maneikis, A., Abrutis, A., Lisauskas, V., Sliuziene, K., Sobolewski, R. Investigation of optically modified $YBa_2Cu_3O_{7-x}$ films by means of X-ray microanalysis technique. *Materials Science (Medžiagotyra)*, 2014, 20, 215–219.

[18] Benzia, P., Bottizzoa, E, Rizzia, N. Oxygen determination from cell dimensions in YBCO superconductors. *Journal of Crystal Growth*, 2004, 269, 625–629.

[19] Stangl, A., Palau, A., Deutscher, G., Obradors, X., Puig, T. Ultrahigh critical current densities of superconducting $YBa_2Cu_3O_{7-\delta}$ thin films in the overdoped state. *Scientific Reports*, 2021, 11, 8176.
[20] Rosenstein, B., Li, D. Ginzburg-Landau theory of type II superconductors in magnetic field. *Reviews of Modern Physics*, 2010, 82, 109–168.
[21] Sueyoshi, T. Modification of critical current density anisotropy in high-T_c superconductors by using heavy-ion irradiations. *Quantum Beam Science*, 2021, 5, 16.
[22] Steponaviciene, L., Sulcas, J., Jukna, A., Barboy, I., Jung, G., Abrutis, A., Sobolewski, R. Current-voltage dependences of $YBa_2Cu_3O_{7-\delta}$ superconducting thin films with laser written channel of easy vortex motion. *Materials Science (Medžiagotyra)*, 2009, 15(4), 291–295.

International Forum on Innovative Technologies and Management for Sustainability – ITMS'2022

International Scientific Conference Intelligent Technologies in Logistics and Mechatronics Systems – ITELMS'2022, 15th September, 2022, Panevėžys, Lithuania

Multi-Criteria Evaluation of the Girder Bridge Beams

Jovita Kaupienė[a,b], Aurimas Česnulevičius[a,b]*

[a]*Kaunas University of Technology, Panevėžys Faculty of Technologies and Business, 33 Nemuno St., Panevėžys LT-37164, Lithuania*
[b]*Panevėžys University of Applied Sciences, 23 Laisvės Sq., Panevėžys LT-35200, Lithuania*

Abstract

Multi-criteria evaluation methods can be applied to find the optimal solution. The Simple Additive Weighting (SAW) method is one of the many used multi-criteria evaluation methods. In this work, the SAW method is applied to search for the most optimal solution in the selection of beams for a girder bridge. Since the application of the SAW method is based on the opinion of experts, 15 experts were interviewed at the initial stage of the research in order to determine the significance of the evaluation criteria that were used for selection of optimal solution. Four possible beam designs were then selected and necessary engineering calculations were performed to select beam parameters. After selecting the characteristics of the considered beams, the SAW method was applied to find the most optimal solution.

© 2022 Jovita Kaupienė, Aurimas Česnulevičius.
Peer-review under responsibility of the Kaunas University of Technology, Panevėžys Faculty of Technologies and Business.

Keywords: Girder bridge; Multi-criteria evaluation; Simple Additive Weighting (SAW).

1. Introduction

Multi-criteria decision making methods are used to find the optimal solution. Multi-criteria evaluation methods usually provide a clear relative weighting system for different criteria. There are quite a number of multi-criteria evaluation methods and their number is constantly growing for several reasons [1, 2]: there are many different types of solutions that meet the wide range of multi-criteria evaluation circumstances; the time within which the analysis can be carried out may vary; the amount or nature of data available for analysis may vary; decision makers may have

* Corresponding author.
E-mail address: aurimas.cesnulevicius@ktu.lt

© 2022 Jovita Kaupienė, Aurimas Česnulevičius.
F916G0004
Peer-review under responsibility of the Kaunas University of Technology, Panevėžys Faculty of Technologies and Business.

different analytical skills. They are divided into two main groups: Multi Objective Decision Making and Multi Attribute Decision Making methods. The primary data of these methods are a vector of significance of indicators and a decision-making matrix consisting of the values of indicators.

The Simple Additive Weighting method (SAW) is one of the simplest and most widely used methods. The rules of the method were summarized by MacCrimmon [3]. Input data – decision matrix and significance values of indicators.

The main tasks of the method are to create a matrix of possible solutions, normalize the values of the members of this matrix and, after applying the significance of each indicator, calculate which alternative is the most effective. The most rational solution is considered to have the highest sum of normalized indicators multiplied by the significance of the corresponding indicators.

Evaluation indicators can be minimized (the choice with the lowest value is the best) or maximized (the choice with the highest value is the best). The minimized and maximized members of the matrix of possible solutions (evaluation indicators) must satisfy the condition:

$$\sum_{j=1}^{n} q_j = 1. \tag{1}$$

The maximized members of the possible decision matrix (evaluation indicators) are normalized accordingly:

$$\overline{x_{ij}} = \frac{x_{ij}}{x_j^{\max}}. \tag{2}$$

The minimization members (evaluation indicators) of the matrix of possible solutions are normalized accordingly:

$$\overline{x_{ij}} = \frac{x_j^{\min}}{x_{ij}}. \tag{3}$$

The corresponding members of the normalized matrix are multiplied by the significance values of the efficiency indicators and the resulting products are summed, when determining the rationality of the option. The sum of the products of the rational variant will be maximum.

$$A = \left\{ \frac{A_i}{\max_i \sum_{j=1}^{n} q_j \cdot \overline{x}_{ij} / \sum_{j=1}^{n} q_j} \right\}; \tag{4}$$

where A_i is a computational alternative; x_{ij} – members of the normalized matrix; q_j – integrated significance; j – indicator; n – number of indicators.

It was chosen to analyze the bridge girders in this study, since they are the main element that distributes the loads acting on the bridge.

2. Study of compatibility of experts' opinions

Since multi-criteria evaluation methods are based on experts' opinions, the initial stage of the research was to interview experts and systematize the results obtained during the interviews.

During the research, experts were given a questionnaire in which they had to answer general information about themselves. The experts were asked their age, which city they are from, their academic degree, field of construction, position held, years of work experience, number of qualification certificates and representative institution. The survey was sent to the employees of the road and bridge construction company AB "Panevėžio keliai". 15 experts participated

in the survey. After answering the general questions, the employees had to number the evaluation criteria from 1 to 6 according to significance.

The experts were presented with 6 beam evaluation criteria, namely: beam material cost, installation cost, structure weight, installation work time, beam bearing capacity and warranty period. The results of expert opinions obtained during the survey are shown in Table 1.

Table 1. Results of expert opinions

	Evaluation indicators					
	Beam material cost, q_1	**Installation cost, q_2**	**Structure weight, q_3**	**Installation work time, q_4**	**Beam bearing capacity, q_5**	**Warranty period, q_6**
Sum of ranks	58	68	22	64	50	53
Average rank	3.87	4.53	1.47	4.27	3.33	3.53
Priority	3	1	6	2	5	4
Subjective importance of the indicator (relative weight)	0.184	0.216	0.070	0.203	0.159	0.168

The average rank is determined by the formula:

$$\bar{t}_j = \left(\sum_{k=1}^{r} t_{jk} \right) \Big/ r; \tag{5}$$

where t_{jk} is the evaluation of the j^{th} indicator by k expert (from 1 to 6); r is the number of experts.

The reliability of experts is expressed by Kendall's concordance coefficient, which describes the degree of closeness of different opinions. When calculating this concordance coefficient, expert assessments are ranked. Determination of the total sum of squares of the unevenness of the individual efficiency indicator:

$$S = \sum_{j=1}^{n} \sum_{k=1}^{r} \left[t_{jk} - \frac{1}{n} \sum_{j=1}^{n} \sum_{k=1}^{r} t_{jk} \right]^2 = \left(58 - \frac{1}{6} \cdot 315 \right)^2 + \left(68 - \frac{1}{6} \cdot 315 \right)^2 + \left(22 - \frac{1}{6} \cdot 315 \right)^2 + \\ + \left(64 - \frac{1}{6} \cdot 315 \right)^2 + \left(50 - \frac{1}{6} \cdot 315 \right)^2 + \left(53 - \frac{1}{6} \cdot 315 \right)^2 = 1339.5 \tag{6}$$

where: n is the number of efficiency indicators.

Determination of concordance factor:

$$W = \frac{12 \cdot S}{r^2 \cdot \left(n^3 - n \right)} = \frac{12 \cdot 1339.5}{15^2 \cdot \left(6^2 - 6 \right)} = 0.3402 \cdot \tag{7}$$

The coefficient is a random variable. To determine Kendall's concordance coefficient, it is necessary to know the number of experts' r and the frequency of distribution of different values of n compared objects. Determination of Kendall's concordance coefficient value:

$$x^2 = \frac{12S}{r \cdot n \cdot \left(n+1 \right)} = \frac{12 \cdot 1339.5}{15 \cdot 6 \cdot \left(6+1 \right)} = 25.514 \cdot \tag{8}$$

Since the obtained value of the concordance coefficient is higher than the normative value (it is equal to 15.09), it is considered that the experts' opinions are harmonized.

3. Study of beam efficiency

After conducting a study on the compatibility of experts' opinions and moving to the calculation part, a calculation scheme should be created, according to which the loads to accept and which beam profiles to choose should be evaluated. In order to carry out the most accurate evaluation, the same conditions are created for all considered elements. The selected cross-section diagram of the bridge is shown in Figure 1.

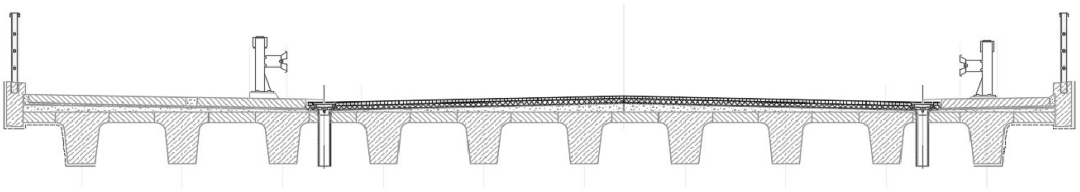


Fig. 1. Bridge calculation scheme

The calculations assume that:

- bridge is an edge path value;
- the length of the bridge beams is 15 meters;
- the width of one carriageway is 4 meters;
- 10 identical girders with a pitch of 1.345 m are used for the bridge deck;
- the structure is calculated as a two-support beam;
- the beam in the support "A" is anchored with bearings restraining in both horizontal and vertical directions, while in the support "B" the displacements are restrained only in the vertical direction; the beam calculation scheme is presented in Figure 2;
- the structure is exposed to atmospheric precipitation (rain);
- in the calculation scheme, the width of the truck is assumed to be 2.3 meters.

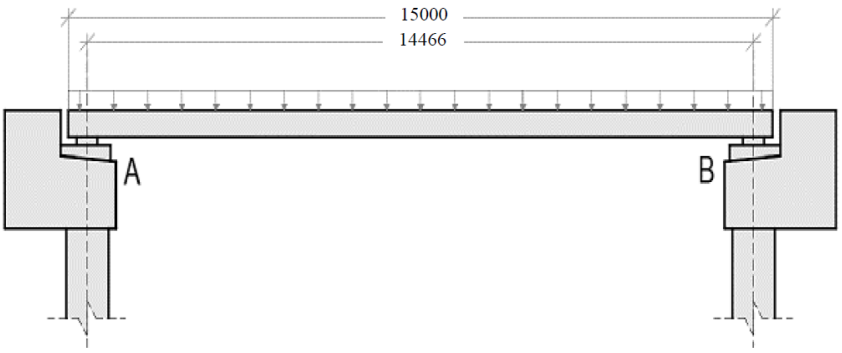


Fig. 2. The calculation scheme of the bridge beam

The slope of the road is estimated at 2.5 %, which distributes the total weight of the truck to its 2 sides, where the side of the slope will be more loaded than the opposite side as shown in Figure 3.

Based on the situation shown in Figure 3, we create a statics problem (diagram shown in Figure 4) and calculate which beams the truck loads the most.

Since the highest calculated load falls on the first beam, it means that the calculations will be performed on it. The maximum load will be on the beam when the entire truck has driven onto the bridge deck as shown in Figure 5.

Based on the truck force distribution scheme (see Fig. 5), we create a calculation scheme for the static problem using *Robot Structural Analysis Professional* 2019 software. The computational scheme is shown in Figure 6.

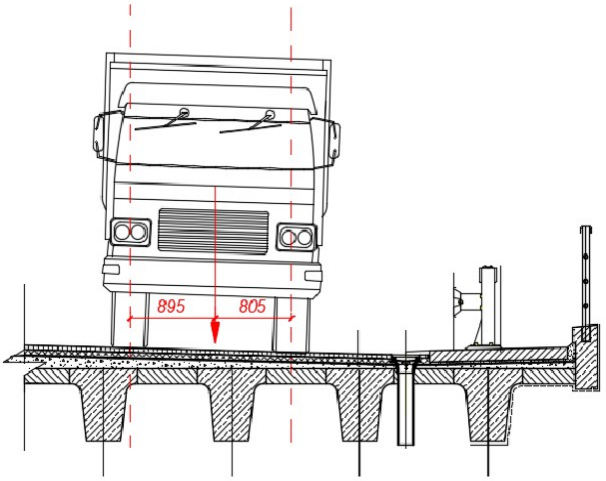


Fig. 3. The weight distribution of the truck when driving on the bridge

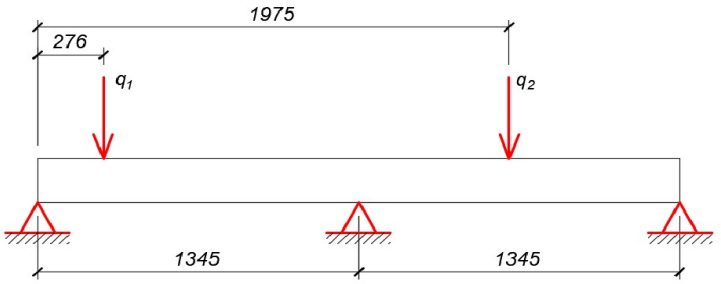


Fig. 4. Diagram of the static problem

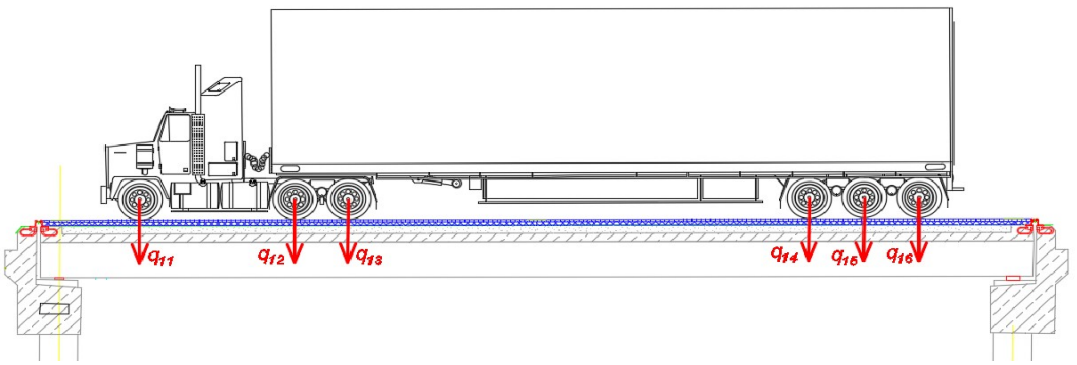


Fig. 5. Distribution of truck forces along the beam

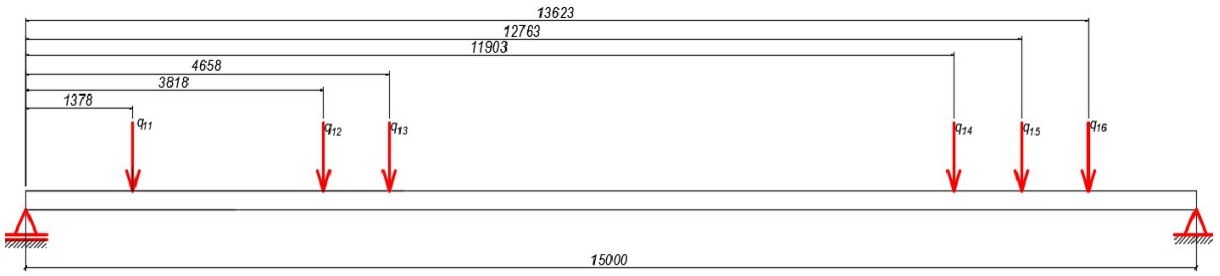


Fig. 6. Calculation diagram of the longitudinal cross-section

After performing the calculations with the given loads, we got that the beam must hold a load of 497.69 kNm to withstand the loads, so we choose rational profiles that would have a storage reserve of more than 20 %.

During the multi-criteria evaluation, we will evaluate 4 beam profiles (HEA700; HEB500; reinforced concrete *T*-shaped beam, the yield zone of which is reinforced with 14 pieces of ø16 steel B400a reinforcement and glass-basalt fiber). The characteristics of the considered beams are presented in Tables 2 and 3.

Table 2. Characteristics of HEA700 and HEB500

Profile	**HEA700**	**HEB500**
Steel	S355	S355
Section height, mm	690	500
Section width, mm	300	300
The cross-sectional thickness of the bearing flanges, mm	27	28
Mass, kg/m	204	187
Cost, €/m	320.3	267.4

Table 3. Characteristics of *T*-beams

Profile	T_{steel}	T_{FRP}
Steel	Steel B400a	Glass-basalt fiber
Section height, mm	750	750
Section width, mm	360	360
The thickness of the cross-section of the supporting reinforcements, mm	16	16
Mass, kg/m	825.6	787.32
Cost, €/m	110.75	97.17

We create the initial decision-making matrix and set the maximization and minimization indicators (see Table 4). The maximized and minimized members of the possible solution matrix are normalized using formulas (2) and (3). Using the formula (4) and the data of the normalized matrix, we create the final matrix of values, which is shown in Table 5.

Table 4. Results of expert opinions

Types of beams	Evaluation indicators					
	Beam material cost, q_1	Installation cost, q_2	Structure weight, q_3	Installation work time, q_4	Beam bearing capacity, q_5	Warranty period, q_6
HEA700	291.7	280	204	6.4	0.800	5
HEB500	267.4	280	187	6.4	0.730	5
The *T*-beam is reinforced with steel	110.75	470	825.6	20	0.790	10
The *T*-beam is reinforced with FRP	97.17	470	787.32	20	0.395	10
Min. or Max. indicator	Min.	Min.	Min.	Min.	Min.	Max.
The best value of the indicator	97.17	280	187	6.4	0.395	10

Table 5. The final matrix of values and priorities

Types of beams	Evaluation indicators						Sum of indicator values	Priority line
	Beam material cost, q_1	Installation cost, q_2	Structure weight, q_3	Installation work time, q_4	Beam bearing capacity, q_5	Warranty period, q_6		
HEA700	0.333	1.000	0.917	1.000	0.494	0.500	0.707	3
HEB500	0.363	1.000	1.000	1.000	0.541	0.500	0.726	1
The *T*-beam is reinforced with steel	0.877	0.596	0.227	0.320	0.500	1.000	0.618	4
The *T*-beam is reinforced with FRP	1.000	0.596	0.238	0.320	1.000	1.000	0.721	2
Min. or Max. indicator	Min.	Min.	Min.	Min.	Min.	Max.		
The best value of the indicator	0.184	0.216	0.070	0.203	0.159	0.168		

4. Conclusions

After carrying out a multi-criteria evaluation using the SAW method, it was found that the most rational solution for choosing a beam is the steel profile HEB500, which has an index of 0.726 (see Table 5). The greatest influence on the choice of the steel profile HEB500 was made by the price of the beam materials, the cost of installation and the time of the installation work, which had the highest significance of the indicators. The second most rational choice is a *T*-beam reinforced with FRP, which has an index of 0.721.

The biggest weight for this beam was the low utilization of its bearing capacity and twice the warranty period compared to steel profiles. The third is the steel profile HEA700, which has the third highest evaluation index of 0.707. The advantages of the beam are the same as those of the HEB500 profile, but the result of the lower values was the higher cost of materials, mass and load-bearing capacity utilization. The fourth most efficient option is the *T*-beam reinforced with steel, which scored a sum of values of 0.618. The beam's indicators did not have significant exceptions, so the evaluation result was average – 4th place.

References

[1] Dodgson, S., Pearman, A., Spackman, M., Phillips, L. *Multi-Criteria Analysis: A Manual*. London, 2009.

[2] Podvezko, V. The comparative analysis of MCDA methods SAW and COPRAS. *Inžinerinė Ekonomika – Engineering Economics*, 2011, 22(2), 134–146. ISSN 2029–5839.

[3] Maccrimmon, K. R. *Decision Making Among Multiple – Attribute Alternatives: A Survey and Consolidated Approach*. RAND Memorandum, RM-4823-ARPA, 1968.

International Forum on Innovative Technologies and Management for Sustainability – ITMS'2022

ktu 1922 panevėžys faculty of technologies and business

International Scientific Conference Intelligent Technologies in Logistics and Mechatronics Systems – ITELMS'2022, 15th September, 2022, Panevėžys, Lithuania

Additive Manufacturing in Hydraulic Systems – The Review

Agnieszka Klimek[a]*, Adam Bartnicki[a]

[a]*Institute of Robots & Machine Design, Faculty of Mechanical Engineering, Military University of Technology, 2 Gen. S. Kaliskiego St., Warsaw 00-908, Poland*

Abstract

Additive Manufacturing is going to become more and more common way of manufacturing. The numerous benefits like saving material and energy, lower cost of prototyping and optimization, opportunity of consolidate an assembly into a single part make Additive Manufacturing an area of interests to hydraulic manufacturers and researchers. This article presents typical usage of Additive Manufacturing in hydraulic systems, like manifolds, hydraulic components parts and actuators.

© 2022 Agnieszka Klimek, Adam Bartnicki.
Peer-review under responsibility of the Kaunas University of Technology, Panevėžys Faculty of Technologies and Business.

Keywords: Additive Manufacturing; Hydraulic systems, Hydraulic components.

1. Introduction

Additive Manufacturing (AM) is "*a process of joining materials to make objects from 3D model data, usually layer upon layer, as opposed to subtractive manufacturing methodologies*" [1]. Importance of AM to commercial manufacturing has enormously grown in the last decades. Nowadays, AM technologies confirm its participation in different industries [2–5], but still the areas of researchers' main interest are technological and process issues [6–14]. AM is a group of different technologies according to different materials and processes. The main features of most common AM technologies are presented in Table 1.

One of the most common and widely used technologies is Material Extrusion (ME) represented by Fused Deposition Modelling (FDM), also named Fused Filament Fabrication (FFF). The principle of this technology is direct usage of 3D CAD files without any 2D drawings for the process preparation. During the process, the plastic wire, also called

* Corresponding author.
E-mail address: agnieszka.klimek@wat.edu.pl

© 2022 Agnieszka Klimek, Adam Bartnicki.
Peer-review under responsibility of the Kaunas University of Technology, Panevėžys Faculty of Technologies and Business.

the filament, is plasticized in the heated nozzle. After the extrusion from the nozzle, plasticized material goes to the building platform where there is the final shape constructed. After the final creation of each layer of material, the building platform is lowered in order to create another layer. The process is repeated to reach the final shape of the element.

Table 1. AM technologies

Technology name	Description according to ISO 17296-1	Material
Binder jetting	Liquid bonding agent is selectively deposited to join powder materials.	Various powders including plasters, sands, and composite materials.
Direct energy deposition	Focused thermal energy is used to fuse materials by melting as they are being deposited.	Various metal powders including titanium, nickel, tool steels, stainless steel, cobalt, aluminium, copper, and various composites.
Material extrusion	Material is selectively dispensed through a nozzle or orifice.	Various thermoplastics including acrylonitrile butadiene styrene (ABS), acrylic-styrene-acrylonitrile (ASA), polyamide, polycarbonate, polypropylene.
Material jetting	Droplets of build material are selectively deposited.	Ceramics, liquid photopolymers, melted waxes.
Powder bed fusion	Thermal energy selectively fuses regions of a powder bed.	Polyamide, polyaryletherketone, polystyrene, and various composites, various alloys including cobalt chrome, titanium, steel.
Sheet lamination	Sheets of material are bonded to form an object.	Various composite thermoplastics.

The second popular technology is the Power Bed Fusion, represented by Selective Laser Melting (SLM). The process starts by loading prepared CAD model into machine software. Next, the process parameters are set. During the process the special recouter applies a layer of material. The distributed layer is melted by laser in places where the section of manufactured element is placed. Then the platform is lowered by the thickness of the layer and the next powder layer is put.

This paper is focused on applying Additive Manufacturing in the hydraulic industry. The article shortly presents the advantages of components manufactured by AM and highlights the main fields for AM in hydraulic systems.

2. Additive Manufacturing in hydraulic systems

2.1. *Hydraulic manifolds*

One of the most popular way to involve Additive Manufacturing in hydraulic system is to design the manifolds (see Fig. 1). Traditional way of manifold manufacturing starts by preparing metal block. After that the channels are drilled, which results in angled junctions and affect energy loses. Usage of AM ensures first of all improving mass of manifold, which is the heaviest part of hydraulic valve. The second benefit is a potential to improve the component characteristics. One of numerous studies in this area is [15]. In their paper Authors presented a holistic development methodology for fluid components with a specific focus on hydraulic manifolds. The stages of development are as follows: creation of the list of requirements, arrangement of part functional structure, conceptual solution, assessment, design and manufacture. Authors implemented their methodology to rail vehicle braking systems. Carried tests show that the weight of the manifold is reduced by 76 % and its width by 18 %.

The other example of manufacturing manifolds with AM is presented in [16]. In their work Alshare et. Al studied a manifold designed with SLM technique. Firstly, they carried out a computational fluid dynamics (CFD) analysis,

which allows them to optimize the structure of manifolds. The optimization managed to achieve an 84 % mass reduction with increased performance in terms of pressure drop. When compared to the base model, the new one has smoother fluid dynamics and is more efficient in terms of load distribution.

Different approach to manifold manufacturing is presented in [17]. In their study the authors are focused on developing "design for Additive Manufacturing" (DfAM). This method mainstage is changing model parameters in order to obtain different flow channel models. Then the flow field and structure strength are calculated. Chosen model is improved by a gradient-based optimization algorithm. The proposed approach was tested on a simplified hydraulic manifold with one flow channel. The further step will be to develop hydraulic manifolds with multi-channels to verify its applicability in practical scenarios.

Another important issue studied in hydraulic systems is pressure. In [18] Authors compared losses in traditional systems and one manufactured with AM technology. To reduce the pressure drop they reduced traditional rectangle and sharp crossings. The tests' results have proved the potential to reduce pressure losses and energy consumption using AM technology. The pressure reduction can reach up to 50 % using a passage with an arch, while pressure drop of the passage with comers can reach up to 20 %.

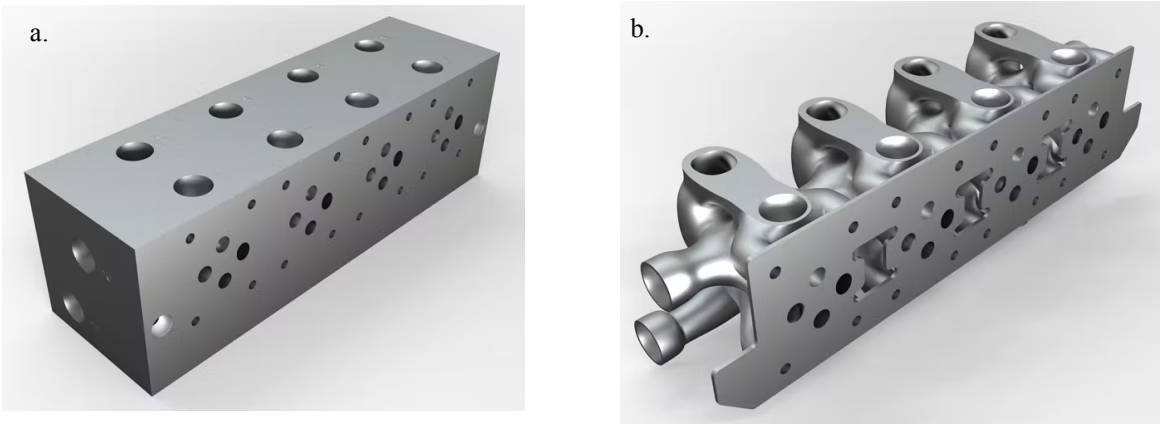


Fig. 1. (a) traditional manifold; (b) AM manufacturing manifold [19]

The specific kind of the manifold is the digital displacement valve manifold. To make digital valve systems competitive with traditional systems it is required to reduce their size and weight. Research in the miniaturization topic has been conducted for years. One of the most interesting proposals is one presented by Chekurov and Lantela [20]. In their work Authors studied a digital valve with 32 pilot operated miniature valves. The prototype was made using SLM technology. Choosing that technology enables creation of the flow channels with a diameter of slightly over 1 mm. The digital valve system was made from "EOS MaragingSteel" MS1 in order to provide operating pressure exceeding 25 MPa. What is more, it is proved that the design with SLM technology makes it possible to optimize the shape of channels, which results in reducing the pressure loss.

2.2. *Parts of hydraulic components*

The main disadvantage of hydraulic equipment is weight. This is why, one of the ends of modern constructors is to make hydraulic components lighter. An interesting solution seems to be replacing some parts of the device with light ones, made from plastic. In their research [21] Krawczyk and Stryczek proposed gears made from POM (Polyoxymethylene) and PPS (Polyphenylene sulfide). Research program included verification of design factors (axial and radial clearance), operational factors (impact of speed, pressure and temperature on the pump characteristics) and definition of durability characteristics. Results of research proves that the pump with gears made of plastics can operate at high speeds (up to 4000 rpm), at temperature of the working fluid in the range 25–50 °C, with the working pressure at the outlet of the pump 4 MPa. Presented results of long-term tests, shows that the pump with gears made of plastics

worked for 40 hours maintaining a constant level of efficiency $Q = 12.5$ dm^3, which represents 80 % of the theoretical volumetric efficiency.

An interesting idea was presented in [22]. Author presents a concept of replacing traditional gear pumps with a new one, made from carbon steel. The main goal of the Author was to improve the pump performance by replacing spur gears by helical ones. The helical gears manufacturing in the traditional way is demanding, and this is why Additive Manufacturing is useful. The new pump was modelled in *SolidWorks* (see Fig.2), and then simulation tests were carried. The carried CFD analysis confirmed the better flow rate (about 17 %), when compared with spur gears. What is more improvement in areas as noise, vibration and fracture were observed.

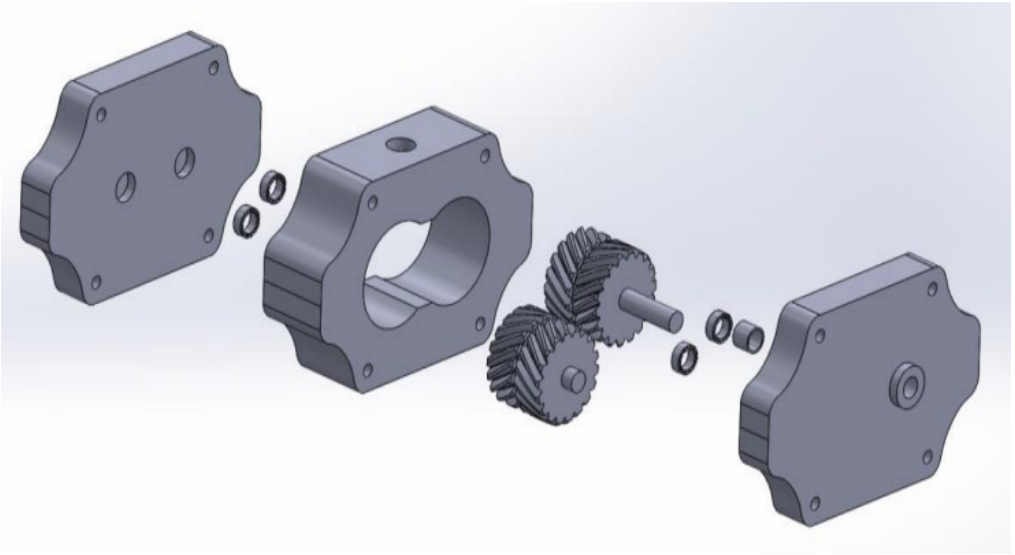


Fig. 2. Innovative hydraulic pump [22]

The innovative way of using Additive Manufacturing in hydraulic systems seems to be manufacturing directional valves spools (see Fig. 3). In traditional systems, spools are manufactured with CNC machines. A new one is printed, which allows to replace the drilled holes with oval ones. It results in significant reduction of pressure drop.

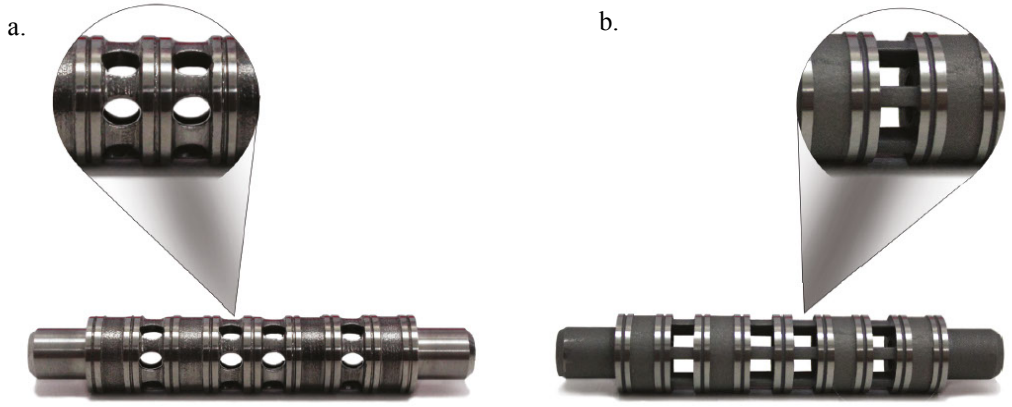


Fig. 3. (a) Traditional spool; (b) AM manufacturing spool [23]

A riveting application of AM in the hydraulic system was presented in [24]. Authors proposed a novel electro-hydraulic system with mini-actuator and low-cost 3D-printed valve (see Fig. 4). The two versions of valve were manufactured, one with steel slave and spool inserted into casing, and second made entirely from PETG. The steady state (neglecting acceleration, valve dynamic etc.) were carried. The result shows that there is little difference in performance between the machined steel spool and the 3D-printed valve. Although the large-quantity cost of a machined spool and sleeve is small, the 3D-printed valve has a very low cost, even in single quantities.

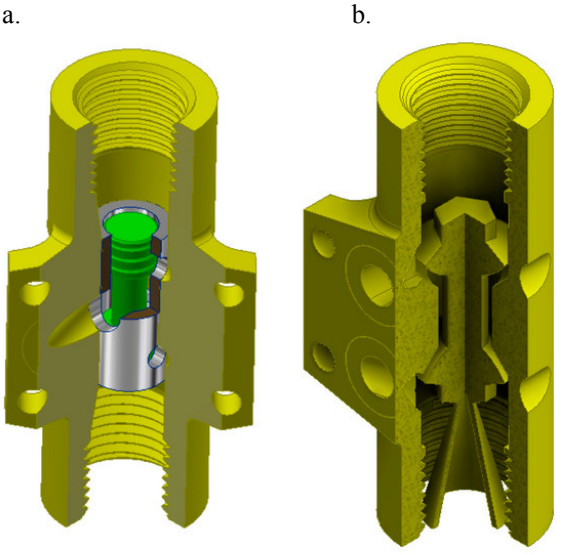


Fig. 4. (a) Valve model A, including 3D-printed PETG casing; (b) Valve model entirely 3D-printed PETG [24]

A visionary way to use Additive Manufacturing in hydraulic equipment was presented by researchers from Institute of Robots & Machine Design at Military University of Technology. In their article [25] they proposed to manufacture spare parts for hydraulic pumps. This topic is of major concern, as due to COVID-19 pandemic the logistic chains were broken. Authors choose a slipper-retainer (see Fig. 5) as a test part.

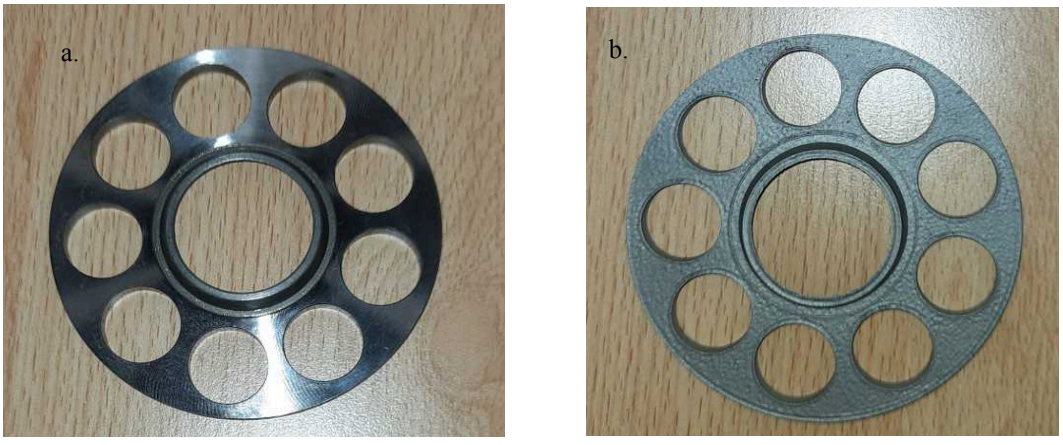


Fig. 5. (a) Original slipper-retainer; (b) AM slipper-retainer

The material of slipper-retainer was identified and replaced with AM powder with similar properties. Then the part was manufactured with SLM technology and tested. A test campaign includes 100 hours of work with different load pressures. The test campaign was divided into 9 stages, after each the wear analysis was carried. Research confirmed that Additive Manufactured spare parts allow the continuation of the exploitation of such devices as hydraulic pumps, until the arrival of a new pump delivery, but they are not recommended for fragile and precise systems.

Important part of researchers' studies is the environmental impact of industry. In their work [26] Tao Peng et. al investigated the sustainability of hydraulic parts manufactured by SLM technology, when compared with conventional manufacturing. The part was first re-designed to achieve a lightweight structure and optimized process parameters. Subsequently, an optimized and a non-optimized sample part were fabricated via SLM. The obtained results show that the environmental impact of SLM without optimization was 37.42 % lower than that of CM with respect to a hydraulic valve body, and the SLM-optimized design can lead to a 10–23 % reduction in environmental impacts.

2.3. *Hydraulic actuators*

An interesting example of usage of Additive Manufacturing in hydraulic systems are actuators, especially actuators for special use like actuators for medical robots. The great sample is an actuator presented in [27]. Authors discuss using polymer Multi-Material Additive Manufacturing (MMAM) to produce miniature hydraulic piston actuators combining rigid structures and flexible seals. This solution is interesting due to the opportunity to use it during special kinds of examinations like *X*-ray or magnetic resonance. The results of this study lead to the conclusion that PolyJet MMAM is a promising technology for the development of polymer hydraulic actuators for custom printed devices. During the test Authors analysed factors like water absorption, dimensions / print quality, leakage, friction and endurance. The experiments were only conducted using water, the results may, therefore, not be applicable for systems using other hydraulic fluids.

3. Conclusions

Additive Manufacturing technologies are an important part of producing hydraulic components. This technology might be useful with production of prototypes or redesigning and optimization of existing parts. The main features of components manufactures with Additive Manufacturing is:

- improving of part performance and flow rate, refer to optimization of internal flow-paths and reduction of stress-strain stage during the melting;
- reduction of the component mass by even 90 %;
- integrating of different components in one;
- much more precise customization of a component to an application (in terms of matching the dimensions to the system's size and capacity and characteristics that are important to dynamics and stability such as leakage, mass, damping).

References

[1] ASTM F2792-12a: *Standard Terminology for Additive Manufacturing Technologies*, 10.04.

[2] Günther, D., Heymel, B., Günther, J. F., Ederer, I. Continuous 3D-printing for Additive Manufacturing [Internet]. *Rapid Prototyping Journal*, 2014, 20, 320–327. Available from: doi:10.1108/RPJ-08-2012-0068 (accessed on 17-06-2022).

[3] Campbell, I., Bourell, D., Gibson, I. Additive Manufacturing: Rapid prototyping comes of age [Internet]. *Rapid Prototyping Journal*, 2012, 18, 255–258. Available from: doi:10.1108/13552541211231563 (accessed on 11-07-2022).

[4] Ivanova, O. S., Williams, C. B., Campbell, T. A. Additive Manufacturing (AM) and nanotechnology: Promises and challenges [Internet]. *International Solid Freeform Fabrication Symposium / 2011 International Solid Freeform Fabrication Symposium*, 2011, 733–749. Available from: doi:10.1108/RPJ-12-2011-0127 (accessed on 17-06-2022).

[5] Glardon, R. Direct rapid tooling: Research. *Rapid Prototyping Journal*, 1998, 4, 77–89.

[6] Gor, M., Soni, H., Wankhede, V., Sahlot, P., Grzelak, K., Szachgluchowicz, I., Kluczyński, J. A Critical review on effect of process parameters on mechanical and microstructural properties of powder-bed fusion Additive Manufacturing of Ss316l [Internet]. *Materials* (Basel), 2021, 14. Available from: doi:10.3390/ma14216527 (accessed on 17-06-2022).

[7] Szachogluchowicz, I., Sniezek, L., Slezak, T., Kluczyński, J., Grzelak, K., Torzewski, J., Fras, T. Mechanical properties analysis of the AA2519-AA1050-Ti6Al4V explosive welded laminate [Internet]. *Materials* (Basel), 2020, 13, 4348. Available from: doi:10.3390/ma13194348 (accessed on 17-06-2022).

[8] Kluczyński, J., Śnieżek, L., Grzelak, K., Oziębło, A., Perkowski, K. Hot isostatic pressing influence on the mechanical properties of selectively laser-melted 316L steel [Internet]. *Bulletin of the Polish Academy of Sciences / Technical Sciences*, 2020, 68, 1413–1424. Available from: doi:10.24425/bpasts.2020.135396 (accessed on 17-06-2022).

[9] Kluczyński, J., Śnieżek, L., Grzelak, K., Torzewski, J., Szachogłuchowicz, I., Oziębło, A., Perkowski, K., Wachowski, M., Małek, M. The influence of heat treatment on low cycle fatigue properties of selectively laser melted 316L steel [Internet]. *Materials* (Basel), 2020, 13, 5737. Available from: doi:10.3390/ma13245737 (accessed on 17-06-2022).

[10] Kravcov, A., Kluczyński, J., Kosturek, R., Franek, O., Morozov, N., Śnieżek, L., Svoboda, P., Kubeček, P. The influence of friction stir welded process parameters of AA2519-T62 on joint quality defined by non-destructive laser amplified ultrasonic method and by microstructure analysis [Internet]. *Proceedings of the Challenges to National Defence in Contemporary Geopolitical Situation*, 2020, 74–78.

[11] Grzelak, K., Łaszcz, J., Polkowski, J., Mastalski, P., Kluczyński, J., Łuszczek, J., Torzewski, J., Szachogłuchowicz, I., Szymaniuk, R. Additive Manufacturing of plastics used for protection against COVID19 ─ The influence of chemical disinfection by alcohol on the properties of ABS and PETG polymers [Internet]. *Materials* (Basel), 2021, 14. Available from: doi:10.3390/ma14174823 (accessed on 11-07-2022).

[12] Szachogłuchowicz, I., Fikus, B., Grzelak, K., Kluczyński, J., Torzewski, J., Łuszczek, J. Selective laser melted M300 maraging steel –Material behaviour during ballistic testing [Internet]. *Materials* (Basel), 2021, 14. Available from: doi:10.3390/ma14102681 (accessed on 11-07-2022)..

[13] Grzelak, K., Kluczyński, J., Szachogłuchowicz, I., Łuszczek, J., Śnieżek, L., Torzewski, J. Modification of structural properties using process parameters and surface treatment of monolithic and thin-walled parts obtained by selective laser melting [Internet]. *Materials* (Basel), 2020, 13, 5662. Available from: doi:10.3390/ma13245662 (accessed on 11-07-2022).

[14] Kluczyński, J., Śniezek, L., Grzelak, K., Oziebło, A., Perkowski, K., Torzewski, J., Szachogłuchowicz, I., Gocman, K., Wachowski, M., Kania, B. Comparison of different heat treatment processes of selective laser melted 316L steel based on analysis of mechanical properties [Internet]. *Materials* (Basel), 2020, 13. Available from: doi:10.3390/ma13173805 (accessed on 11-07-2022).

[15] Rolinck, N., Schmitt, M., Schneck, M., Schlick, G., Schilp, J. Development workflow for manifolds and fluid components based on laser powder bed fusion [Internet]. *Applied Sciences*, 2021, 11, 7335. Available from: https://doi.org/10.3390/app11167335 (accessed on 11-07-2022).

[16] Alshare, A. A., Calzone, F., Muzzupappa, M. Hydraulic manifold design via Additive Manufacturing optimized with CFD and fluid-structure interaction simulations [Internet]. *Rapid Prototyping Journal*, 2019, 25(9), 1516–1524. Available from: https://doi.org/10.1108/RPJ-03-2018-0064 (accessed on 11-07-2022).

[17] Ji, H., Zou, B., Ma, Y., Lange, C. F., Liu, J., Li, L. Intelligent design optimization system for additively manufactured flow channels based on fluid – Structure interaction [Internet]. *Micromachines*, 2022, 13, 100. Available from: https://doi.org/10.3390/mi13010100 (accessed on 11-07-2022).

[18] Liu, G., Zhang, J., Xu, B. Structure optimization for passages in hydraulic manifolds using metal Additive Manufacturing technology [Internet]. *IEEE 8th International Conference on Fluid Power and Mechatronics* (FPM), 2019, 485–492. Available from: doi: 10.1109/FPM45753.2019.9035877 (accessed on 11-07-2022).

[19] *Additive Manufacturing Shapes a New Manifold* [Internet]. Available from: https://www.machinedesign.com/3d-printing-cad/article/21183396/additive-manufacturing-shapes-a-new-manifold (accessed on 11-07-2022).

[20] Chekurov, S., Lantela, T. Selective laser melted digital hydraulic valve system [Internet]. *3D Printing and Additive Manufacturing*, 2017, 4(4), 215–221. Available from: https://doi.org/10.1089/3dp.2017.0014 (accessed on 11-07-2022).

[21] Krawczyk, J., Strycek, J. Construction and experimental research on plastic cycloidal gears used in gerotor pumps. *Proceedings of the 8th FPNI Ph.D Symposium on Fluid Power*, 2014.

[22] Al-Zaidi, A. Design of a hydraulic pump of tractor for manufacturing with 3D printer technology. *DJES*, 2022, 15(2), 31–39.

[23] *Additive Manufacturing Aidro: 3D Printing for Hydraulic Components, Ames Valves* [Internet]. Available from: https://aidro.it/additive-manufacturing/ (accessed on 11-07-2022).

[24] Wiens, T., Deibert, B. A low-cost miniature electrohydrostatic actuator system [Internet]. *Actuators*, 2020, 9, 130. Available from: https://doi.org/10.3390/act9040130 (accessed on 11-07-2022).

[25] Klimek, A., Kluczyński, J., Łuszczek, J., Bartnicki, A., Grzelak, K., Małek, M. Wear analysis of additively manufactured slipper-retainer in the axial piston pump [Internet]. *Materials*, 2022, 15, 1995. Available from: https://doi.org/10.3390/ ma15061995 (accessed on 11-07-2022).

[26] Tao Peng, Yanan Wang, Yi Zhu, Yang Yang, Yiran Yang, Renzhong Tang. Life cycle assessment of selective-laser-melting-produced hydraulic valve body with integrated design and manufacturing optimization: A cradle-to-gate study [Internet]. *Additive Manufacturing*, 2020, 36. Available from: https://doi.org/10.1016/j.addma.2020.101530 (accessed on 11-07-2022).

[27] Siegfarth, M., Pusch, T. P., Pfeil, A., Renaud, P., Stallkamp, J. Multi-material 3D printed hydraulic actuator for medical robots [Internet]. *Rapid Prototyping Journal*, 2020, 26(6), 1019–1026. Available from: https://doi.org/10.1108/RPJ-07-2019-0205 (accessed on 11-07-2022).

International Forum on Innovative Technologies and Management for Sustainability – ITMS'2022

ktu 1922 panevėžys faculty of technologies and business

International Scientific Conference Intelligent Technologies in Logistics and Mechatronics Systems – ITELMS'2022, 15th September, 2022, Panevėžys, Lithuania

Additive Manufacturing of Polyphenylene Sulfide: Material's Behavior During Tensile Testing

Janusz Kluczyński[a]*

[a]*Institute of Robots & Machine Design, Faculty of Mechanical Engineering, Military University of Technology, 2 Gen. S. Kaliskiego St., Warsaw 00-908, Poland*

Abstract

The paper includes research about the influence of the orientation of Polyphenylene sulfide parts manufactured by means of Additive Manufacturing on mechanical properties. To better describe the material's behavior during tensile testing, a digital image correlation and a microscopic investigation of the fractures have been made. The results revealed high isotropy of all samples which is a very rare phenomenon in parts obtained by using such technologies.

© 2022 Janusz Kluczyński.
Peer-review under responsibility of the Kaunas University of Technology, Panevėžys Faculty of Technologies and Business.

Keywords: Additive Manufacturing; Fused Filament Fabrication; Polyphenylene sulfide; Mechanical properties analysis.

1. Introduction

The usage of Additive Manufacturing (AM) technologies is still growing. The last decade revealed some improvements which caused an increase in the industry in all types of AM devices – especially in Research and Development (R&D) departments [1–3]. Such success was possible because of the main principle of AM technology, where the material is deposited layer-by-layer. That kind of approach allows the creation of complex geometries or the use of different materials during the process [4]. It is additionally important for AM technologies development, that layered materials are of significant interest in the novel, high-tech solutions [5–12]. A really characteristic

* Corresponding author. Tel.: +48 683 837 646.
E-mail address: janusz.kluczynski@wat.edu.pl

© 2022 Janusz Kluczyński.
Peer-review under responsibility of the Kaunas University of Technology, Panevėžys Faculty of Technologies and Business.

structure (layered) of the AM parts creates a need for very diverse research, which creates an enormous field of research for many scientists and engineers [13–16]. Scientific outcomes in a form of tensile, fatigue, dynamic and structural analysis are in significant use to allow using AM technologies in some industrial applications. A layered structure of additively manufactured parts causes an anisotropy of mechanical properties related to the build orientation during AM process [17–19]. For that reason, there are a lot of different types of postprocessing that are suitable for different AM technologies [20–23]. Because of the development of AM technologies and different types of post-processes, there is a growth of application case studies dedicated to different industries. Klimek et al. [24] analyzed the behavior of the axial pump with a replaced retainer- slipper holder which was additively manufactured. The most important outcome of that research is a successful work of such part for 100 hours with different load regimes. In a different application, Szachogłuchowicz et al. [25] analyzed how AM material behaves during ballistic testing. Their analysis revealed that AM parts in as-built conditions are characterized by lower fragmentation than heat-treated counterparts. In another research Małek et al. [26] analyzed how additively manufactured scaffolding affects the thermal and mechanical properties of cement bricks. In the last two years, AM technologies were also used during the COVID-19 pandemic to fill the production gap of many different medical tools [3, 27–29].

Because of the relatively low cost, and very good accessibility of devices, Material Extrusion (ME) technologies such as Fused Filament Fabrication (FFF) are one of the most popular. Such a phenomenon causes the development of different materials dedicated to the FFF technology. One of the most interesting materials is high-temperature polymers which could be a kind of substitute even for aluminum alloys. A very good example of such materials is Polyphenylene sulfide (PPS) which is a semi-crystalline thermoplastic polymer, resistant to high temperatures. Due to its structure, PPS is also chemically resistant with high mechanical strength, even at temperatures above 200 °C. In addition to low water absorption, the PPS polymer also has good dimensional stability and excellent electrical properties. PPS thermoplastic is chemically very stable, even at high temperatures, which is very important in the FFF process because the distortion of produced parts is relatively low.

In this research, the influence of the orientation of PPS parts on mechanical properties has been examined. To better describe the material's behavior during tensile testing, a microscopic investigation of the fractures has been made.

2. Materials and methods

PPS material was supplied by the "Spectrum Filaments Ltd. Company". To produce specimens, an "Intamsys Funmat HT" was used. The main reason for using this exact device is the possibility of exceeding 300 °C by the extrusion nozzle and closed building chamber with active heating technology.

To reach desirable elements properties it was used the following process parameters:

- hotend temperature – 320 °C;
- heatbed temperature – 120 °C;
- chamber temperature – 80 °C;
- layer thickness – 0.2 mm;
- outline shell thickness – 2 mm;
- infill – 100 %;
- part cooling intensity – 40 %;
- printing speed – 50 mm/s;
- nozzle diameter – 0.4 mm.

To determine the mechanical properties, dog-bone-shaped parts were produced (three samples for each combination of orientation) ASTM D638 "*Standard Test Method for Tensile Properties of Plastics*". The geometry of the designed sample is shown in Figure 1.

Tensile tests were made at room temperature by means of an "Instron" 8802 axial servo-hydraulic testing machine, equipped with an "Instron" 8800 controller. To allow more precise data acquisition, a uniaxial extensometer "Instron" 2630-112 with a gauge length of 50 mm (axial travel +50 %) was used.

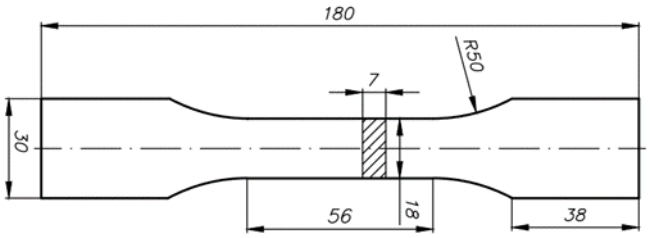


Fig. 1. Sample part for tensile testing used in the research (dimensions in mm)

Sample parts were oriented along each of the three axes (see Fig. 2) to allow the determination of how layer deposition of the FFF parts affects tensile properties.

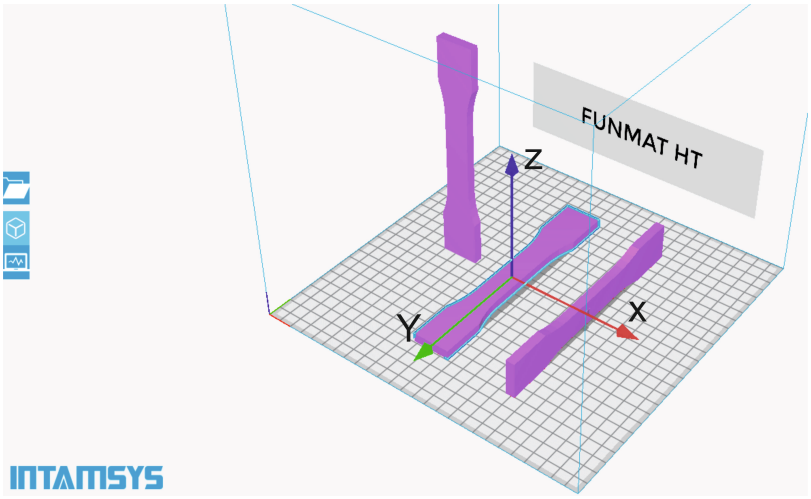


Fig. 2. Samples' orientation in the substrate plate

To improve the tensile test results, a Digital Image Correlation (DIC) analysis was used to measure the distribution of deformation during the tensile tests. The measure was made by the use of a "Dantec Dynamics" device and *ISTRA* 4D software. To allow structural characterization, and cracking propagation of the samples during the tensile tests, fractographic research was performed. These observations were made by means of the "KEYENCE" VHX-7000 digital microscope.

3. Results and discussion

Before the tests, samples were also prepared for DIC analysis by using dotted structures on their surfaces. Samples before and after tests are shown in Figure 3. The obtained parts' properties including tensile strength and elongation at the break of the samples are presented in Table 1.

Table 1. Mechanical properties of samples tested (total values)

Type of property	**Value for *X*-orientation**	**Value for *Y*-orientation**	**Value for *Z*-orientation**
Ultimate tensile strength (MPa)	36.18	48.96	24.67
Strain at break (%)	1.95	3.38	1.20

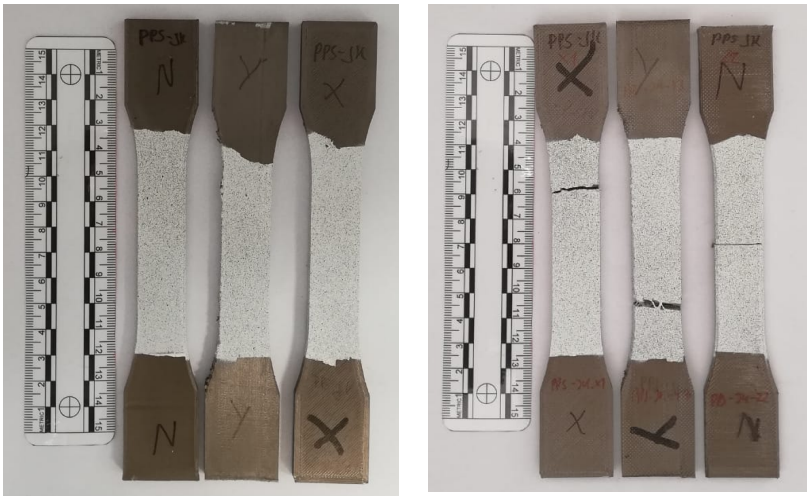


Fig. 3. Samples' before (left side) and after tensile tests (right side)

For a better presentation of the obtained tensile tests, a stain-stress chart was generated for three tested samples from each orientation. The chart is shown in Figure 4.

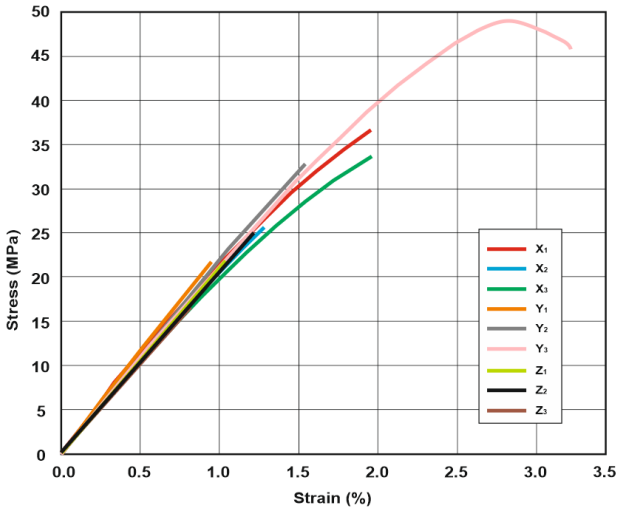


Fig. 4. Strain-stress chart for *X*, *Y*, and *Z*-oriented samples made of the PPS material

As is visible in Figure 4, all samples, despite their orientation are characterized by high isotropy, especially in the Hook law area. The highest obtained UTS has been registered for *Y*-oriented samples, as well as the highest strain (3.38 %). The analysis of the deformation during tensile testing obtained by the DIC method revealed very low strain even at the UTS level, which indicates a significant brittleness of the material.

Additionally, based on the DIC analysis results (see Fig. 5), the significant isotropy of the mechanical properties is proven. Despite the different ways of single material lines deposition, and material layers arrangement during the FFF process, there are no visible deformations related to the technological process, which is typical for the kind of parts, obtained by AM technologies with the use of different materials.

To better describe the material's behaviour during tensile testing, fracture images were captured (see Fig. 6). It could be visible typical brittle-like cracking in the case of *X*, and *Y*-oriented samples. Also, in case *X*, and *Y* orientation

there is a similarity in the number of internal pores. Such a phenomenon results in similar material strength and affected crack generation, which ran almost the same in both orientations (which also proves the high isotropy of the material).

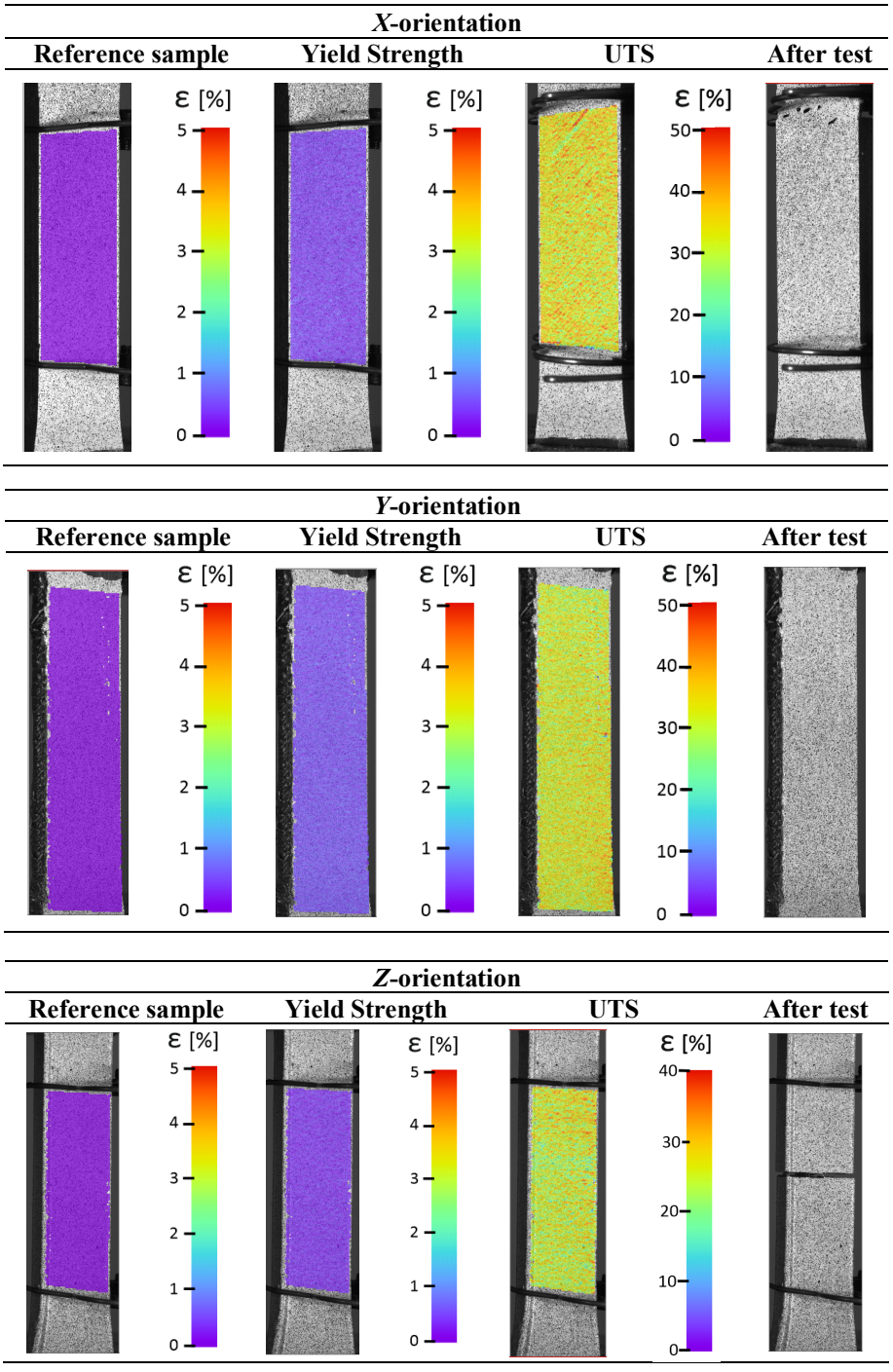


Fig. 5. DIC analysis of all samples

Fractures of the *X* and *Y*-orientations indicate structural heterogeneity connected with local stress damping, which promoted a cracking initiation. It is possible to observe that cracking went through several layers which finally made an irregular, multiplanar crack. In the case of samples made along the *Z*-axis, the fracture has the same nature as the two previous materials.

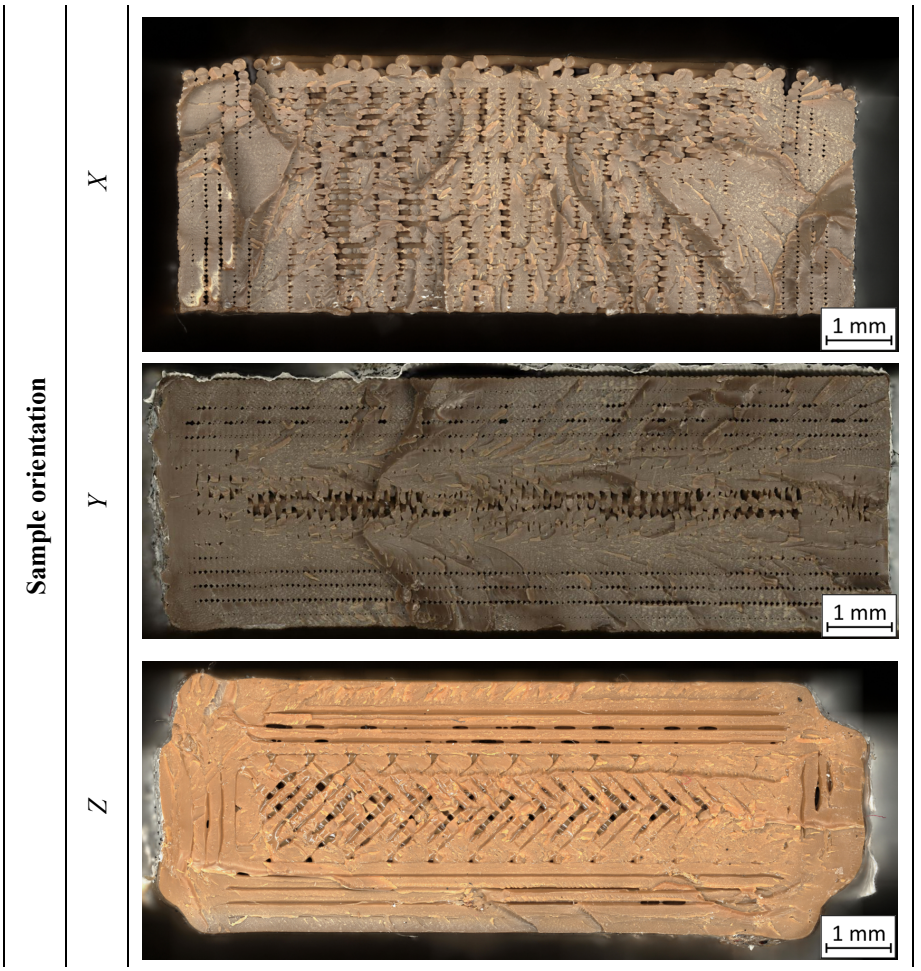


Fig. 6. Fracture images for *X*, *Y*, and *Z*-oriented samples made of the PPS material

In the case of *Z* orientation, there is visible a typical fracture for that kind of arrangement in the substrate plate [30]. What is very interesting is a course of the tensile curves (see Fig. 4) of samples made along the *Z*-axis. Such a phenomenon indicates that the adhesion between layers is almost comparable with the UTS of the material.

4. Conclusions

Based on the obtained results, the following conclusion could be drawn:

1. Parts produced with the use of the FFF technology made of PPS material are characterized by UTS similar to other popular materials available for that kind of AM technology.
2. Samples produced in *Z*-orientation are characterized by high adhesive strength between layers close to the UTS of the PPS material.

3. Fractures of the samples produced along *X* and *Y* directions indicate brittle-like cracking similar to conventionally made materials.

References

[1] Mohanavel, V., Ashraff Ali, K. S., Ranganathan, K., Jeffrey, A. J., Ravikumar, M. M., Rajkumar, S. The roles and applications of Additive Manufacturing in the aerospace and automobile sector [Internet]. *Materials Today Proceedings*, 2021. Available from: doi:https://doi.org/10.1016/j.matpr.2021.04.596 (accessed on 02-08-2022).

[2] Mellor, S., Hao, L., Zhang, D. Additive Manufacturing: A framework for implementation [Internet]. *International Journal of Production Economics*, 2014, 149, 194–201. Available from: doi:10.1016/j.ijpe.2013.07.008 (accessed on 02-08-2022).

[3] Aydin, A., Demirtas, Z., Ok, M., Erkus, H., Cebi, G., Uysal, E., Gunduz, O., Ustundag, C. B. 3D Printing in the battle against COVID-19 [Internet]. *Emergent Materials*, 2021. Available from: doi:10.1007/s42247-021-00164-y (accessed on 02-08-2022).

[4] Kluczyński, J., Śnieżek, L., Kravcov, A., Grzelak, K., Svoboda, P., Szachogłuchowicz, I., Franek, O., Morozov, N., Torzewski, J., Kubeček, P. The examination of restrained joints created in the process of multi-material FFF Additive Manufacturing technology [Internet]. *Materials* (Basel), 2020, 13, 903. Available from: doi:10.3390/ma13040903 (accessed on 02-08-2022).

[5] Sniezek, L., Szachogluchowicz, I., Wachowski, M., Torzewski, J., Mierzynski, J. High cycle fatigue properties of explosively welded laminate AA2519/AA1050/Ti6Al4V [Internet]. *Procedia Structural Integrity*, 2017, 5, 422–429. Available from: doi:10.1016/j.prostr.2017.07.191(accessed on 02-08-2022).

[6] Szachogluchowicz, I., Sniezek, L., Sulym, H., Gloc, M. Testing and verification modeling of wave-shape formation under explosion welding to laminate AA 2519-Ti6Al4V [Internet]. *Procedia Structural Integrity*, 2016, 2, 2375–2380. Available from: doi:10.1016/j.prostr.2016.06.297 (accessed on 02-08-2022).

[7] Sniezek, L., Szachogluchowicz, I., Gocman, K. The mechanical properties of composites AA.2519-Ti6Al4V obtained by detonation method. *Proceedings of the Intelligent Technologies in Logistics and Mechatronics Systems*, 2013, 214–219.

[8] Fras, T., Szachogluchowicz, I., Sniezek, L. Ti6Al4V-AA1050-AA2519 explosively-cladded plates under impact loading [Internet]. *The European Physical Journal Special Topics*, 2018, 227, 17–27. Available from: doi:10.1140/epjst/e2018-00114-9 (accessed on 02-08-2022).

[9] Szachogłuchowicz, I., Śnieżek, L., Ślęzak, T. Mechanical properties analysis of explosive welded sheet of AA2519-Ti6Al4V with interlayer of AA1050 subjected to heat-treatment [Internet]. *Materials* (Basel), 2022, 15. Available from: doi:10.3390/ma15114023 (accessed on 02-08-2022).

[10] Szachogluchowicz, I., Sniezek, L., Slezak, T., Kluczyński, J., Grzelak, K., Torzewski, J., Fras, T. Mechanical properties analysis of the AA2519-AA1050-Ti6Al4V explosive welded laminate [Internet]. *Materials* (Basel), 2020, 13, 1–16. Available from: doi:10.3390/ma13194348 (accessed on 02-08-2022).

[11] Kluczynski, J., Kravcov, A., Kosturek, R., Śnieżek, L., Kluczyński, J., Franek, O., Morozov, N., Maciejewski, P. The influence of friction stir welded process parameters of AA2519-T62 on joint quality defined by non-destructive laser amplified ultrasonic method and by microstructure analysis [Internet]. *Acta Polytechnica*, 2020. Available from: doi:10.14311/AP.2020.60.0415 (accessed on 02-08-2022).

[12] Kravcov, A., Kluczyński, J., Kosturek, R., Franek, O., Morozov, N., Śnieżek, L., Svoboda, P., Kubeček, P. The Influence of friction stir welded process parameters of AA2519-T62 on joint quality defined by non-destructive laser amplified ultrasonic method and by microstructure analysis. *Proceedings of the Challenges to National Defence in Contemporary Geopolitical Situation*, 2020, 74–78.

[13] Gor, M., Soni, H., Wankhede, V., Sahlot, P., Grzelak, K. A Critical review on effect of process parameters on mechanical and microstructural properties of powder-bed fusion Additive Manufacturing of SS316L. *Materials* (Basel), 2021, 14(21), 6527.

[14] Prakash, K. S., Nancharaih, T., Rao, V. V. S. Additive Manufacturing techniques in manufacturing – An overview [Internet]. *Materials Today Proceedings*, 2018, 5, 3873–3882. Available from: doi:10.1016/j.matpr.2017.11.642 (accessed on 02-08-2022).

[15] Labeaga-Martínez, N., Sanjurjo-Rivo, M., Díaz-Álvarez, J., Martínez-Frías, J. Additive Manufacturing for a moon village [Internet]. *Procedia Manufacturing*, 2017, 13, 794–801. Available from: doi:10.1016/j.promfg.2017.09.186 (accessed on 02-08-2022).

[16] Łuszczek, J. Review of the method design and Additive Manufacturing of gears [Internet]. *Biuletyn Wojskowej Akademii Technicznej*, 2021, 70, 15–34. Available from: doi:10.5604/01.3001.0015.7008 (accessed on 02-08-2022).

[17] Gu, D., Chen, H. Selective laser melting of high strength and toughness stainless steel parts: The roles of laser hatch style and part placement strategy [Internet]. *Materials Science and Engineering: A*, 2018, 725, 419–427. Available from: doi:10.1016/j.msea.2018.04.046 (accessed on 02-08-2022).

[18] Mooney, B., Kourousis, K. I. *Metals a Review of Factors a FF Ecting the Mechanical A Review of of Maraging Factors Affecting Properties of Powder Bed Fusion*, 2020.

[19] Fergani, O., Bratli Wold, A., Berto, F., Brotan, V., Bambach, M. Study of the effect of heat treatment on fatigue crack growth behaviour of 316L stainless steel produced by selective laser melting [Internet]. *Fatigue and Fracture Engineering Materials and Structures*, 2018, 41, 1102–1119. Available from: doi:10.1111/ffe.12755 (accessed on 02-08-2022).

[20] Kluczyński, J., Śniezek, L., GRZELAK, K., Oziębło, A., Perkowski, K., Torzewski, J., Szachogłuchowicz, I., Gocman, K., Wachowski, M., Kania, B. Hot isostatic pressing influence on the mechanical properties of selectively laser-melted 316L steel [Internet]. *Bulletin of the Polish Academy of Sciences: Technical Sciences*, 2020, 68, 1413–1424. Available from: doi:10.24425/bpasts.2020.135396 (accessed on 02-08-2022).

[21] Kluczyński, J., Śniezek, L., Grzelak, K., Oziebło, A., Perkowski, K., Torzewski, J., Szachogłuchowicz, I., Gocman, K., Wachowski, M., Kania, B. Comparison of different heat treatment processes of selective laser melted 316L steel based on analysis of mechanical properties [Internet]. *Materials* (Basel). 2020, 13. Available from: doi:10.3390/ma13173805 (accessed on 02-08-2022).

[22] Kluczyński, J., Śnieżek, L., Grzelak, K., Torzewski, J., Szachogłuchowicz, I., Ozikebło, A., Perkowski, K., Wachowski, M., Małek, M. The influence of heat treatment on low cycle fatigue properties of selectively laser melted 316L steel [Internet]. *Materials* (Basel), 2020, 13, 5737. Available from: doi:10.3390/ma13245737 (accessed on 13-08-2022).
[23] Grzelak, K., Kluczyński, J., Szachogłuchowicz, I., Łuszczek, J., Śnieżek, L., Torzewski, J. Modification of structural properties using process parameters and surface treatment of monolithic and thin-walled parts obtained by selective laser melting [Internet]. *Materials* (Basel), 2020, 13, 1–12. Available from: doi:10.3390/ma13245662 (accessed on 13-08-2022).
[24] Klimek, A., Kluczyński, J., Łuszczek, J., Bartnicki, A., Grzelak, K., Małek, M. Wear analysis of additively manufactured slipper-retainer in the axial piston pump [Internet]. *Materials* (Basel), 2022, 15. Available from: doi:10.3390/ma15061995 (accessed on 13-08-2022).
[25] Szachogłuchowicz, I., Fikus, B., Grzelak, K., Kluczyński, J., Torzewski, J., Łuszczek, J. Selective laser melted M300 maraging steel – material behaviour during ballistic testing [Internet]. *Materials* (Basel), 2021, 14. Available from: doi:10.3390/ma14102681 (accessed on 13-08-2022).
[26] Małek, M., Grzelak, K., Łasica, W., Jackowski, M., Kluczyński, J., Szachogłuchowicz, I., Torzewski, J., Łuszczek, J. Cement-glass composite bricks (CGCB) with interior 3D printed PET-G scaffolding [Internet]. *Journal of Building Engineering*, 2022, 52. Available from: doi:10.1016/j.jobe.2022.104429 (accessed on 13-08-2022).
[27] Tino, R., Moore, R., Antoline, S., Ravi, P., Wake, N., Ionita, C. N., Morris, J. M., Decker, S. J., Sheikh, A., Rybicki, F. J., et al. COVID-19 and the role of 3D printing in medicine [Internet]. *3D Printing in Medicine*, 2020, 6, 1–8. Available from: doi:10.1186/s41205-020-00064-7 (accessed on 13-08-2022).
[28] Roman, N., Cojocaru, D., Coman, C., Repanovici, A., Bou, S. F., Miclaus, R. S. Materials for respiratory masks in the context of COVID-19 pandemic [Internet]. *Materiale Plastice*, 2021, 57, 236–247. Available from: doi:10.37358/MP.20.4.5423 (accessed on 13-08-2022).
[29] Grzelak, K., Łaszcz, J., Polkowski, J., Mastalski, P., Kluczyński, J., Łuszczek, J., Torzewski, J., Szachogłuchowicz, I., Szymaniuk, R. Additive Manufacturing of plastics used for protection against COVID-19 – the influence of chemical disinfection by alcohol on the properties of ABS and PETG polymers [Internet]. *Materials* (Basel), 2021, 14. Available from: doi:10.3390/ma14174823 (accessed on 13-08-2022).
[30] Mazurkiewicz, M., Kluczyński, J., Jasik, K., Sarzyński, B., Szachogłuchowicz, I., Łuszczek, J., Torzewski, J., Śnieżek, L., Grzelak, K., Małek, M. Bending strength of polyamide-based composites obtained during the fused filament fabrication (FFF) process [Internet]. *Materials* (Basel), 2022, 15, 5079. Available from:doi:10.3390/ma15145079 (accessed on 13-08-2022).

International Forum on Innovative Technologies and Management for Sustainability – ITMS'2022

International Scientific Conference Intelligent Technologies in Logistics and Mechatronics Systems – ITELMS'2022, 15th September, 2022, Panevėžys, Lithuania

Mechanical Properties Comparison of the Additively Manufactured Gears Made of Polymeric Materials with Improved Wear Resistance

Jakub Łuszczek[a]*, Lucjan Śnieżek[a], Krzysztof Grzelak[a]

[a]*Institute of Robots & Machine Design, Faculty of Mechanical Engineering, Military University of Technology, 2 Gen. S. Kaliskiego St., Warsaw 00-908, Poland*

Abstract

Additive Manufacturing (AM) is currently one of the fastest growing manufacturing technology in the industry area. One of the applications of the AM technology is the production of gears using polymer materials. This paper presents the results of comparative tests on measurement accuracy, as well as static and fatigue strength of gears made of ABS polymers, and "Igumid" P150-PF, "Iglidur" I150-PF dedicated to the production of this type of elements. The gears made with the use of ABS were characterized by the lowest dimensional accuracy due to the susceptibility of this material to thermal shrinkage. Static and fatigue tests in the field of bending teeth showed the highest stiffness and durability of wheels made of "Igumid" P150-PF. The work has been shown that ABS material can be used for elements of drive systems, the loads of which will be static. In the case of static loads, the material shows a significant weakening by 50 % in the initial phase of the test, unlike the other tested materials. In addition, the paper contains descriptions and photos of the course of tooth deformation in the field of fatigue and static tests.

© 2022 Jakub Łuszczek, Lucjan Śnieżek, Krzysztof Grzelak.
Peer-review under responsibility of the Kaunas University of Technology, Panevėžys Faculty of Technologies and Business.

Keywords: Additive Manufacturing; Fused Filament Fabrication; Gears; Mechanical properties analysis.

1. Introduction

Additive Manufacturing (AM) is currently one of the most dynamically developing technology for the production of various types of elements, especially in terms of their prototyping and unit production [1]. Its main advantage is

* Corresponding author.
E-mail address: jakub.luszczek@wat.edu.pl

© 2022 Jakub Łuszczek, Lucjan Śnieżek, Krzysztof Grzelak.
F916G0007
Peer-review under responsibility of the Kaunas University of Technology, Panevėžys Faculty of Technologies and Business.

the ability to produce complex geometries due to the nature of the process where the material is applied layer by layer, as opposed to subtractive techniques such as turning or milling, where the material is removed [2–4]. It is related to the anisotropy of strength properties as in other layered materials [5–8]. One of the areas where an increase in interest in additive technology has been noticed is the production of drive system components, including gears. Gears, due to the geometry of the toothing, require many specialized machines and tools for their production. In addition, the number of types of gears (bevel gears, conical gears, etc.) increases the equipment of the machine park of a given production company. Additive Manufacturing allows any type of gear to be manufactured using metals or polymers using only one machine. One of the few limitations is the working area of the machine. For this reason, AM seems to be an attractive alternative in the production of drive system components.

Many authors of works [16–19] made an attempt to implement AM technology for the production of gears using various materials. However, in order to determine the usefulness of this technology in the discussed scope, it is necessary to conduct experimental tests of model elements in conditions reflecting the actual operation of these elements.

For the Additive Manufacturing of gears, the authors of the works most often use the FDM (Fused Deposid Modeling) technology, which according to ISO/ASTM 52900 standard belongs to the Extrusion Material group. The most commonly used materials for the production of parts using the FDM technique include: PLA (PolyLactic Acid), ABS (Acrylonitrile Butadiene Styrene), PETG (PolyEthylene Terephthalate Glycol) [9] as well as high-temperature materials such as ULTEM or PEEK, which require much more advanced equipment and are also characterized by a higher purchase price. Recently, materials dedicated to FDM printing of gears, such as "Igumid" P150-PF and "Iglidur" I150-PF, have appeared on the market, however, apart from the data on the manufacturer's website, there is no research on the suitability of these materials in this area in the literature. Additive Manufacturing also enables production from metal powders [10–12]. However, popularly available materials such as 316L steel [12, 13] or M300 maraging steel [14] are not materials dedicated to this type of application. The broader aspect of manufacturing wheels using AM techniques was discussed in the previous work [15].

Research on AM gears in terms of their fatigue strength has been conducted by many researchers [16–22]. One of the main wear mechanisms is abrasive wear, plastic deformation or tooth melting due to high temperature, and tooth breaking [23, 24]. Cader et al. [16] investigated the wear of gears produced by the FDM method from the ULTEM 9 085 material. They used a different arrangements of successive layers in the manufactured gear, while the tests were carried out on the actual machine in which the gears were to be ultimately applied. The research showed that the best results were obtained in the case of wheels where successive layers were arranged alternately at an angle of 60 and 45. The importance of the arrangement of individual layers during the production of gears was also mentioned by [25] and [26]. It was shown in these works that in order to obtain uniform stiffness of the teeth along the entire circumference of the gear, the toothed rim should be made of only outlines. However, attention should be paid to possible voids that may appear between successive contours at low module values, which may reduce the strength of the teeth.

Harsha et al. [17] compared wheels made of three materials: PLA, ABS and PA (Polyamide) using the FDM method. The tests carried out on the test rig showed that the main wear mechanism is abrasive wear and plastic deformation of the teeth as a result of high temperature during operation. The wheels made of PA showed the greatest service life. Similar studies were carried out by Zhang et al. [15]. The authors of the study point out that the wear resistance of wheels made of Polyamide 618, with the use of Additive Manufacturing, depends mainly on the temperature conditions and the quality of the connection of individual layers of the material.

In the discussed works, the tests were carried out at different speeds of rotational gear of the tested gearboxes. The resulting friction increases the temperature on the tooth flanks, thus becoming one of the main causes of damage to the tested gears. However, in low-speed mechanisms, such as manual drives or short-cycle gears, such as gate sliding mechanisms, the operating temperature is not the key factor. Therefore, the test with low temperature change is single tooth bending on pulsators according to the method described in ISO 6336-5 (Method B).

In the literature on the study of gears manufactured with the use of the FDM technology, there are residual data on this subject. This knowledge seems to be necessary to determine the suitability of this technique in the field of gear production. This paper presents the results of comparative tests in terms of bending strength at the base of the tooth of gears manufactured with the use of ABS and materials with increased strength and wear resistance – "Igumid" P150-PF, "Iglidur" I150-PF.

2. Materials and methods

The geometry of the gear sample was established in accordance with ISO 6336-5:2016. The designed gear with the geometry parameters has been presented in Figure 1 and Table 1.



Fig. 1. 3D model of the sample gear used in the research

Table 1. Geometry parameters of the gear sample

Name of parameters	Value
Number of teeth, z	25
Module, m [mm]	3.5
Pressure angle, α [deg]	20
Face width, b [mm]	15
Pitch circle diameter, D [mm]	87.5
Hub diameter, D_h [mm]	30

For the production of gear samples, it was used the ABS, material provided by "Spectrum Filaments Ltd Company" (Poland, Pęcice) and "Igumid" P150-PF, "Iglidur" I150-PF provided by "Igus GmbH" (German, Colonia). The ABS is one of the most popular materials used in FDM technology. Is characterized by high strength, good ductility and susceptibility to machining.

Table 2. Process parameters of materials used to produce gear samples by means of FDM technology

Material	Hotend temperature, °C	Heatbed temperature, °C	Layer thickness	Infill, %	Perimeters	Part cooling intensity, %	Printing speed	Nozzle diameter
ABS	235	90				0		
"Igumid" P150-PF	260	70	0.2	100	9	0	40	0.4
"Iglidur" I150-PF	240	40				40		

The "Igumid" P150-PF ang "Iglidur" I150-PF are "Igus" proprietary materials, referred to as tribo-filaments. "Igumid" P150-PF is a robust and rigid material with fiber reinforcement and characterized by high flexural strength. "Iglidur" I150-PF is doped with solid lubricants, which increases their wear resistance, improved mechanical properties and additional can be used in the food and packing industry (agree with the norm UE 10/2011).

"Igumid" P150-PF and "Iglidur" I150-PF can be processed just as easily as standard PLA and PETG filaments. To produce the test samples "Mass Portal Pharaoh" printer from "Mass Portal" (Latvia, Riga) and dedicated software *Simplify3D* was used. The process parameters which was used during the production of the gears samples have been presented in Table 2.

Tests in the field of determining the accuracy of gear manufacturing were carried out with the use of the GOM Atos 3D scanner by GOM (German, Brunswick). The scans performed were compared with the three-dimensional reference model. Measurements of the addendum circle diameter (outside diameter) and dedendum circle diameter (root

diameter) were made. Measurements are made in a plane perpendicular to the axis of rotation of the gear, located in the middle of the face width.

The static bending test and fatigue test was performed using "MTS Criterion" C42 and "MTS Landmark" 370.50 (USA, Eden Prairie). The special handle has been designed to correctly carry out the static and fatigue bending tests, which are illustrated in Figure 2.

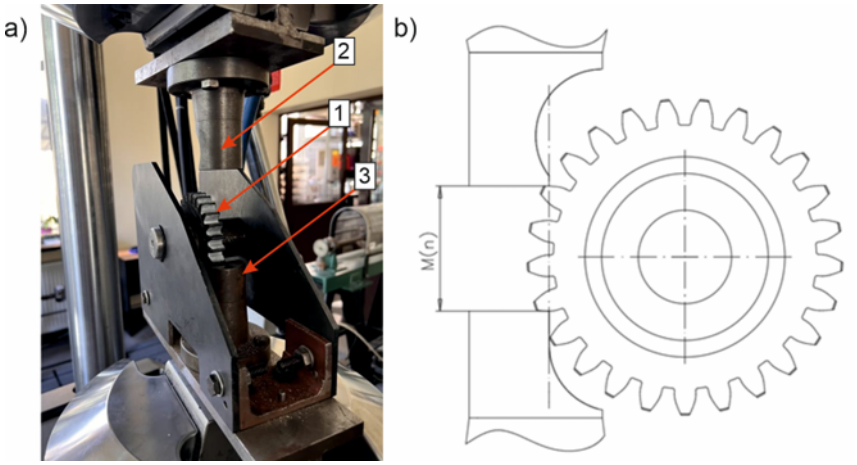


Fig. 2. a) Laboratory station for single tooth bending (1 – Test gear; 2 – Loading pin; 3 – Support pin); b) Diagram of test gear tooth loading

The $M(n)$ parameter (see Fig. 2a) was established using equation (1) [1]. $M_{tab}(n)$ is a table value of the distance between the pins depending on the number of teeth ($M_{tab}(4) = 7.73$); n – a number of teeth between the mandrels; x – coefficient of displacement of the outline (for the gear samples, $x = 0.035$); α_0 – a value of the profile angle (for the sample wheel $\alpha_0 = 20°$); m – tooth module (for the gear samples, $m = 3.5$). The value of given coefficients ($M_{tab}(n)$, x) was chosen to form the literature [1].

$$M(n) = (M_{tab}(n) + 2 \cdot x \cdot sin\alpha_0 + \pi \cdot cos\alpha_0) \cdot m; \quad (1)$$
$$M(4) = 37{,}46\ mm.$$

On the base of assumption and counting, the special holder for the bending test of gear was designed and produced (see Fig. 2a). The gear sample (1) is placed between two pins, where one is the loading pin (2) and the second is the support pin (3). Due to the difference between the length of the arm on which the bending moment is generated, the tooth on the side of the loading pin is the main loaded tooth. A tooth that was a support tooth in a given test did not participate as a load or support tooth in a subsequent test. The first stage of the bending tests was carried out under static loading using the "MTS Criterion" C42. Then a series of tests with cyclic loads were carried out. Due to the size of the testing machine and the range of possible forces to generate (up to 80 kN), the "MTS Landmark" 370.50 machine did not allow for the maintenance of the specified load values during the tests (< 2kN). Therefore it was decided to load individual gears with a constant value of the load pin displacement. As a result, the system responded in the form of a force. The decrease in force over time (after a certain number of cycles) meant the weakening of the tooth material, and its total decrease – the destruction of the sample and the end of the test. Static and fatigue tests were carried out with the use of the same handle in an identical configuration.

3. Geometry measurements – results and discussion

During the manufacturing process of components using gears, high temperature gradients occur due to the large temperature difference between the environment and the material being extruded through the nozzles. In some cases, this can result in component deformation due to material shrinkage. Geometrical accuracy is of particular importance

in the case of gears (see Fig. 3). A cross-section with geometry deviations on the tooth heads and in the roots are shown. Regardless of the material used, the gears show different deviation values along the toothed rim. Negative deviations are marked in blue, while positive deviations are marked in green. The distribution of deviations with negative values shows local deformation of the gears, which is the effect of thermal shrinkage of the material. Positive values are the result of overlapping individual material paths, which during deposit are deformed by nozzles in order to ensure proper adhesion to the previously unfolded layer, a phenomenon that often accompanies elements produced by the FDM method.

Table 3 shows the mean values of the outer diameters and the root diameter, calculated based on the mean value of the deviation obtained from the measurements in photo 3.

Table 3. Process parameters of materials used to produce gear samples by means of FDM technology

Material	The average value of outside diameter, D_0 [mm]	Standard deviation, D_0 [mm]	The average value of root diameter, D_R [mm]	Standard deviation, D_R [mm]
ABS	94.12	0.32	78.22	0.26
"Igumid" P150-PF	94.23	0.27	78.40	0.23
"Iglidur" I150-PF	94.20	0.28	78.27	0.22
Model CAD	94.50	-	78.75	-

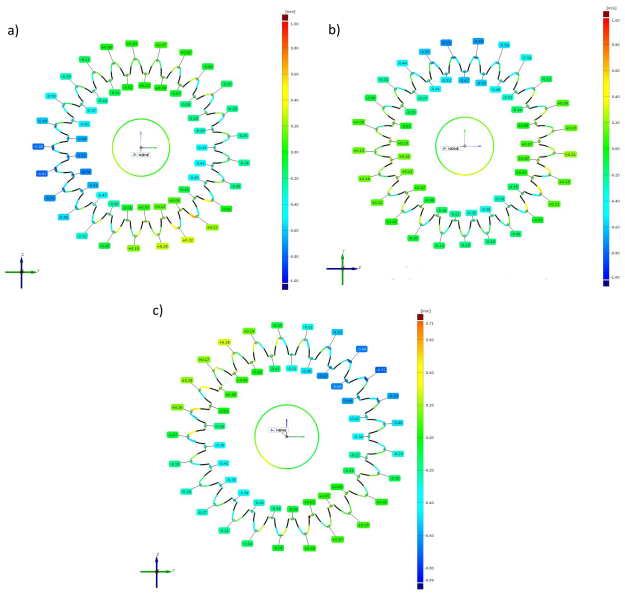


Fig. 3. Distribution of geometrical deviations of gears additive manufactured in relation to the reference model: a) ABS; b) "Igumid" P150-PF; c) "Iglidur" I150-PF

The table also contains the values of standard deviations for the calculated diameters, as well as the reference values determined from the CAD model. The largest deviations in both diameters were observed in gears made of ABS polymer. This means that this material exhibits higher deformation shrinkage than the other two materials. Gears made of "Igumid" P150-PF and "Iglidur" I150-PF are more dimensionally stable. In each of the cases, the standard deviations take values over 0.22 mm, which proves a large variation in the values of deviations along the circumference of the gears.

The deviation values are similar to those obtained by the authors of the work [27]. Therefore, the deviation wheels may have a negative effect on the operation of the transmission, and as a result may accelerate the abrasive wear and increase the operating temperature. Moreover, the manufactured gears cannot be assigned to any of the manufacturing accuracy classes according to DIN 3962, because the values of geometric deviations are too high.

4. Static and fatigue bending – results, and discussion

The first stage of research on the mechanical properties of the gears was the single tooth bending. Table 4 shows the results of the static tooth bending test. From the recorded force being the load on the tooth during the test, the values of stresses at the base of the tooth were calculated on the basis of the relationships contained in the ISO 6336 standard. The highest values of stresses at the base of the tooth were shown by wheels made of "Igumid" P150-PF (126.2 MPa), with the lowest value of registered displacements – 3.3 mm. This is due to the significant reinforcement of the material by the fibers unlike the other two. On the other hand, the teeth made of "Iglidur" I150-PF had the lowest stiffness. Similar studies were carried out by the authors of the study [26]. Kim et al. statically tested gears made of fiber-reinforced polyamide. From the data contained in the article, it was calculated that the stresses at the root of the tooth (made of perimeters only) amount to about 116 MPa, which is a value similar to that obtained in the case of ABS gears. However, the fundamental difference was noticed in the deformation, which in the case of polyamide was 2.2 mm, which makes it much stiffer than the materials considered in this paper.

Table 4. Static bending test results for Additive Manufacturing gears

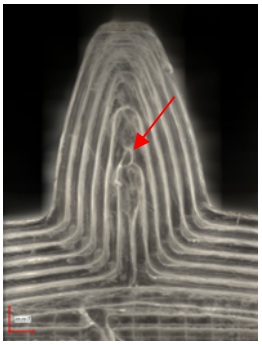
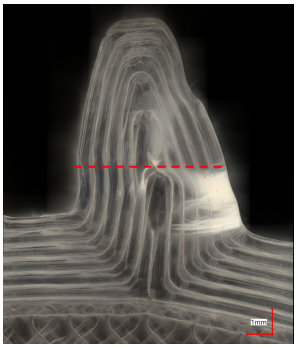
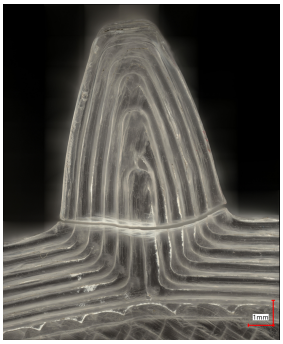
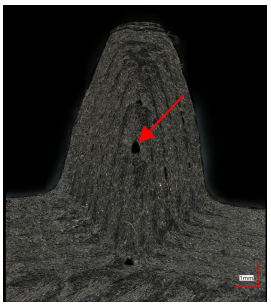
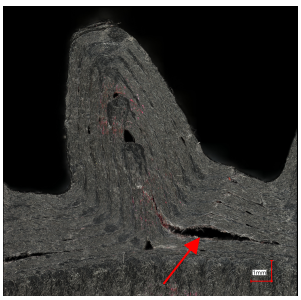
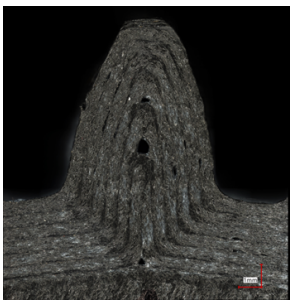
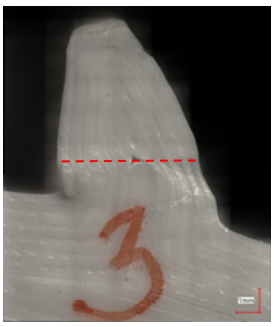
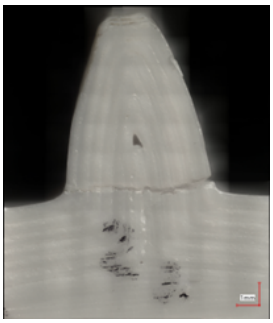
Material	Static bending strength [MPa]	Standard deviation [MPa]	Average max. displacement [mm]	Standard deviation [mm]
ABS	111.2	4.4	4.6	0.4
"Igumid" P150-PF	126.2	3.5	3.3	0.3
"Iglidur" I150-PF	79.6	1.5	5.1	0.2

Table 4 contains pictures of the teeth of given gears in three states: before the test (as a reference tooth), after the static test and the fatigue test. Before the examination, the teeth were compact, with slight defects in the tooth axis. It is caused by inaccurate generation of the material deposition path.

However, the software used to prepare the manufacturing process does not have the option of manually modifying the course of the tracks. This defect clearly affects the way the teeth are deformed during static tests. In the case of ABS and "Iglidur" I150-PF, the defect in the form of a hole resulting from the lack extrusion (red narrow on the reference tooth picture) is on the edge of the plastic deformation of the tooth.

It is caused by a sudden change of the tooth cross-sectional area, which results in a concentration of stresses in this area. In the case of "Igumid" P150-PF material, the tooth was deformed as a result of breaking the connection between successive contours. This proves that a single fiber is stronger than the connections between the contours. The reduction of the adhesive strength may be influenced by the impurities of fibers in the material, which improve the properties of the fiber itself but reduce the ability to create connections between them.

Table 5. Photos of teeth before and after bending tests

Materials	Reference tooth	After static bending test	After fatigue bending test
ABS			
"Igumid" P150-PF			
"Iglidur" I150-PF			

In Figure 4 presents the results of fatigue bending tests of the teeth of gears made of the considered materials. The tests were carried out with a total deformation value of 0.7 mm. This value was determined on the basis of a static tooth bending test, so that it belonged to the elastic-plastic range of the material.

The study was stopped when 10^5 cycles were reached or a tooth was broken. Due to the different stiffness of the teeth made of given materials, the generated load was varied. Each of the tested materials showed cyclical weakening, in particular ABS, the load value of which in half the number of cycles needed to fail (2 500) decreased by 50 %. "Iglidur" I150-PF, which, due to its higher plasticity, was destroyed after more than six times the number of cycles.

However, unlike ABS, the material weakening during the test was 34 %. The teeth made of "Igumid" P150-PF showed the higher durability. The material reached the cycle limit of 10^5 with a material weakening of 33 %. The photos of the teeth in Table 5 show the fracture site. Broken teeth break in the area of the tooth root, and the course of the crack is similar to that of steel teeth.

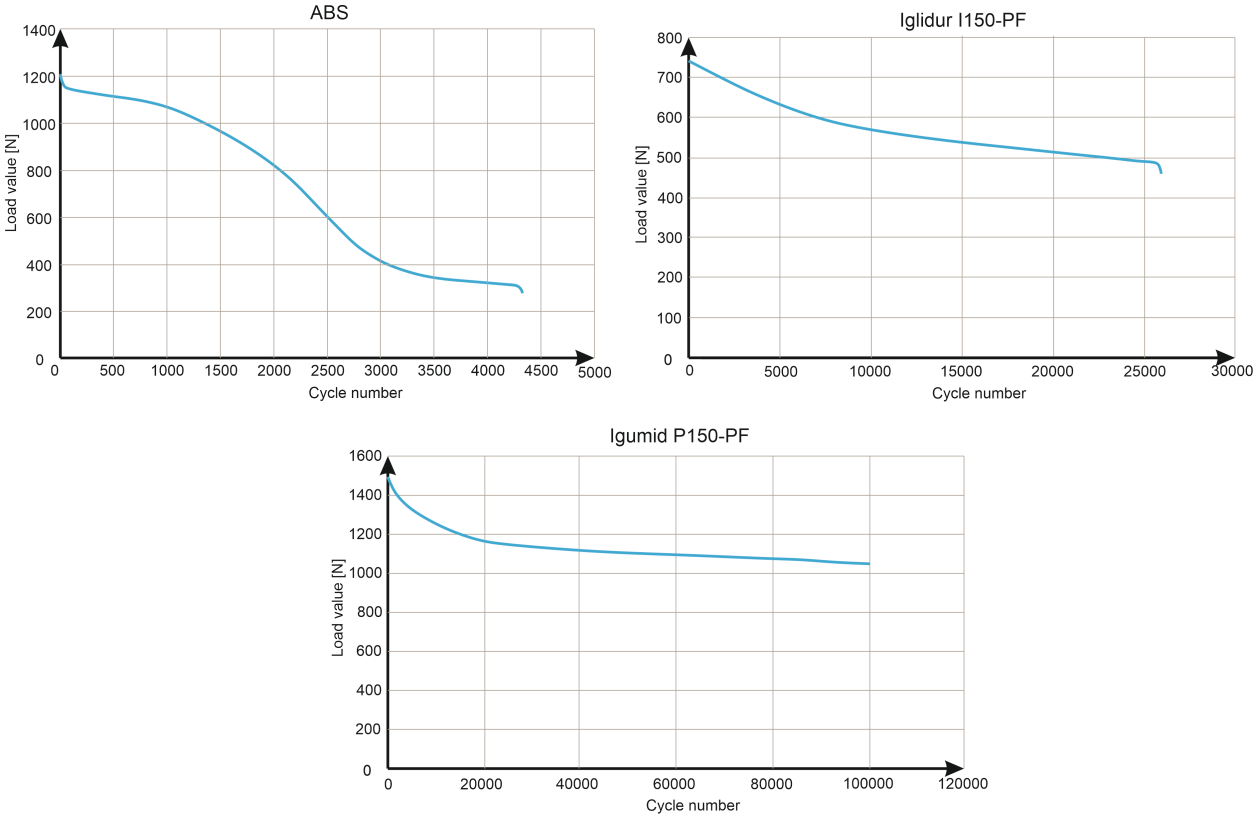


Fig. 4. Results of pilot fatigue tests of tooth bending at the base of gears made of ABS, "Igumid" P150-PF, "Iglidur" I150-PF made using the FDM technology

This proves that the defect located in the tooth axis has no influence on the bending fatigue strength at the base of the tooth.

5. Conclusions

The tests carried out in the field of dimensional accuracy, as well as static and fatigue strength, showed the usefulness of Additive Manufacturing in the production of gears, but with certain limitations. The analysis of the obtained research results allows for the following conclusions:

- gears manufactured using the FDM technology are characterized by low dimensional accuracy, which does not allow to be assigned any class of accuracy according to DIN 3962;
- the gears made of ABS were characterized by the highest geometrical deviations, the main reason of which was the thermal shrinkage of the material;
- the highest stiffness during the static bending tests was registered in the case by the teeth made of "Igumid" P150-PF (the highest load value at the lowest displacement);
- the mechanism of tooth destruction during the static bending test is mainly based on the plastic deformation of the tooth head;
- the highest fatigue strength was characteristic of "Igumid" P150-PF gears, which were not damaged in the considered load range and number of cycles;
- the use of ABS can be an alternative to "Igumid" P150-OF material in the field of static loads, but its low fatigue life does not justify its use in the field of cyclic loads.

Future work will focus on extending the load range of fatigue tests, as well as additional observations of fractures to determine the course of cracking.

References

[1] Klimek, A., Kluczyński, J., Łuszczek, J., Bartnicki, A., Grzelak, K. Małek, M. Wear analysis of additively manufactured slipper-retainer in the axial piston pump [Internet]. *Materials* (Basel), 2022, 15. Available from: https://doi.org/10.3390/ma15061995 (accessed on 16-06-2022).

[2] Campbell, I., Bourell, D., Gibson, I. Additive Manufacturing: Rapid prototyping comes of age [Internet]. *Rapid Prototyping Journal*, 2012, 18, 255–258. Available from: https://doi.org/10.1108/13552541211231563 (accessed on 16-06-2022).

[3] Gibson, I., Rosen, D. W., Stucker. B. *Additive Manufacturing Technologies: Rapid Prototyping to Direct Digital Manufacturing* [Internet]. Springer US, 2010. Available from: https://doi.org/10.1007/978-1-4419-1120-9 (accessed on 16-06-2022).

[4] Levy, G., Schindel, R., Kruth, J. Rapid manufacturing and rapid tooling with Layer Manufacturing (LM) technologies, state of the art and future perspectives. *CIRP Annals*, 2003, 52.

[5] Szachogłuchowicz, I., Śnieżek, L., Ślęzak, T. Mechanical properties analysis of explosive welded sheet of AA2519-Ti6Al4V with interlayer of AA1050 subjected to heat-treatment [Internet]. *Materials* (Basel), 2022, 15. Available from: https://doi.org/10.3390/ma15114023 (accessed on 16-06-2022).

[6] Fras, T., Szachogluchowicz, I., Sniezek, L. Ti6Al4V-AA1050-AA2519 explosively-cladded plates under impact loading [Internet]. *European Physical Journal-Special Topics*, 2018, 227, 17–27. Available from: https://doi.org/10.1140/epjst/e2018-00114-9 (accessed on 16-06-2022).

[7] Sniezek, L., Szachogluchowicz, I., Wachowski, M., Torzewski, J., Mierzynski, J. High cycle fatigue properties of explosively welded laminate AA2519/AA1050/Ti6Al4V [Internet]. *Procedia Structural Integrity*, 2017, 5, 422–429. Available from: https://doi.org/10.1016/j.prostr.2017.07.191 (accessed on 16-06-2022).

[8] Szachogluchowicz, I., Sniezek, L., Sulym, H., Gloc, M. Testing and verification modeling of wave-shape formation under explosion welding to laminate AA 2519-Ti6Al4V [Internet]. *Procedia Structural Integrity* 2016, 2, 2375–2380. Available from: https://doi.org/10.1016/j.prostr.2016.06.297 (accessed on 16-06-2022).

[9] Grzelak, K., Łaszcz, J., Polkowski, J., Mastalski, P., Kluczyński, J., Łuszczek, J., Torzewski, J., Szachogłuchowicz, I., Szymaniuk, R. Additive Manufacturing of plastics used for protection against COVID-19 – The influence of chemical disinfection by alcohol on the properties of ABS and PETG polymers [Internet]. *Materials* (Basel), 2021, 14. Available from: https://doi.org/10.3390/ma14174823 (accessed on 27-06-2022).

[10] Gor, M., Soni, H., Wankhede, V., Sahlot, P., Grzelak, K., Szachgluchowicz, I., Kluczyński, J. A critical review on effect of process parameters on mechanical and microstructural properties of powder-bed fusion Additive Manufacturing of SS316l [Internet]. *Materials* (Basel), 2021, 14. Available from: https://doi.org/10.3390/ma14216527 (accessed on 27-06-2022).

[11] Grzelak, K., Kluczyński, J., Szachogłuchowicz, I., Łuszczek, J., Śnieżek, L., Torzewski, J. Modification of structural properties using process parameters and surface treatment of monolithic and thin-walled parts obtained by selective laser melting [Internet]. *Materials* (Basel), 2020, 13, 1–12. Available from: https://doi.org/10.3390/ma13245662 (accessed on 27-06-2022).

[12] Kluczyński, J., Śnieżek, L., Grzelak, K., Torzewski, J., Szachogłuchowicz, I., Oziębło, A., Perkowski, K., Wachowski, M., Małek, M. The influence of heat treatment on low cycle fatigue properties of selectively laser melted 316l steel [Internet]. *Materials* (Basel), 2020, 13, 1–20. Available from: https://doi.org/10.3390/ma13245737 (accessed on 27-06-2022).

[13] Kluczyński, J., Śniezek, L., Grzelak, K., Oziębło, A., Perkowski, K., Torzewski, J., Szachogłuchowicz, I., Gocman, K., Wachowski, M., Kania, B. Hot isostatic pressing influence on the mechanical properties of selectively laser-melted 316L steel [Internet]. *Bulletin of the Polish Academy of Sciences / Technical Sciences*, 2020, 68, 1413–1424. Available from: https://doi.org/10.24425/bpasts.2020.135396 (accessed on 27-06-2022).

[14] Fikus, B., Grzelak, K., Torzewski, J. *Selective Laser Melted M300 Maraging Steel – Material*, 2021.

[15] Łuszczek, J. Review of the method design and Additive Manufacturing of gears [Internet]. *Bulletin of the Military University of Technology*, 2021, 70, 15–34. Available from: Available from: https://doi.org/10.5604/01.3001.0015.7008 (accessed on 27-06-2022).

[16] Cader, M., Blicharz, B. The analysis of wear of thermoset material gears manufactured using Additive Manufacturing [Internet]. *Mechanik*, 2015, 557/93-557/100. Available from: https://doi.org/10.17814/mechanik.2015.7.218 (accessed on 27-06-2022).

[17] Harsha, K. M., Seetharama Rao, Y., Jagannadha Rao, D. Comparison of wear behaviour of polymer spur gears using FDM process [Internet]. *IOP Conference Series: Materials Science and Engineering*, 2021, 1168, 012028. Available from: https://doi.org/10.1088/1757-899x/1168/1/012028 (accessed on 27-06-2022).

[18] Pandian, A K., Gautam, S. S., Senthilvelan, S. Effect of layer orientation on the single tooth bending fatigue strength of polymer gears manufactured by selective laser sintering [Internet]. *Proceedings of the Institution of Mechanical Engineers, Part L: Journal of Materials: Design and Applications*, 2022, 236, 1557–1573. Available from: https://doi.org/10.1177/14644207221074902 (accessed on 27-06-2022).

[19] Pandian, A. K., Gautam, S. S., Senthilvelan, S. Comparison of the bending fatigue performances of selective laser sintered and injection moulded nylon spur gears [Internet]. *Proceedings of the Institution of Mechanical Engineers, Part L: Journal of Materials: Design and Applications*, 2022, 236, 513–523. Available from: https://doi.org/10.1177/14644207211047376 (accessed on 27-06-2022).

[20] Zmindak, M., Kaco, M., Sapietova, A. Analysis of the contact stresses of spur gears manufactured by 3D printing from composite materials [Internet]. *MATEC Web of Conferences*, 2022, 357, 06003. Available from: https://doi.org/10.1051/matecconf/202235706003 (accessed on 27-06-2022).

[21] Bharti, S., Selvaraj, S. Performance of selective laser sintered polyamide spur gear under dry and lubricated conditions [Internet]. *Proceedings of the Institution of Mechanical Engineers, Part J: Journal of Engineering Tribology*, 2022, 1–11. Available from: https://doi.org/10.1177/13506501221116221 (accessed on 27-06-2022).

[22] Pisula, J., Budzik, G., Turek, P., Cieplak, M. An analysis of polymer gear wear in a spur gear train made using FDM and FFF methods based on tooth surface topography assessment [Internet]. *Polymers* (Basel), 2021, 13. Available from: https://doi.org/10.3390/polym13101649 (accessed on 27-06-2022).
[23] Zumofen, L., Kirchheim, A. Feasibility investigation of gears manufactured by fused filament fabrication [Internet]. *Conference Proceedings Industrializing Additive Manufacturing*, 2021. Available from: https://doi.org/10.1007/978-3-030-54334-1 (accessed on 16-06-2022).
[24] Dennig, H.-J., Monn, S., Vodermayer, A. Thermoplastic high performance composite gears [Internet]. *International Conference on Gears*, 2019, 1279–1290. Available from: https://doi.org/10.51202/9783181023556-1279 (accessed on 16-06-2022).
[25] Skawiński, P., Siemiński, P., Błazucki, P. Applications of Additive Manufacturing (FDM method) in the manufacturing of gear [Internet]. *Mechanik*, 2015, 976/173-976/179. Available from: https://doi.org/10.17814/mechanik.2015.12.582 (accessed on 16-06-2022).
[26] Kim, J., Kang, B. S. Enhancing structural performance of short fiber reinforced objects through customized tool-path [Internet]. *Applied Sciences*, 2020, 10, 1–19. Available from: https://doi.org/10.3390/app10228168 (accessed on 16-06-2022).
[27] García-García, R., González-Palacios, M. A. Method for the geometric modeling and rapid prototyping of involute bevel gears [Internet]. *The International Journal of Advanced Manufacturing Technology*, 2018, 98, 645–656. Available from: https://doi.org/10.1007/s00170-018-2246-9 (accessed on 16-06-2022).

International Forum on Innovative Technologies and Management for Sustainability – ITMS'2022

ktu 1922 panevėžys faculty of technologies and business

International Scientific Conference Intelligent Technologies in Logistics and Mechatronics Systems – ITELMS'2022, 15th September, 2022, Panevėžys, Lithuania

Selecting Military Transport Options, Taking Into Account Cost Analysis, Part 1 – Theoretical Basis

Jarosław Ziółkowski[a]*, Volodymyr Hutsaylyuk[a], Daniel Łukasiak[a]

[a]*Military University of Technology, Faculty of Mechanical Engineering, 2 Gen. S. Kaliskiego St., Warsaw 00-908, Poland*

Abstract

Transportation costs represent significant part of entire logistic costs incurred by companies and that is why a considerable significance is attached to seek solutions to reduce expenditure in this area. Company managers specializing in logistics may need support because they often face decision problem related with selecting the most economical transportation option. The objective of this paper are methods for assessing available variants of realization carriages and they are based on analysing components such as cost structure, demand for transportation services, expected value and break-even point. The example that was taken to implement developed methodology were freights carried out within a military distribution network. This network was reflected on the basis of the Regional Logistic Base notes operating in the Polish Armed Forces.

© 2022 Jarosław Ziółkowski, Volodymyr Hutsaylyuk, Daniel Łukasiak.
Peer-review under responsibility of the Kaunas University of Technology, Panevėžys Faculty of Technologies and Business.

Keywords: Road transport; Distribution networks; Transport problems; Costs.

1. Introduction

Contemporary road transport is a popular field of scientific research. There is a vast portfolio of mathematical methods that apply to measuring effectiveness of both transport systems and the vehicles themselves or their fleet. The publication in this domain often include issues associated with linear programming [1–3], constitute an outline (concept) for new methods [4–6], algorithm [7] or optimization techniques [8] of the analysed decision-related

* Corresponding author. Tel.: +48 22 261 837301.
E-mail address: jaroslaw.ziolkowski@wat.edu.pl

© 2022 Jarosław Ziółkowski, Volodymyr Hutsaylyuk, Daniel Łukasiak. F916G0008
Peer-review under responsibility of the Kaunas University of Technology, Panevėžys Faculty of Technologies and Business.

problem. Such an issue is often associated with the transport of goods [9], for which basic effectiveness measures are calculated [10–12]. In turn, these measures, supported by appropriate indices, impact customer service level [13, 14].

As part of the research in the field of supplies, the source literature presents various mathematical models regarding decision problems [15, 16], as well as algorithms used to optimize transport processes [17, 18]. For example, the authors of [19, 20] developed mathematical models that simulate the functioning of supply logistic systems enabling the determination of minimum logistics costs, assuming optimal supply schedule arrangements (supply volume at subsequent project implementation stages). The authors of other publications, in their attempt to streamline a studied process or system, focused on:

- minimizing selected cost components [21];
- increasing vehicle fleet efficiency [22, 23];
- improving routing [24, 25] in urban logistics;
- improving planning [26] and optimizing transport routes [27];
- the issue of sustainable development in an urban agglomeration [28];
- reducing the emission of harmful substances into the atmosphere [29, 30];
- minimizing lead time [31] for "perishable" products [32];
- possible application of hydrogen in public transport [33].

The concept of optimizing road transport is extensive in terms of meaning and covers a set of numerous components, such as selecting the quickest and / or shortest route [34], minimizing empty runs [35] or forecasting transports within a distribution network [35]. The possibilities above essentially come down to optimizing the costs of a vehicle fleet managed by a public owner [37]. The aforementioned set of publications did not focus adequate attention on the methodology that enables selecting one of the options that is rational from the cost perspective. Exactly this topic constitutes the subject matter of this paper. The methodology suggested in this article has been verified using an actual military distribution network, based on existing, relatively permanent locations of the hubs under a Regional Logistics Base that functions within the Polish Armed Forces.

2. Procedure

The decision-related problem often experienced by people responsible for organizing a distribution network is selecting the transport option. In particular, the deliberations relate to varied, potentially available options, in other words, whether it is worth investing (buying) or use own fleet in securing own transport needs or acquire fleet through leasing or maybe commission these tasks entirely to a carrier.

The methodology presented in this paper includes taking into account such factors as fixed and variable costs, analysis of expected value and the break-even point. The 3 below variants were taken into account to satisfy transport needs within a military distribution network:

1. Option 1: Transport with own means of transport and using own personnel.
2. Option 2: Using the services of a transport company (carrier) in the on-call mode.
3. Option 3: Acquiring fleet through leasing along with driver remuneration calculations.

The next section presents fundamental cost components for each option.

2.1. *Calculating costs and consumed fuel with respect to each selection option*

a) Transport with own means of transport and using full-time personnel

The calculations commenced with determining the average variable costs from the formula (1):

$$k = d \cdot s; \tag{1}$$

where k – variable cost (distance-dependent); d – distance; s – transport rate [zł/km].

In the case in question, the average variable cost was calculated according to the dependence (2) as:

$$k_{1-1} = \frac{d_1 \cdot \sum_{j=A}^{F}(s_{j,ekspl.} \cdot t_{1,j})}{\sum_{j=A}^{F}(t_{1,j})}; \tag{2}$$

where

d_1 – distance to depot No. 1 [km];

k_{1-1} – average variable cost to depot No. 1 [$\frac{PLN}{delivery}$];

$s_{j,ekspl.}$ – unit operating cost index for the j group of vehicles [$\frac{PLN}{km}$];

$t_{1,j}$ – number of runs to depot No. 1 for the j group.

In order to calculate the average variable cost for the entire distribution network in question, the authors used a weighted average for the total number of runs to all depots, in accordance with the formula below (3):

$$k_{śr.zm.-1} = \frac{\sum_{i=1}^{11}\sum_{j=A}^{F}(d_i \cdot s_{j,ekspl.} \cdot t_{i,j})}{\sum_{i=1}^{11}\sum_{j=A}^{F}(t_{i,j})}; \tag{3}$$

where

d_i – distance to the i depot [km];

$t_{i,j}$ – number of runs to the i depot for the j group of vehicles.

Total fuel consumption for all runs was calculated based on fundamental consumption standards and the dependence below (4) as:

$$Z = \frac{\sum_{i=1}^{11}\sum_{j=A}^{F}(d_i \cdot z_j \cdot t_{i,j})}{100}; \tag{4}$$

where z_j – fuel consumption for the j group of vehicles [$\frac{dm^3}{100\ km}$].

While the average fuel consumption was calculated as:

$$\emptyset Z = \frac{\sum_{i=1}^{11}\sum_{j=A}^{F}(d_i \cdot z_j \cdot t_{i,j})}{\sum_{i=1}^{11}\sum_{j=A}^{F}(d_i \cdot t_{i,j})}. \tag{5}$$

Therefore, the average variable cost due to fuel consumption amounted to:

$$k_{śr.zm.-1} = \frac{\sum_{i=1}^{11}\sum_{j=A}^{F}(d_i \cdot s_{i,MPS} \cdot t_{i,j})}{\sum_{i=1}^{11}\sum_{j=A}^{F}(t_{i,j})} \tag{6}$$

where $s_{j,MPS}$ – unit operating cost index for the j group of vehicles [$\frac{PLN}{km}$].

b) Using the services of a transport company (carrier) in the on-call mode

Option 2 takes into account transport rates for a given tonnage group of runs. The average variable cost within the analysed military transport network was calculated from the formula (7) as:

$$k_{1-2} = \frac{d_1 \cdot \sum_{k=1}^{3}(s_k \cdot t_{1,k})}{\sum_{k=1}^{3}(t_{1,k})}; \quad (7)$$

where k_{1-2} – average variable cost to depot No. 1 $[\frac{PLN}{delivery}]$; s_k – transport rate in the k transport group $[\frac{PLN}{km}]$.

Therefore, the average variable cost within the entire military transport network is (8):

$$k_{śr.zm.-2} = \frac{\sum_{i=1}^{11}\sum_{k=1}^{3}(d_i \cdot s_k \cdot t_{i,k})}{\sum_{i=1}^{11}\sum_{k=1}^{3}(t_{i,k})}. \quad (8)$$

The average fuel consumption in the case of this transport option was not calculated due to its specificity. However, the option takes into account the rate per kilometres.

c) Acquiring fleet through leasing along with driver remuneration calculations

The average variable costs in this case will be calculated based on the average fuel consumption as (9):

$$k_{1-3} = \frac{d_1 \sum_{k=1}^{3}(z_k \cdot t_{1,k}) \cdot c_{ON}}{100 \cdot \sum_{k=1}^{3}(t_{1,k})}; \quad (9)$$

where z_k – average fuel consumption for the k vehicle$[\frac{dm^3}{100\ km}]$; c_{ON} – diesel oil price $[\frac{PLN}{dm^3}]$.

Therefore, the average variable cost for the analysed option within the military transport network is (10):

$$k_{śr.zm.-3} = \frac{\sum_{i=1}^{11}\sum_{k=1}^{3}(d_i \cdot z_k \cdot t_{i,k}) \cdot c_{ON}}{100 \cdot \sum_{i=1}^{11}\sum_{k=1}^{3}(t_{i,k})}. \quad (10)$$

The total fuel consumption for all transports implemented within a year amounted to (11):

$$Z = \frac{\sum_{i=1}^{11}\sum_{j=A}^{F}(d_i \cdot z_k \cdot t_{i,k})}{100}. \quad (11)$$

The average fuel consumption was calculated as (12):

$$\emptyset Z = \frac{\sum_{i=1}^{11}\sum_{j=A}^{F}(d_i \cdot z_j \cdot t_{i,j})}{\sum_{i=1}^{11}\sum_{j=A}^{F}(d_i \cdot t_{i,j})}. \quad (12)$$

2.2. *Expected value, decision tree and break-even analysis*

In order to make a decision on selecting the transport option, it is important to conduct an analysis that determines the cost structure for the options in question; however, the knowledge of the expected demand value is also important. The absence of such information prevents determining, which option generates the lowest expenses. Only combining the cost structure analysis and the demand prediction enables making the ultimate decision.

The expected value is calculated according to formula (13) in order to take into account the assumed demand level and its probability. This value is the product of probability and the financial result for a given scenario.

$$WO_j = \sum_{i=1}^{n} P_i C_{i,j}; \quad (13)$$

where: WO_j – expected value of the j option; P_i – probability of the i scenario becoming a reality; $C_{i,j}$ – financial result of the i scenario for the j option [PLN].

Moreover, decision trees are also used within the decision-making theory. They constitute a graphic representation of the possible transport options within a case in question, and their objective behind developing them is making the right choice. The help visualizing even very complex decision series and their financial outcomes, as well as taking into account the risk level associated with individual options. They contain a decision node (*i.e.*, the addressed issue), with branches symbolizing possible choice variants. The nodes where a decision has to be made are symbolized by rectangles, while random points (representing demand), which are beyond the control of the decision-maker are in the form of circles. Each of the branches should be assigned the probability of a given outcome, bearing in mind, however, that the total probability branching from a single random node must be equal to 1. Decisions based on expected value analysis require calculating the financial results individually for each branch (scenario), followed by calculating weighted averages for thicker branches (choice variants) based on the probability of different outcomes. The analysis in commercial enterprises also takes the break-even point into account. It is interpreted as an operation intensity level measured by the number of deliveries, at which total revenue is higher than total costs. Therefore, above this point, the enterprises start making profits, while below it, which is understandable, loses money. The break-even point is calculated from the formula (14):

$$PR = \frac{K_S}{P_j - K_{zj}}; \tag{14}$$

where PR – break-even point; K_S – fixed costs [PLN]; P_j – unit revenue [PLN], K_{zj} – average variable unit cost [PLN].

It is difficult to speak of the break-even point in the case in question, which refers to a military transport network, since the Polish Armed Forces are not a profit-oriented institution (enterprise), and the primary objective of transport operations is the execution of specific tasks. For this reason, no break-event points for the considered options were calculated within this paper (see part 2 – numerical example).

3. Conclusions

The issue discussed in this elaboration is significant due to the fact that transport costs constitute a considerable part in the total expenses incurred by an enterprise. As can be seen in the example above, depending on the chosen transport method, the transport costs can differ significantly between individual methods and making the optimal choice may considerably impact the expenses incurred. The suitability of the presented methodology can be observed in practical embodiments related to real problems associated with selecting the transport option. The presented transport option selection methodology can be applied in relation to other transport issues, also occurring within civilian enterprises. The operational algorithm does not differ much in other cases from the one presented on the example of a military transport network. The second part (Selecting military transport options, taking into account cost analysis, part 2 – numerical example) contains a practical application example of the methodology described in this publication.

References

[1] An, J., Mikhaylov, A., Jung, S. U. A linear programming approach for robust network revenue management in the airline industry [Internet]. *Journal of Air Transport Management*, 2021, 91. Available from: doi:10.1016/j.jairtraman.2020.101979 (accessed on 01-08-2022).

[2] Park, C. H., Lim, H. A parametric approach to integer linear fractional programming: Newton's and hybrid-newton methods for an optimal road maintenance problem [Internet]. *European Journal of Operational Research*, 2021, 289, 1030–1039. Available from: doi:10.1016/j.ejor.2019.07.010 (accessed on 01-08-2022).

[3] Angelelli, E., Morandi, V., Savelsbergh, M., Speranza, M. G. System optimal routing of traffic flows with user constraints using linear programming [Internet]. *European Journal of Operational Research*, 2021, 293, 863–879. Available from: doi:10.1016/j.ejor.2020.12.043 (accessed on 01-08-2022).

[4] Karagul, K., Sahin, Y. A novel approximation method to obtain initial basic feasible solution of transportation problem [Internet]. *Journal of King Saud University – Engineering Sciences*, 2020, 32, 211–218. Available from: doi:10.1016/j.jksues.2019.03.003 (accessed on 01-08-2022).
[5] Karthiyayini, P. G., Ananthalakshmi, S., Parameswari, U. R. An innovative method to solve transportation problem based on a statistical tool [Internet]. *Advances in Mathematics: Scientific Journal*, 2020, 9, 2533–2539. Available from: doi:10.37418/amsj.9.5.16 (accessed on 05-08-2022).
[6] Pargar, F., Ganji, A. P., Bajgan, H. R. A novel approach for obtaining initial basic solution of transportation problem [Internet]. International *Journal of Industrial and Systems Engineering*, 2012, 12, 84–99. Available from: doi:10.1504/IJISE.2012.048286 (accessed on 05-08-2022).
[7] Mnif, M., Bouamama, S. A New multi-objective firework algorithm to solve the multimodal planning network problem [Internet]. *International Journal of Applied Metaheuristic Computing*, 2020, 11, 91–113 Available from: doi:10.4018/IJAMC.2020100105 (accessed on 05-08-2022).
[8] Theeraviriya, C., Pitakaso, R., Sethanan, K., Kaewman, S., Kosacka-Olejnik, M. A new optimization technique for the location and routing management in agricultural logistics [Internet]. *Journal of Open Innovation: Technology, Market, and Complexity*, 2020, 6. Available from: doi:10.3390/joitmc6010011 (accessed on 05-08-2022).
[9] Hosseini, A., Sahlin, T. An optimization model for management of empty containers in distribution network of a logistics company under uncertainty [Internet]. *Journal of Industrial Engineering International*, 2019, 15, 585–602. Available from: doi:10.1007/s40092-018-0286-2 (accessed on 05-08-2022).
[10] Sharafutdinova, N., Palyakin, R., Shafigullina, A. Development of employee performance indicators in the online environment [Internet]. *Lecture Notes in Civil Engineering*, 2022, 190, 257–268. Available from: doi:10.1007/978-3-030-86047-9_27 (accessed on 05-08-2022).
[11] Tikhonov, A. I., Sazonov, A. A., Chursin, A. A. The analysis of foreign planning, development, and quality systems for the production of helicopter technology in the world market [Internet]. *Lecture Notes in Networks and Systems*, 2020, 115, 663–674. Available from: doi:10.1007/978-3-030-40749-0_79 (accessed on 05-08-2022).
[12] Stawowy, M., Rosiński, A., Siergiejczyk, M., Perlicki, K. Quality and reliability-exploitation modelling of power supply systems [Internet]. *Energies*, 2021, 14. Available from: doi:10.3390/en14092727 (accessed on 05-08-2022).
[13] Rassam, A. R., Tammim, K., Abualrejal, H. M. E., Mohammed, F., Al-kumaim, N. H., Fazea, Y. The impact of sales promotion on consumer of GSM in Yemen: MTN-Yemen [Internet]. *Lecture Notes in Networks and Systems*, 2022, 299, 638–645. Available from: doi:10.1007/978-3-030-82616-1_52 (accessed on 05-08-2022).
[14] Singhvi, V., Srivastava, P. Evaluation of consumer reviews for adidas sports brands using data mining tools and *Twitter* APIs [Internet]. *International Journal of Service Science, Management, Engineering, and Technology*, 2021, 12, 89–104. Available from: doi:10.4018/IJSSMET.2021110106 (accessed on 05-08-2022).
[15] Aydoğdu, B., Özyörük, B. Mathematical model and heuristic approach for solving dynamic vehicle routing problem with simultaneous pickup and delivery: Random iterative local search variable neighborhood descent search [Internet]. *Journal of the Faculty of Engineering and Architecture of Gazi University*, 2020, 35, 563–580. Available from: doi:10.17341/gazimmfd.490179 (accessed on 01-08-2022).
[16] Ghayour-Baghbani, F., Asadpour, M., Faili, H. MLPR: Efficient influence maximization in linear threshold propagation model using linear programming [Internet]. *Social Network Analysis and Mining*, 2021, 11. Available from: doi:10.1007/s13278-020-00704-0 (accessed on 01-08-2022).
[17] Al Theeb, N., Smadi, H. J., Al-Hawari, T. H., Aljarrah, M. H. Optimization of vehicle routing with inventory allocation problems in cold supply chain logistics [Internet]. *Computers and Industrial Engineering*, 2020, 142. Available from: doi:10.1016/j.cie.2020.106341 (accessed on 01-08-2022).
[18] Mandal, J., Goswami, A., Wang, J., Tiwari, M. K. Optimization of vehicle speed for batches to minimize supply chain cost under uncertain demand [Internet]. *Information Sciences*, 2020, 515, 26–43. Available from: doi:10.1016/j.ins.2019.12.009 (accessed on 01-08-2022).
[19] Ziółkowski, J., Zieja, M., Oszczypała, M. *Forecasting of the Traffic Flow Distribution in the Transport Network*, 2019, 1476–1480.
[20] Ziółkowski, J., Lęgas, A. Problem of modelling road transport [Internet]. *Journal of Konbin*, 2019, 49, 159–193. Available from: doi:10.2478/jok-2019-0055 (accessed on 01-08-2022).
[21] Zieja, M., Ziółkowski, J., Oszczypała, M. *Comparative Analysis of Available Options for Satisfying Transport Needs Including Costs*, 2019, 1433–1438.
[22] Guimarães, L. R., Athayde Prata, B. D., De Sousa, J. P. *Models and Algorithms for Network Design in Urban Freight Distribution Systems*, 2020, 47, 291–298.
[23] Schaefer, M., Cap, M., Mrkos, J., Vokrinek, J. *Routing a Fleet of Automated Vehicles in a Capacitated Transportation Network*, 2019, 8223–8229.
[24] Yaghoubi, A., Akrami, F. Proposing a new model for location – Routing problem of perishable raw material suppliers with using meta-heuristic algorithms [Internet]. *Heliyon*, 2019, 5. Available from: doi:10.1016/j.heliyon.2019.e03020 (accessed on 05-08-2022).
[25] Pourazarm, S., Cassandras, C. G., Wang, T. Optimal routing and charging of energy-limited vehicles in traffic networks [Internet]. *International Journal of Robust and Nonlinear Control*, 2016, 26, 1325–1350. Available from: doi:10.1002/rnc.3409 (accessed on 05-08-2022).
[26] Liu, Z., Song, Z. Strategic planning of dedicated autonomous vehicle lanes and autonomous vehicle / toll lanes in transportation networks [Internet]. *Transportation Research Part C: Emerging Technologies*, 2019, 106, 381–403. Available from: doi:10.1016/j.trc.2019.07.022 (accessed on 05-08-2022).

[27] Ahmed, L., Mumford, C., Heyken-Soares, P., Mao, Y. *Optimising Bus Routes with Fixed Terminal Nodes: Comparing Hyper-Heuristics with NSGAII on Realistic Transportation Networks*, 2019, 1102–1110.
[28] Torbacki, W. Achieving sustainable mobility in the Szczecin metropolitan area in the post-COVID-19 era: The DEMATEL and PROMETHEE II approach [Internet]. *Sustainability* (Switzerland), 2021, 13. Available from: doi:10.3390/su132212672 (accessed on 05-08-2022).
[29] Szkutnik-Rogoż, J., Ziółkowski, J., Małachowski, J., Oszczypała, M. Mathematical programming and solution approaches for transportation optimisation in supply network [Internet]. *Energies*, 2021, 14. Available from: doi:10.3390/en14217010 (accessed on 05-08-2022).
[30] Wróblewski, P., Lewicki, W. A Method of analyzing the residual values of low-emission vehicles based on a selected expert method taking into account stochastic operational parameters [Internet]. *Energies*, 2021, 14. Available from: doi:10.3390/en14216859.
[31] Ziółkowski, J., Lęgas, A., Szymczyk, E., Małachowski, J., Oszczypała, M., Szkutnik-Rogoż, J. Optimization of the delivery time within the distribution network, taking into account fuel consumption and the level of carbon dioxide emissions into the atmosphere [Internet]. *Energies*, 2022, 15. Available from: doi:10.3390/en15145198.
[32] Małachowski, J., Zrek, J., Ziółkowski, J., Lęgas, A. Application of the transport problem from the criterion of time to optimize supply network with products "Fast-Running". *Journal of Konbin*, 2020, 49, 127–137 Available from: doi:10.2478/jok-2019-0079 (accessed on 01-08-2022).
[33] Pyza, D., Gołda, P., Sendek-Matysiak, E. Use of hydrogen in public transport systems [Internet]. *Journal of Cleaner Production*, 2022, 335. Available from: doi:10.1016/j.jclepro.2021.130247 (accessed on 01-08-2022).
[34] Hussein, H. A., Shiker, M. A. K. *A Modification to Vogel's Approximation Method to Solve Transportation Problems*, 2020, 1591.
[35] Ziółkowski, J., Lęgas, A. Minimisation of empty runs in transport [Internet]. *Journal of Konbin*, 2018, 48, 465–491. Available from: doi:10.2478/jok-2018-0067 (accessed on 01-08-2022).
[36] Hosseini, B., Tan, B. Modeling and analysis of a cooperative service network [Internet]. *Computers and Industrial Engineering*, 2021, 161. Available from: doi:10.1016/j.cie.2021.107620 (accessed on 01-08-2022).
[37] Andrzejczak, K., Selech, J. Quantile analysis of the operating costs of the public transport fleet [Internet]. *Transport Problems*, 2017, 12, 103–111. Available from: doi:10.20858/tp.2017.12.3.10 (accessed on 01-08-2022).

International Forum on Innovative Technologies and Management for Sustainability – ITMS'2022

International Scientific Conference Intelligent Technologies in Logistics and Mechatronics Systems – ITELMS'2022, 15th September, 2022, Panevėžys, Lithuania

Selecting Military Transport Options, Taking Into Account Cost Analysis, Part 2 – Numerical Example

Jarosław Ziółkowski[a]*, Volodymyr Hutsaylyuk[a], Daniel Łukasiak[a]

[a]*Military University of Technology, Faculty of Mechanical Engineering, 2 Gen. S. Kaliskiego St., Warsaw 00-908, Poland*

Abstract

Transportation costs represent significant part of entire logistic costs incurred by companies and that is why a considerable significance is attached to seek solutions to reduce expenditure in this area. Company managers specializing in logistics may need support because they often face decision problem related with selecting the most economical transportation option. The objective of this paper are methods for assessing available variants of realization carriages and they are based on analyzing components such as cost structure, demand for transportation services, expected value and break-even point. The example that was taken to implement developed methodology were freights carried out within a military distribution network. This network was reflected on the basis of the Regional Logistic Base notes operating in the Polish Armed Forces.

© 2022 Jarosław Ziółkowski, Volodymyr Hutsaylyuk, Daniel Łukasiak.
Peer-review under responsibility of the Kaunas University of Technology, Panevėžys Faculty of Technologies and Business.

Keywords: Road transport; Distribution networks; Transport problems; Costs.

1. Introduction

The issue related to transport costs is gaining particular importance due to global inflation caused by, among others, the aggression of the Russian Federation on independent Ukraine. The main cost components in relation to a vehicle fleet are the rising fuel prices and driver salaries. Therefore, it is crucial to look for solutions aimed at maintaining entity competitiveness on the market. One of the methods of looking for savings is ecodriving, which has a tangible value in enterprises with a fleet of a dozen or so or several dozen vehicles. In addition, the age structure of the fleet is

* Corresponding author. Tel.: +48 22 261 83 73 01.
E-mail address: jaroslaw.ziolkowski@wat.edu.pl

© 2022 Jarosław Ziółkowski, Volodymyr Hutsaylyuk, Daniel Łukasiak. F916G0009
Peer-review under responsibility of the Kaunas University of Technology, Panevėžys Faculty of Technologies and Business.

significant, due to the fact that newer vehicle consume less fuel and are more reliable. The topic of cost reduction has been widely addressed in scientific publications.

The authors of [1] proposed vehicle speed optimization for a batch in order to minimize supply chain costs upon an uncertain demand, while Andrzejczak and Selech [2] analysed operating costs for a public transport fleet. In turn, the authors of [3] selected transport options taking into account costs. A considerable part of the source literature contains issues associated with linear programming [4–6], transport modelling [7, 8] and optimization [9–11], including multi-criteria [12–15].

Based on a literature review, it can be concluded that there is a number of studies on transport modelling, including transport optimization. However, the lack of a basic methodology that enables selecting a given transport option, taking into account the cost analysis, is evident. For this reason, a large part of this paper presents an example of estimating the total costs associated with a selected specific transport option (variant) within a military transport network.

2. Analysis of a military distribution network – assumptions

The analysed transport network example is the Regional Logistics Base (RBLog). It is a logistic military unit, the task of which primarily involve satisfying the material and technical needs in the field of reliability. As part of its operations, the unit transports various material and technical goods to several dozen depots.

A transport option selection methodology will be developed based on the information provided by the RBLog that include a list of runs completed in 2020. A diagram of this network after the process of anonymising sensitive data associated with depot location is shown in Figure 1.

Table 1 contains a collective list of transports completed within a given calendar year, as well as distances to individual depots.

The numbers mean the amount of runs on a given route and using given means of transport. The letters of the alphabet symbolize the following vehicles.

- A – “Iveco Eurocargo”;
- B – “Iveco Stralis”;
- C – “Jelcz” P862;
- D – “VW Crafter”;
- E – “Star” 12.220 / “Star” 200 / “Star” 944;
- F – “Fiat Ducato” / “Opel Vivaro”, “Opel Movano” / “Ford Transit” / “Lublin”.

Cost calculations will be conducted in two variants, *i.e.*, based on the total operating costs and based only on fuel consumption. Three transport options will be analysed:

1. Option 1: Transport with own means of transport and using own personnel.
2. Option 2: Using the services of a transport company in the on-call mode.
3. Option 3: Acquiring fleet through leasing along with driver remuneration calculations.

The costs for the first option will be calculated based on [16]. This document is a collective list of costs associated with means of transport maintenance. These values refer to the operation process unit of measure – a kilometre or engine hour.

Table 2 below contains an excerpt from the aforementioned order regarding vehicles operated within the transport network in question.

Fundamental fuel consumption standards that will be required to calculate the consumption have also been listed.

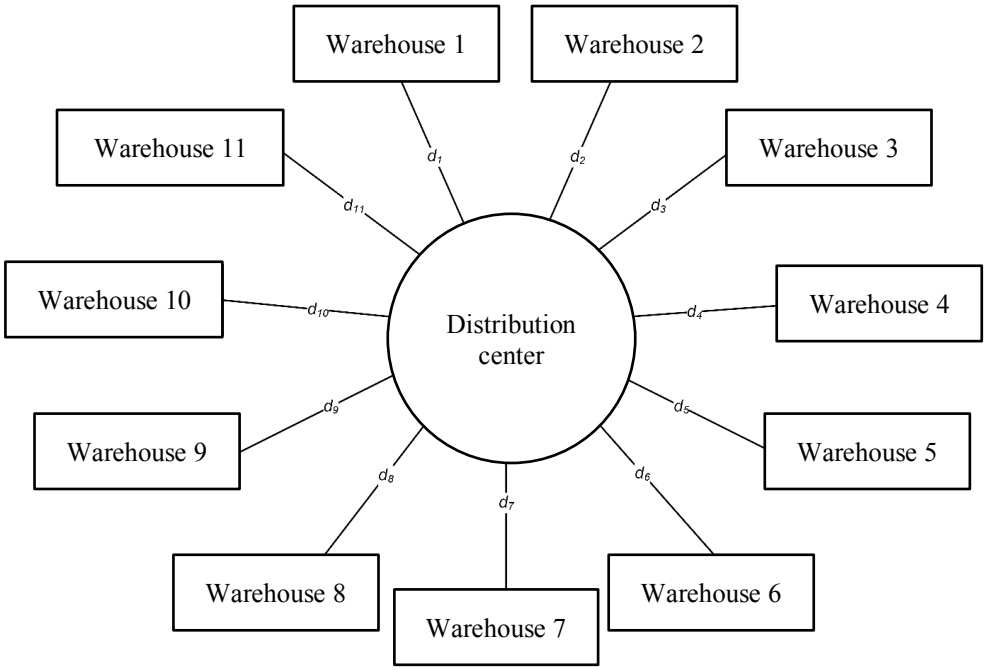


Fig. 1. Schematic diagram of a military transport network

Table 1. Structure of transport tasks executed at 2. RBlog

i	Warehouse	Distance, d_i [km]	Number of cruise trips for each means of transport, $t_{i,j}$						Total cruises, t_i	Percentage, w_i
			Group, j							
			A	B	C	D	E	F		
1	Warehouse 1	93	8	5	2	19	0	0	34	0.033
2	Warehouse 2	51	0	25	0	0	0	29	54	0.052
3	Warehouse 3	156	15	0	12	2	0	9	38	0.037
4	Warehouse 4	73	0	0	31	0	2	0	33	0.032
5	Warehouse 5	208	40	21	0	0	18	0	79	0.076
6	Warehouse 6	202	71	17	0	0	0	115	203	0.196
7	Warehouse 7	192	48	0	9	3	0	42	102	0.098
8	Warehouse 8	296	0	33	0	18	18	0	69	0.066
9	Warehouse 9	219	1	35	0	62	13	10	121	0.117
10	Warehouse 10	255	70	5	0	74	95	39	283	0.273
11	Warehouse 11	32	19	0	0	0	0	3	22	0.021
	TOTAL		**272**	**141**	**54**	**178**	**146**	**247**	**1038**	

After vehicles were grouped (groups with several vehicles) the costs and standards were calculated using the arithmetic mean, based on data from RBLog (see Table 3).

Table 2. Unit cost indicators for the MPS (propellant and lubricant material service) and operation, as well as fundamental fuel consumption standards [16]

i	Name of means of transport	Unit cost index MPS, $s_{i,MPS}$ [zł/km]	Unit operating cost index, $s_{i,ekspl.}$ [zł/km]	Basic fuel consumption standard, z_i [$\frac{dm^3}{100\ km}$]
1	"Iveco Eurocargo"	2.24	15.00	27.7
2	"Iveco Stralis"	2.63	10.80	27.8
3	"Jelcz" P862	3.78	43.02	56.5
4	"VW Crafter"	0.79	3.67	11.5
5	"Star" 12.220	1.46	10.17	29.0
6	"Star" 200	1.43	6.73	22.0
7	"Star" 944	1.72	17.73	22.5
8	"Fiat Ducato"	0.74	2.67	12.3
9	"Opel Vivaro"	0.83	3.05	8.3
10	"Opel Movano"	0.83	4.05	13.5
11	"Ford Transit"	0.77	2.45	12.0
12	"Lublin"	0.83	2.15	14.3

Table 3. Unit costs indicators and standards after consolidation

Group, j	Name of means of transport	Unit cost index MPS, $s_{j,MPS}$ [$\frac{zł}{km}$]	Unit operating cost index, $s_{j,ekspl.}$ [$\frac{zł}{km}$]	Basic fuel consumption standard, z_j [$\frac{dm^3}{100\ km}$]
A	"Iveco Eurocargo"	2.24	15.00	27.67
B	"Iveco Stralis"	2.63	10.80	27.75
C	"Jelcz" P862	3.78	43.02	56.5
D	"VW Crafter"	0.79	3.67	11.50
E	"Star" 12.220, "Star" 200, "Star" 944	1.59	13.95	24.50
F	"Fiat Ducato", "Opel Vivaro", "Opel Movano", "Ford Transit", "Lublin"	0.80	2.87	12.05

In order to consider the second and third options, transports were divided into 3 groups according to the weight criterion, *i.e.*, high-tonnage, medium-tonnage and delivery (marked with the letters "W", "Ś" and "D"). Transports marked with "B" and "C" (high-tonnage), "A" and "E" (medium-tonnage) and "D" and "F" (delivery) were assigned accordingly to these groups. The numbers of transport runs were also aggregated (see Table 4). Total number of runs for individual sets, taking into account three transport types, are listed in Table 5.

The third option assumes purchasing own fleet through leasing (Option 3), while employing own drivers. In order to authoritatively compare each of the variants, it was assumed that leased vehicles would be similar to or same as the means of transport used in the military. In light of the above the following was assumed:

- high-tonnage truck – "Iveco S-Way" (as an equivalent of the no longer manufactured "Stralis" used in the Polish Armed Forces); a configuration with the following parameters was selected: DMC 26.0 t, 6 × 2 pusher axle drive, "Cursor" 9 Euro VI 360 KM engine, 16-speed manual gearbox;
- medium-tonnage truck – "Iveco Eurocargo"; parameters: DMC 16.0 t, 4 × 2 rear axle drive, "Tector" 7 250 KM engine, 9-speed synchronized gearbox;
- delivery van – "VW Crafter"; parameters: DMC 3.5 t, 4 × 4 drive, 2.0,177 KM engine, 6-speed gearbox.

Table 4. List of transport runs completed in 2020 within RBLog, divided into tonnage groups

	I			II			III			IV			V			VI			VII			VIII			IX			X			XI			XII		
	H	M	V	H	M	V	H	M	V	H	M	V	H	M	V	H	M	V	H	M	V	H	M	V	H	M	V	V	H	M	V	H	M	V	H	M
Warehouse 1	0	0	1	2	3	4	0	0	1	0	0	1	0	1	1	0	0	0	1	0	1	2	0	2	0	0	2	2	2	3	0	2	2	0	0	1
Warehouse 2	0	0	1	4	0	4	2	0	2	1	0	1	3	0	5	3	0	1	1	0	2	2	0	1	4	0	3	2	0	3	3	0	2	1	0	4
Warehouse 3	0	0	0	3	3	0	2	3	0	2	3	1	1	0	2	0	1	1	1	0	1	2	0	1	0	2	0	0	1	2	0	1	1	1	1	2
Warehouse 4	1	0	0	1	1	0	5	1	0	1	0	0	1	0	0	5	0	0	3	0	0	3	0	0	3	0	0	3	0	0	3	0	0	2	0	0
Warehouse 5	0	1	0	3	2	0	2	1	0	0	2	0	0	5	0		3	0	0	12	0	5	0	0	3	4	0	3	10	0	3	14	0	0	4	0
Warehouse 6	0	6	2	0	17	11	2	9	12	2	3	11	2	5	8	1	1	10	1	4	4	3	2	12	1	5	8	4	10	14	1	7	13	0	2	10
Warehouse 7	0	2	5	1	7	4	0	2	1	1	6	4	0	1	2	1	2	3	1	5	3	0	3	4	1	7	6	2	6	5	2	5	4	0	2	4
Warehouse 8	2	1	3	4	1	0	1	3	0	2	0	1	4	2	2	6	0	2	0	0	2	3	2	1	3	2	1	0	3	1	3	3	4	5	1	1
Warehouse 9	3	0	1	1	3	2	4	0	6	3	0	2	5	0	8	3	0	10	3	1	9	1	0	4	5	1	8	3	1	2	0	8	10	4	0	10
Warehouse 10	0	7	7	0	13	7	4	17	17	0	15	9	0	10	8	1	10	21	0	12	8	0	8	0	0	23	7	0	13	10	0	24	10	0	13	9
Warehouse 11	0	0	0	0	2	0	0	0	0	0	2	0	0	4	0	0	1	0	0	2	0	0	1	0	0	7	0	0	0	0	0	0	3	0	0	0
TOTAL	**6**	**17**	**20**	**19**	**52**	**32**	**25**	**36**	**39**	**12**	**31**	**30**	**15**	**28**	**36**	**22**	**18**	**4S**	**11**	**36**	**30**	**21**	**16**	**25**	**20**	**51**	**35**	**19**	**46**	**40**	**15**	**64**	**49**	**13**	**23**	**41**
	43			**103**			**97**			**73**			**79**			**88**			**77**			**62**			**106**			**105**			**128**			**77**		

Table 5. Structure of transport tasks executed at 2.RBLog, divided into tonnage groups

i	Warehouse	Distance, d_i [km]	Number of cruise trips for each means of transport, $t_{i,k}$		
			Group, k		
			High-tonnage	Medium-tonnage	Vans
1	Warehouse 1	93	7	8	19
2	Warehouse 2	51	25	0	29
3	Warehouse 3	156	12	15	11
4	Warehouse 4	73	31	2	0
5	Warehouse 5	208	21	58	0
6	Warehouse 6	202	17	71	115
7	Warehouse 7	192	9	48	45
8	Warehouse 8	296	33	18	18
9	Warehouse 9	219	35	14	72
10	Warehouse 10	255	5	165	113
11	Warehouse 11	32	0	19	3

The second option (Option 2) assumes calling and using the services of a transport company in the on-call mode, *i.e.*, every time such a need arises. In order to conduct calculations for this option, the authors obtained actual transport rates applicable in domestic transport. The information was provided by the transport company "BBA Transport System Sp. z o.o. Sp. K.". Estimated rates are shown in Table 6. Averaged values were adopted for the calculations.

Table 6. Transport rates applied in the industry. Source: generic data obtained from "BBA Transport System"

k	Type of transport	Transport rate [PLN/km]
1	High-tonnage	3.3–4.5
2	Medium-tonnage	2.8–3.3
3	Vans	1.5–2

In the case of this option, it was necessary to indicatively estimate fixed costs that would primarily be the expenses associated with fleet maintenance and hiring drivers. Due to the maximum monthly load criterion, it was agreed that it would be necessary to purchase at least one car of the first, three of the second and two of the third type. Moreover, it will be necessary to employ six drivers.

The representatives of "Iveco" and "Volkswagen" were contacted in order to obtain financial information with respect to leasing the aforementioned cars. When purchasing "Iveco" vehicles, it was possible to sign a leasing

agreement for a period of 72 months, and 60 months for "Volkswagen" vehicles. The representatives of the 10th "Warsaw Motor Regiment" (10 WPSAM) and the RBLog provided information on the salaries of civilian drivers. The calculation takes into account a third-party liability insurance offer from "Uniqa". Due to the absence of manufacturer data (except for "VW Crafter" – 9.56 dm^3/100km), fuel consumption was assumed identical as for military equivalents. Fuel prices was obtained from PKN "Orlen" (wholesale price as at 17 December 2021). The data is shown in Table 7.

Table 7. Numerical data for calculating leasing costs. Source: data obtained from Iveco, Volkswagen, 10WPSAM, RBLog and PKN Orlen

k	Type of transport	Unit	Monthly lease payment [PLN]	Monthly driver's rate [PLN]	Average fuel consumption, z_k $[\frac{dm^3}{100\ km}]$
1	"Iveco S-Way"	1	4 559.6	4 160	27.8
2	"Iveco Eurocargo"	3	3 409.93	4 160	27.7
3	"VW Crafter"	2	2 642.44	3 840	9.56
Wholesale price of diesel fuel c_{ON} $[\frac{zł}{m^3}]$					4 746.00

The total annual fixed costs for the presented fleet (human factor included) amounted to PLN 539 332.

3. Fixed and variable cost calculation for individual transport options

The source literature contains a number of cost classification criteria; however, not all are equally significant. In the case in question, it is important to distinguish costs into two basic groups, *i.e.*, fixed and variable. Fixed costs in the analysed transport options generally occur only when purchasing own fleet. The components of these expenses include leasing instalments, driver salaries and third-party liability insurance premiums. Whereas the amount of variable costs varied depending on the selected option. Table 8 lists calculated fixed and variable cost values, as well as expenditure on fuel consumption, as being the main variable cost source.

Table 8. Fixed and variable cost structure

	Option		
	1	2	3
Type	Own transport	Transport on request	Leasing
Fixed costs [PLN]	none	None	539 332
Variable costs [PLN]	2 079	539	195
Fuel consumption $[dm^3]$	45 222.67	-	42 740.61
Average fuel consumption $[\frac{dm^3}{100\ km}]$	21.43	-	20.25
Average variable cost due to fuel consumption [PLN]	331.43	-	195.42

Knowing cost nature and structure enables plotting a dependence of total costs on the transport performance (see Fig. 2). In addition, the data above allows to determine the operation intensity level, at which two selected options generate the same expenses, so-called points of indifference.

The point of indifference analysis (see Fig. 2) indicate that for an intensity level of approximately 286 deliveries, it is unimportant from the cost perspective, which of the two options (own transport or leasing) is selected, since they both generate the same expenses. Similarly, the same costs were obtained for the on-call and leasing transport for an intensity level of approximately 1 568. From the long-term costs perspective, the most beneficial option beyond 1 568 deliveries is leasing.

Table 9 shows total cost calculations for 3 different demand levels. As indicated by the compiled data, option selection depends on demand quantity, *i.e.*, the best option for a small demand is on-call, while in the case of many orders, considering leasing is worthwhile.

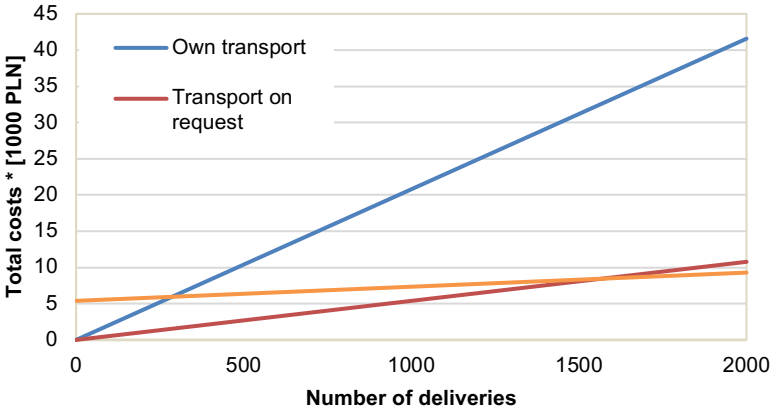


Fig. 2. Total cost dependence as a function of operating intensity for the transport options considered

Table 9. Total cost for various demand levels

Total cost	300 cruise (low demand)	1000 cruise (average demand)	1600 cruise (high demand)
Own transport	623 700	2 079 000	3 326 400
Transport on request 0 zł + x · 539 zł	**161 700**	**53 9000**	862 400
Leasing 539 332 zł + x · 195 zł	597 832	734 332	**851 332**

Table 9 above is only an example of calculations involving selected costs for three hypothetical scenarios. The selection methodology should be based on the probability of each of them, since, de facto, not much is evident from the information that the best option above 1 568 deliveries is leasing, if such a scenario would be unlikely in reality. In such a case, and based on historical (forecast) data, it would be required to determine several possible scenarios and calculate their probability. The results in this respect are shown in Table 10.

Table 10. Selected demand scenarios and their probability

Number of deliveries per month	Number of deliveries per year	Number of realization	Probability [%]
to 70	to 840	2	17
70–90	960	5	42
90–110	1 200	4	33
over 110	over 1 320	1	8

Table 11 lists the financial results for all options, taking into account the four scenarios considered in question.

Table 11. Financial results for the three considered options and four scenarios

Financial result of the i-th scenario for the j-th option, C_{ij} [PLN]			Variant j		
i	Amount of demand [deliveries / year]	Probability of occurrence of a given scenario, P_i [%]	Option 1	Option 2	Option 3
1	to 840	17	1 746 360	**452 760**	703 132
2	960	42	1 995 840	**517 440**	726 532
3	1 200	33	2 494 800	**646 800**	773 332
4	1 320	8	2 744 280	**711 480**	796 732

The expected costs for the considered options were calculated according to the formula (13), with the results depicted in Figure 3.

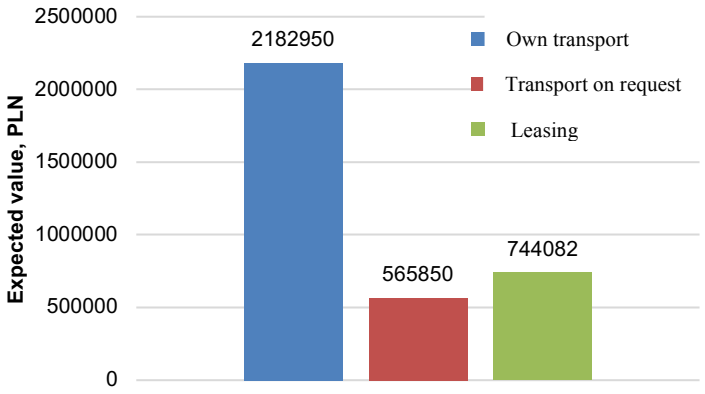


Fig. 3. Expected values for the considered transport options [PLN]

A decision tree for the discussed issue was developed based on the principles above (see Fig. 4).

The conducted analysis enabled demonstrating the rightness in the statement that option 2, which involves using a transport company in the on-call mode is the most suitable for the analysed case, if the cost criterion is taken into account. This does not mean that it is the best solution in general. But if the issue is approached from the economic perspective, it would be the most rational choice. Please note that rather few transport companies would be even willing to accept so many orders at such a small distance, hence, in practice, this type of transport organization would be impossible to implement at all.

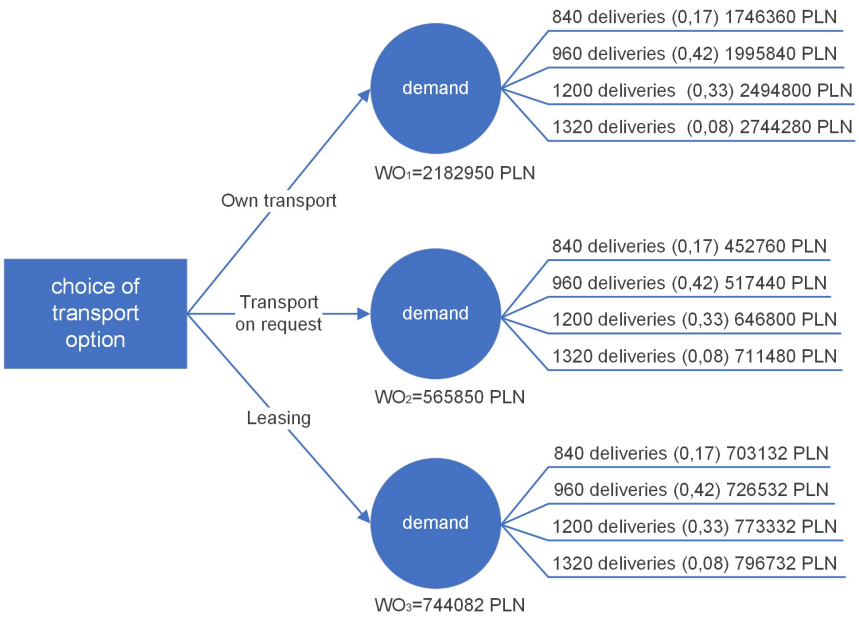


Fig. 4. A decision tree for the choice of transport option

In addition, the supply system of the Polish Armed Forces, in terms of purposefulness, does not function to generate profit. Its main task is to maintain constant availability and task worthiness, which is why it is important for it to have an own transport base. Despite the fact that the option associated with using own fleet is the least economically justified, the Polish Armed Forces should maintain and use own fleet, due to the specificity of its functional objective.

4. Conclusions

Based on paper, it is possible to formulate the following conclusions:

1. Military logistics networks have other objectives than commercial ones, *i.e.*, operating within a civilian market, characterized by the so-called business processes. Their activity is not profit-oriented. Instead, it focuses on maintaining task worthiness.
2. Transport costs are always a significant contributor to the total expenses incurred by an enterprise. Propellant and lubricant consumption is an important component therein.
3. A transport option selection methodology should take into account not only the cost structure but also the forecast demand. Such an approach ensures making an optimal selection decision.
4. Within the analysed case study, transport organization should be based on calling a transport company in each case, while military transport executed using own means of transport turned out the least advantageous in terms of economy. In the case of the on-call transport option, one transport run would cost an average of PLN 539/delivery, while in the case of own transport, the cost would amount to PLN 2 079/delivery.
5. The option associated with leasing would turn out the best only upon a large demand of at least 1 568 deliveries per year; however, such a demand level in military distribution networks is unlikely, which is confirmed by the analysed example. The best option below this demand level would be the on-call transport mode.
6. The average cost per delivery varied depending on the analysed option. Own transport turned out unprofitable due to the significant share of costs associated with fuel consumption – an average of PLN 331.43/delivery. Purchasing vehicles within option 3 (leasing) was also uneconomical due to the high fixed cost of PLN 539 332 per annum. The said variant would be a cost-effective solution only upon a large number of executed deliveries.
7. An analysis of the expected value, which takes the probability of a given scenario into account indicated that, in the considered situation, it would be best to go with the option involving calling a transport company in each case, since the expected value was the lowest and amounted to PLN 565 850 (for comparison, the expected values for the other two options, *i.e.*, own transport and leasing were PLN 2 182 950 and PLN 744 082).
8. However, formulating the above conclusions does not mean that the Polish Army should withdraw from maintaining and using own fleet, since the functional objective of this network is not income-oriented.

References

[1] Mandal, J., Goswami, A., Wang, J., Tiwari, M. K. Optimization of vehicle speed for batches to minimize supply chain cost under uncertain demand [Internet]. *Information Sciences*, 2020, 515, 26–43. Available from: doi:10.1016/j.ins.2019.12.009 (accessed on 05-08-2022).

[2] Andrzejczak, K., Selech, J. Quantile analysis of the operating costs of the public transport fleet [Internet]. *Transport Problems*, 2017, 12, 103–111. Available from: doi:10.20858/tp.2017.12.3.10 (accessed on 05-08-2022).

[3] Zieja, M., Ziółkowski, J., Oszczypała, M. *Comparative Analysis of Available Options for Satisfying Transport Needs Including Costs*, 2019, 1433–1438.

[4] An, J., Mikhaylov, A., Jung, S.-U. A linear programming approach for robust network revenue management in the airline industry. *Journal of Air Transport Management*, 2021, 91. Available from: doi:10.1016/j.jairtraman.2020.101979 (accessed on 05-08-2022).

[5] Park, C. H., Lim, H. A parametric approach to integer linear fractional programming: Newton's and hybrid-newton methods for an optimal road maintenance problem [Internet]. *European Journal of Operational Research*, 2021, 289, 1030–1039. Available from: doi:10.1016/j.ejor.2019.07.010 (accessed on 09-08-2022).

[6] Angelelli, E., Morandi, V., Savelsbergh, M., Speranza, M. G. System optimal routing of traffic flows with user constraints using linear programming [Internet]. *European Journal of Operational Research*, 2021, 293, 863–879. Available from: doi:10.1016/j.ejor.2020.12.043 (accessed on 09-08-2022).

[7] Ziółkowski, J., Lęgas, A. Problem of modelling road transport [Internet]. *Journal of Konbin*, 2019, 49, 159–193. Available from: doi:10.2478/jok-2019-0055 (accessed on 09-08-2022).

[8] Hosseini, B., Tan, B. Modelling and analysis of a cooperative service network [Internet]. *Computers and Industrial Engineering*, 2021, 161. Available from: doi:10.1016/j.cie.2021.107620 (accessed on 09-08-2022).

[9] Al Theeb, N., Smadi, H. J., Al-Hawari, T. H., Aljarrah, M. H. Optimization of vehicle routing with inventory allocation problems in cold supply chain logistics [Internet]. *Computers and Industrial Engineering*, 2020, 142. Available from: doi:10.1016/j.cie.2020.106341 (accessed on 09-08-2022).

[10] Bagheri, M., Ghafourian, H., Kashefiolasl, M., Pour, M. T. S., Rabbani, M. Travel management optimization based on air pollution condition using markov decision process and genetic algorithm (Case study: Shiraz city) [Internet]. *Archives of Transport*, 2020, 53, 89–102. Available from: doi:10.5604/01.3001.0014.1746 (accessed on 05-08-2022).

[11] Cui, H., Qiu, J., Cao, J., Guo, M., Chen, X., Gorbachev, S. Route optimization in township logistics distribution considering customer satisfaction based on adaptive genetic algorithm [Internet]. *Mathematics and Computers in Simulation*, 2023, 204, 28–42. Available from: doi:10.1016/j.matcom.2022.05.020 (accessed on 05-08-2022).

[12] Lee, H. J., Shim, J. K. Multi-objective optimization of a dual mass flywheel with centrifugal pendulum vibration absorbers in a single-shaft parallel hybrid electric vehicle powertrain for torsional vibration reduction [Internet]. *Mechanical Systems and Signal Processing*, 2022, 163. Available from: doi:10.1016/j.ymssp.2021.108152 (accessed on 05-08-2022).

[13] Wu, P., Chu, F., Che, A., Zhao, Y. Dual-objective optimization for lane reservation with residual capacity and budget constraints [Internet]. *IEEE Transactions on Systems, Man, and Cybernetics: Systems*, 2020, 50, 2187–2197. Available from: doi:10.1109/TSMC.2018.2810114 (accessed on 05-08-2022).

[14] Qin, W., Shi, Z., Li, W., Li, K., Zhang, T., Wang, R. Multiobjective routing optimization of mobile charging vehicles for UAV power supply guarantees [Internet]. *Computers and Industrial Engineering*, 2021, 162. Available from: doi:10.1016/j.cie.2021.107714 (accessed on 09-08-2022).

[15] Wang, C., Ma, C., Xu, X. Multi-objective optimization of real-time customized bus routes based on two-stage method [Internet]. *Physica A: Statistical Mechanics and Its Applications*, 2020, 537. Available from: doi:10.1016/j.physa.2019.122774 (accessed on 09-08-2022).

[16] Rozkaz Nr. 25 Szefa Inspektoratu Wsparcia Sił Zbrojnych z dnia 19 lutego 2020 r. *w Sprawie Aktualizacji Jednostkowych Wskaźników Kosztów Eksploatacji Wybranego Sprzętu Służby Czołgowo-Samochodowe*j.

International Forum on Innovative Technologies and Management for Sustainability – ITMS'2022

International Scientific Conference Intelligent Technologies in Logistics and Mechatronics Systems – ITELMS'2022, 15th September, 2022, Panevėžys, Lithuania

The Influence of Aramide Fibers Addition on the Tensile Properties of the Acrylonitrile Butadiene Styrene Dedicated for the FFF Technology

Ireneusz Szachogluchowicz[a]*

[a]*Institute of Robots & Machine Design, Faculty of Mechanical Engineering, Military University of Technology, 2 Gen. S. Kaliskiego St., Warsaw 00-908, Poland*

Abstract

In this article, the results of a study of the mechanical properties of samples produced using the Additive Manufacturing Fused Filament Fabrication technique are presented. The material used to manufacture the test pieces is Acrylonitrile Butadiene Styrene doped with Kevlar. Three variants of printing sample layouts were adopted for the respective fabrication parameters. Monotonic tensile tests were performed and yield strength, tensile strength and total strain were determined. Micro-fractography of the fracture of the samples was presented. The mechanism of the fracture process was determined. It was shown that the pores between the bonding paths are also important. They weaken the material by reducing the surface area and additionally act as notches. This often leads to stress concentrations and the formation of a fracture source. Digital image correlation studies were also carried out on the tested variants. As a result of the tests, the most favourable arrangement of the specimens depending on the loading axis was determined. The test results showed a significant difference between the variants of the specimen arrangement. The force value differs by about 20 % between the variants, while the strain range differs by 280 %. These values indicate how important the correct positioning of the specimens is in relation to the Additive Manufacturing specimen alignment.

© 2022 Ireneusz Szachogluchowicz.
Peer-review under responsibility of the Kaunas University of Technology, Panevėžys Faculty of Technologies and Business.

Keywords: Additive Manufacturing; Fused Filament Fabrication; ABS; Kevlar; Mechanical properties analysis.

* Corresponding author.
E-mail address: ireneusz.szachogluchowicz@wat.edu.pl

© 2022 Ireneusz Szachogluchowicz.
F916G0010
Peer-review under responsibility of the Kaunas University of Technology, Panevėžys Faculty of Technologies and Business.

1. Introduction

The current global economic situation has led to an intensification in the search for new manufacturing and prototyping techniques [1–4]. One of the main developments is the attempt to join materials that are difficult to weld, or not wieldable, by traditional methods [5–7]. A second further direction is rapid material prototyping techniques [8–11]. One of the most popular incremental manufacturing technologies is Fused Filament Fabrication (FFF). The principle of this technology is the direct use of 3D models to prepare the process. During this process, a plastic wire, called filament, is plasticised in a heated nozzle. Once extruded from the nozzle, the plasticised material is transferred to the build platform, where the final shape is created. After the final formation of each layer of material, the build platform is lowered to allow the next layer to be formed. The process is repeated to achieve the final shape of the component. One of the most popular incremental manufacturing technologies is Fused Filament Fabrication (FFF). The principle of this technology is the direct use of 3D models to prepare the process. During this process, a plastic wire, called filament, is plasticised in a heated nozzle. Once extruded from the nozzle, the plasticised material is transferred to the build platform, where the final shape is created. After the final formation of each layer of material, the build platform is lowered to allow the next layer to be formed. The process is repeated to achieve the final shape of the component. The current very popular materials used in the FFF technique are ABS, PLA, PET-G [12–15]. ABS is a scratch-resistant material, as it has high hardness and impact strength. It is safe for humans, non-toxic and resistant to diluted acids, lies, grease and salts. It has very good thermal insulating properties and at the same time does not deform itself when temperatures change. It does not absorb moisture from the air and is unfortunately not resistant to UV radiation. ABS is most commonly used for the manufacture of housings for consumer electronics, electronic devices, automotive components (such car parts as trusses, wheel arches, some body parts). It can also be found in toys, and is used in the manufacture of pipes (resistant to various aggressive environments) and many everyday products. Aramid fibres are a material with enhanced strength properties. It is used in many industries, automotive, special constructions as well as in the defence industry. The current trend is to design layered performance materials with enhanced ballistic resistance [16–18]. This trend also applies to incrementally manufactured materials, which are increasingly being subjected to a range of toughness tests [19–22]. The ever-growing interest in the use of FFF technology and layered materials [23–25] in research and industry was the motivation to analyse the impact of using aramid fibres in an FFF-based material. The aim of this study is to analyse the effect of different orientations on the tensile properties of ABS material reinforced with aramid fibres (10 % of the total volume).

2. Materials and methods

For the test, it was used the Acrylonitrile Butadiene Styrene material provided by the "Spectrum Filaments Ltd. Company". ABS_Kevlar consists of 90 % ABS and 10 % aramid fibers. ABS_Kevlar is a constructive composite fabricated on the basis of ABS with aramid fibers. The addition of fibers used ensures less shrinkage and very good adhesion to the working platforms. The addition of aramid fibers reduces the weight of the material. Excellent dimensional stability allows for 3D printing of objects with exact dimensions, which is especially important in projects consisting of many elements. ABS_Kevlar, which makes the material more thermal-resistant and improved from a mechanical properties point of view.

To reach desirable elements properties it had been designed the following process parameters:

- hotend temperature – 280 °C;
- heatbed temperature – 100 °C;
- chamber temperature – 60 °C;
- layer thickness – 0.2 mm;
- infill – 100 %;
- part cooling intensity: 40 %;
- printing speed – 50 mm/s;
- nozzle diameter – 0.4 mm.

To obtain proper plastic samples, "Intamsys Funmat HT" 3D printer was used. Thanks to the heating building chamber, high-temperature hotend, and heated plate up to 160 °C, proper manufacturing of samples without thermal-stresses was possible. The samples were made in three variants presented in Figure 1.

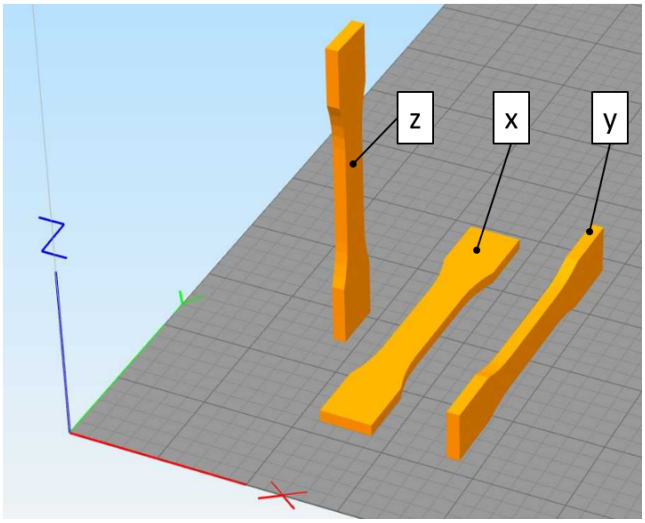


Fig. 1. Orientation of *XYZ* samples relative to the platform

To evaluate the mechanical properties, dog-bone shaped parts were fabricated by the FFF additive technology printer according to ASTM D638 "*Standard Test Method for Tensile Properties of Plastics*". For each test, five same samples were prepared to make sure the obtained values of designed joints mechanical properties reliable. The geometry of designed sample is shown in Figure 2.

a) b)

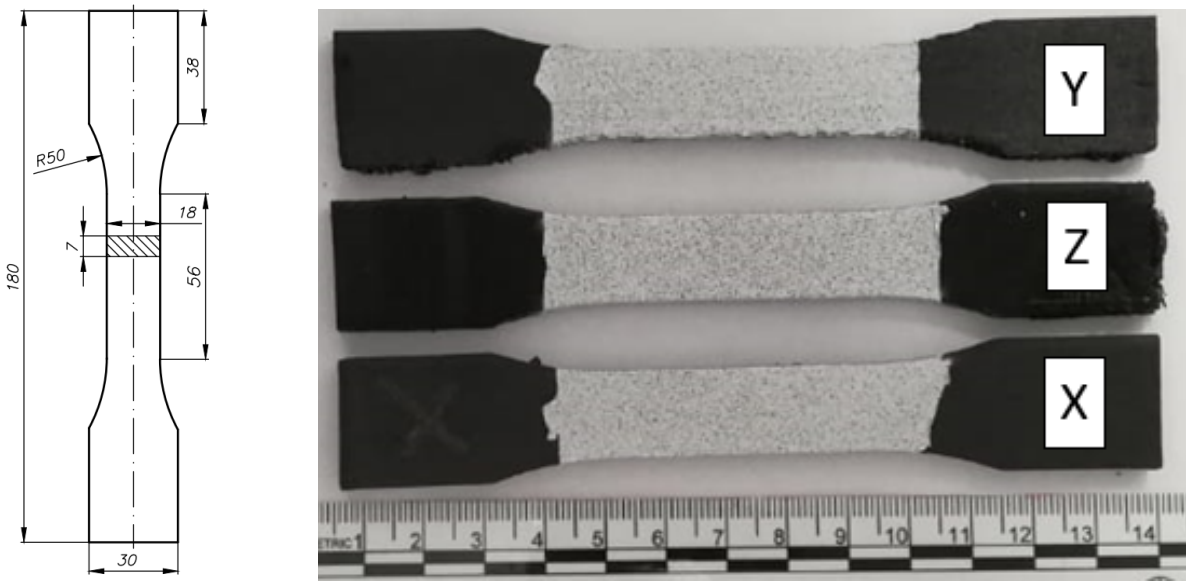


Fig. 2. a) Geometry of plain flat specimen tested under tensile loading (dimensions in mm); b) Sample picture of the picture

Tensile tests and low cycle fatigue tests have been performed at room temperature by adopting an "Instron" 8802 axial servo-hydraulic testing machine ("Instron", Norwood, MA, USA), with a load capacity of 250 kN and equipped with an "Instron" 8800 controller. The uniaxial extensometer "Instron" 2630-112 with a gauge length of 50 mm (axial travel +50 %) has been adopted to measure the axial strain during tensile tests. The dynamic extensometer "Instron" 2620-602 with a gauge length of 25 mm (axial travel ±5 %) was used for strain-controlled tests. DIC – non-contact, optical method from "Dantec Dynamics" (Ulm, Germany).

3. Tensile test – results, and discussion

All tensile tests were performed under room temperature conditions using a universal testing machine "Instron" 8802 with a quasi-static loading condition (5 mm/min). The results of the monotonic stretching curves are shown in Figure 3.

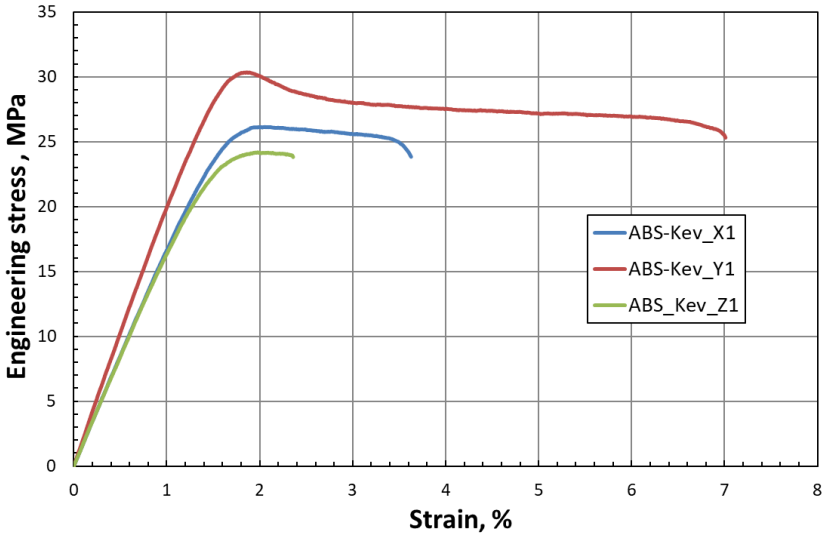


Fig. 3 Monotonic stretching curves

The *Y*-orientation had the highest tensile strength above 30 MPa and an elongation of 7 %. The *X*-orientation achieved a strength of 26 MPa and an elongation of 3.7 %. The weakest performance is characterized by the *Z*-orientation at 24 MPa and an elongation of 2.35 %. The obtained material properties included tensile strength and elongation at break of the samples are presented in Table 1.

Table 1. Mechanical properties of samples tested

Type of property	Value for *X*-orientation	Value for *Y*-orientation	Value for *Z*-orientation
Ultimate tensile strength (MPa)	26.14	30.35	24.19
Yield Strength (MPa)	25.4	28.1	22.40
Strain at break (%)	3.7	7	2.35

4. Digital image correlation – results and discussion

Digital image correlation allowed to observe the mechanism of deformation and cracks formation during the monotonic tensile test. The results showed that in the elastic tensile range of the specimen, all orientations maintained

a uniform level of strain. Only at the time of the UTSW of the *X*-orientation, traces of excessive deformation are visible, these are places of filament delamination that run at an angle of 45 degrees to the sample axis. The remaining *Y* and *Z* variants at the UTS point of the sample delaminated to form horizontal bands (see Fig. 5).

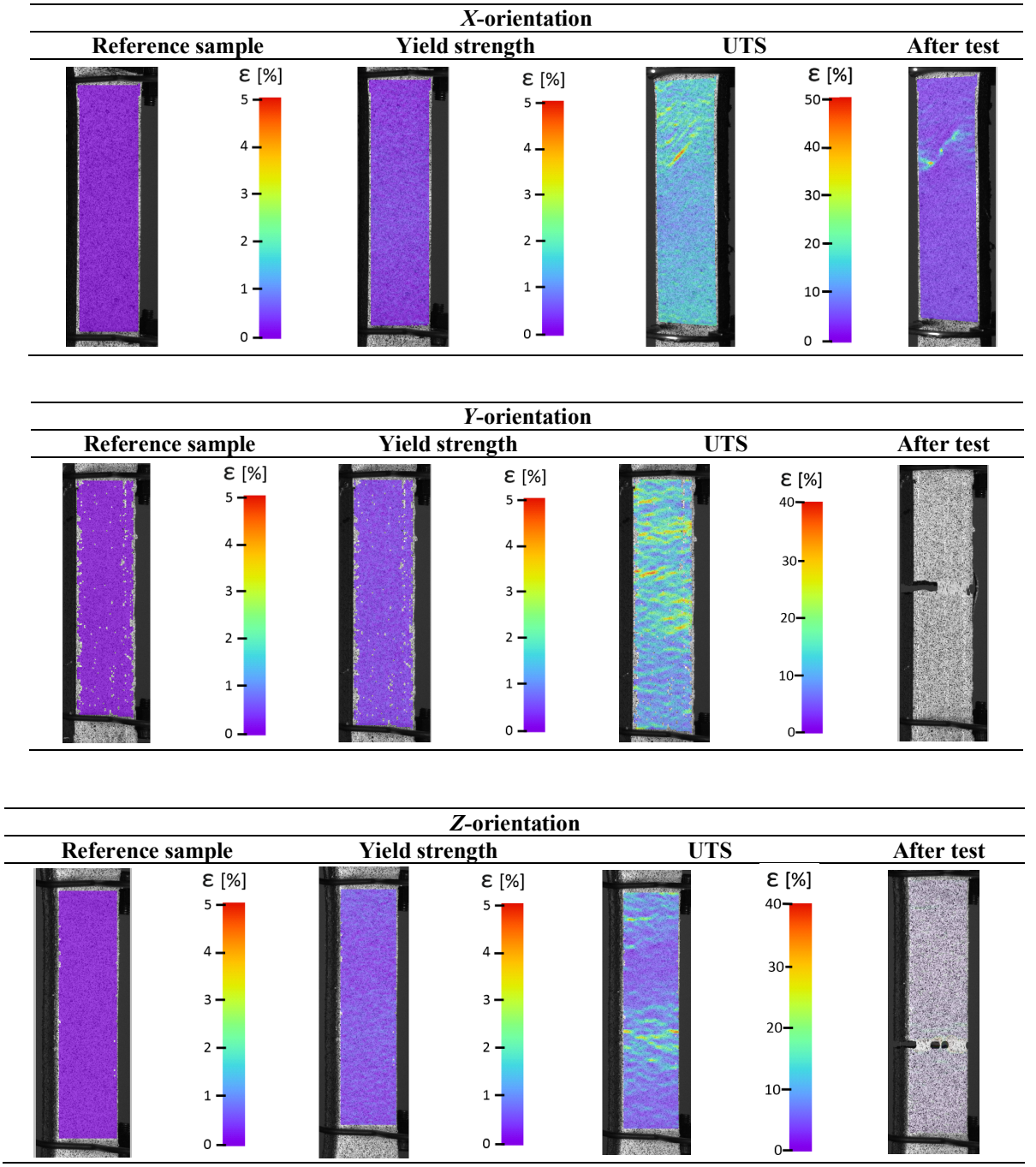


Fig. 5. DIC analysis of all samples

The resulting fractures were subjected to microfractographic examination. The results of these tests allow to determine the cracking mechanism. No specific sources of crack formation can be seen in the *X*- and *Y*-orientation. The *X*-orientation is characterized by brittle and plastic fracture at the same time. The orientation is characterized by a course of plastic fracture. Orientation With a typical brittle fracture course (see Fig. 6).



Fig. 6. Fracture images for *X*, *Y*, and *Z*-oriented samples made of the ABS_Kev material

In any of the fractures, the fiber fragment does not cause a crack. The process of cracking occurs in the place where the print lines and their delamination are joined. The resulting pores in the 7 orientation will reduce the volume of the material and do not cause additional grooving due to the high plasticity of the material.

5. Conclusions

Based on the results obtained, the following conclusion can be drawn:

1. Parts made in the FFF technology made of ABS_Kev material are characterized by UTS higher UTS strength than other popular materials available for this type of AM technology.
2. Samples made in *Y*-orientations are characterized by high adhesion between the layers similar to the UTS of the ABS material.
3. Cracks on samples fabricated in the *Z* directions indicate brittle failure similar to conventionally made materials
4. The *Y*-oriented test is characterized by properties similar to those of cast materials.

References

[1] Günther, D., Heymel, B., Günther, J. F., Ederer, I. Continuous 3D-printing for Additive Manufacturing [Internet]. *Rapid Prototyping Journal*, 2014, 20, 320–327. Available from: doi:10.1108/RPJ-08-2012-0068 (accessed on 24-06-2022).

[2] Campbell, I., Bourell, D., Gibson, I. Additive Manufacturing: Rapid prototyping comes of age [Internet]. *Rapid Prototyping Journal*, 2012, 18, 255–258. Available from: doi:10.1108/13552541211231563 (accessed on 24-07-2022).

[3] Ivanova, O. S., Williams, C. B., Campbell, T. A. Additive Manufacturing (AM) and nanotechnology: Promises and challenges [Internet]. *International Solid Freeform Fabrication Symposium / 2011 International Solid Freeform Fabrication Symposium*, 2011, 733–749. Available from: doi:10.1108/RPJ-12-2011-0127 (accessed on 15-06-2022).

[4] Glardon, R. Direct rapid tooling: Research. *Rapid Prototyping Journal*, 1998, 4, 77–89.

[5] Szachogluchowicz, I., Sniezek, L., Sulym, H., Gloc, M. Testing and verification modeling of wave-shape formation under explosion welding to laminate AA 2519-Ti6Al4V [Internet]. *Procedia Structural Integrity*, 2016, 2, 2375–2380. Available from: doi:10.1016/j.prostr.2016.06.297 (accessed on 24-07-2022).

[6] Sniezek, L., Szachogluchowicz, I., Gocman, K. The mechanical properties of composites AA.2519-Ti6Al4V obtained by detonation method. *Intelligent Technologies in Logistics and Mechatronics Systems* (ITELMS 2013), 2013, 214–219.

[7] Kluczyński, J., Śnieżek, L., Grzelak, K., Oziębło, A., Perkowski, K. Hot isostatic pressing influence on the mechanical properties of selectively laser-melted 316L steel [Internet]. *Bulletin of the Polish Academy of Sciences / Technical Sciences*, 2020, 68, 1413–1424. Available from: doi:10.24425/bpasts.2020.135396 (accessed on 17-06-2022).

[8] Klimek, A., Kluczyński, J., Łuszczek, J., Bartnicki, A., Grzelak, K., Małek, M. Wear analysis of additively manufactured slipper-retainer in the axial piston pump [Internet]. *Materials*, 2022, 15, 1995. Available from: https://doi.org/10.3390/ ma15061995 (accessed on 11-07-2022).

[9] Grzelak, K., Łaszcz, J., Polkowski, J., Mastalski, P., Kluczyński, J., Łuszczek, J., Torzewski, J., Szachogłuchowicz, I., Szymaniuk, R. Additive Manufacturing of plastics used for protection against COVID-19 ─ The influence of chemical disinfection by alcohol on the properties of ABS and PETG polymers [Internet]. *Materials* (Basel), 2021, 14. Available from: doi:10.3390/ma14174823 (accessed on 11-07-2022).

[10] Kluczyński, J., Śnieżek, L., Kravcov, A., Grzelak, K., Svoboda, P., Szachogłuchowicz, I., Franek, O., Morozov, N., Torzewski, J., Kubeček, P. The examination of restrained joints created in the process of multi-material FFF Additive Manufacturing technology [Internet]. *Materials* (Basel), 2020, 13, 903. Available from: doi:10.3390/ma13040903 (accessed on 11-07-2022).

[11] Łuszczek, J. Review of methods of designing and Additive Manufacturing of gears [Internet]. *Bulletin of the Military University of Technology*, 70(2), 15–34, 2021. Available from: doi:10.5604/01.3001.0015.7008 (accessed on 11-07-2022).

[12] Małek, M., Grzelak, K., Łasica, W., Jackowski, M., Kluczyński, J., Szachogłuchowicz, I., Torzewski, J., Łuszczek, J. Cement-glass composite bricks (CGCB) with interior 3D printed PET-G scaffolding [Internet]. *Journal of Building Engineering*, 2022, 52, 104429. Available from: https://doi.org/https://doi.org/10.1016/j.jobe.2022.104429 (accessed on 11-07-2022).

[13] Gao, X., Zhang, D., Qi, S., Wen, X., Su, Y. Mechanical properties of 3D parts fabricated by fused deposition modeling: Effect of various fillers in polylactide [Internet]. *Journal of Applied Polymer Science*, 2019, 136, 1–10. Available from: doi:10.1002/app.47824 (accessed on 11-07-2022).

[14] Yao, Y., Li, M., Lackner, M., Herfried, L. A Continuous fiber-reinforced Additive Manufacturing processing based on PET fiber and PLA [Internet]. *Materials* (Basel), 2020, 13. Available from: doi:10.3390/ma13143044 (accessed on 11-07-2022).

[15] García, E., Núñez, P. J., Chacón, J. M., Caminero, M. A., Kamarthi, S. Comparative study of geometric properties of unreinforced PLA and PLA-graphene composite materials applied to Additive Manufacturing using FFF technology [Internet]. *Polymer Testing*, 2020, 91. Available from: doi:10.1016/j.polymertesting.2020.106860 (accessed on 11-07-2022).

[16] Fras, T., Szachogluchowicz, I., Sniezek, L. Ti6Al4V-AA1050-AA2519 explosively-cladded plates under impact loading [Internet]. *European Physical Journal-Special Topics*, 2018, 1–2, 17–27. Available from: doi:10.1140/epjst/e2018-00114-9 (accessed on 11-07-2022).

[17] Szachogłuchowicz, I., Fikus, B., Grzelak, K., Kluczyński, J., Torzewski, J., Łuszczek, J. Selective laser melted M300 maraging steel – Material behaviour during ballistic testing [Internet]. *Materials* (Basel), 2021, 14. Available from: doi:10.3390/ma14102681 (accessed on 11-07-2022).

[18] Szachogluchowicz, I., Sniezek, L., Slezak, T., Kluczyński, J., Grzelak, K., Torzewski, J., Fras, T. Mechanical properties analysis of the AA2519-AA1050-Ti6Al4V explosive welded laminate [Internet]. *Materials* (Basel), 2020, 13, 434. Available from: doi:10.3390/ma13194348 (accessed on 11-07-2022).

[19] Kluczyński, J., Śnieżek, L., Grzelak, K., Oziębło, A., Perkowski, K. Hot isostatic pressing influence on the mechanical properties of selectively laser-melted 316L steel [Internet]. *Bulletin of the Polish Academy of Sciences / Technical Sciences*, 2020, 68, 1413–1424. Available from: doi:10.24425/bpasts.2020.135396 (accessed on 22-07-2022).

[20] Kluczyński, J., Śnieżek, L., Grzelak, K., Torzewski, J., Szachogłuchowicz, I., Oziębło, A., Perkowski, K., Wachowski, M., Małek, M. The influence of heat treatment on low cycle fatigue properties of selectively laser melted 316L steel [Internet]. *Materials* (Basel), 2020, 13, 5737. Available from: doi:10.3390/ma13245737 (accessed on 22-07-2022).
[21] Kravcov, A., Kluczyński, J., Kosturek, R., Franek, O., Morozov, N., Śnieżek, L., Svoboda, P., Kubeček, P. The influence of friction stir welded process parameters of AA2519-T62 on joint quality defined by non-destructive laser amplified ultrasonic method and by microstructure analysis [Internet]. *Proceedings of the Challenges to National Defence in Contemporary Geopolitical Situation*, 2020, 74–78.
[22] Grzelak, K., Kluczyński, J., Szachogłuchowicz, I., Łuszczek, J., Śnieżek, L., Torzewski, J. Modification of structural properties using process parameters and surface treatment of monolithic and thin-walled parts obtained by selective laser melting [Internet]. *Materials* (Basel), 2020, 13, 5662. Available from: doi:10.3390/ma13245662 (accessed on 22-07-2022).
[23] Szachogluchowicz, I., Sniezek, L., Slezak, T., Kluczyński, J., Grzelak, K., Torzewski, J., Fras, T. Mechanical properties analysis of the AA2519-AA1050-Ti6Al4V explosive welded laminate [Internet]. *Materials* (Basel), 2020, 13, 434. Available from: doi:10.3390/ma13194348 (accessed on 22-07-2022).
[24] Szachogluchowicz, I., Sniezek, L., Hutsaylyuk, V. Low cycle fatigue properties laminate AA2519-TI6AL4V [Internet]. *Procedia Engineering*, 2015, 114, 26–33. Available from: doi:10.1016/j.proeng.2015.08.022 (accessed on 22-07-2022).
[25] Wachowski, M., Śnieżek, L., Szachogłuchowicz, I., Kosturek, R., Płociński, T. Microstructure and fatigue life of Cp-Ti/316L bimetallic joints obtained by means of explosive welding [Internet]. *Bulletin of the Polish Academy of Sciences. Technical Sciences*, 2018, 66, 925–933. Available from: doi:10.24425/bpas.2018.125940 (accessed on 22-07-2022).

International Forum on Innovative Technologies and Management for Sustainability – ITMS'2022

International Scientific Conference Intelligent Technologies in Logistics and Mechatronics Systems – ITELMS'2022, 15th September, 2022, Panevėžys, Lithuania

Glass Hollow Spheres Reinforced Polyamide for Additive Manufacturing: Strength Analysis

Janusz Torzewski[a]*

[a] *Institute of Robots & Machine Design, Faculty of Mechanical Engineering, Military University of Technology, 2 Gen. S. Kaliskiego St., Warsaw 00-908, Poland*

Abstract

The study researched the strength properties of glass hollow spheres reinforced Polyamide of additively manufactured elements (AM). The research shows the influence of the production direction of polyamide-based (PA) composites on the fundamental strength parameters. All samples were tested in the three principal directions during the FFF process. In order to broaden the scope of the research, additional digital-image-correlation tests were performed. The results indicate a high dependence of the production directionality on the strength properties.

© 2022 Janusz Torzewski.
Peer-review under responsibility of the Kaunas University of Technology, Panevėžys Faculty of Technologies and Business.

Keywords: Additive Manufacturing; Fused Filament Fabrication; Polyamide GK10; Mechanical properties analysis.

1. Introduction

Polyamide-based materials are characterized by relatively high-performance properties, such as strength, hardness, stiffness, fatigue, and good frictional properties. Due to their properties, PA materials are increasingly used in Additive Manufacturing (AM) [1–3]. The following methods can realize elements made of PA-based materials with the use of AM: Fused Filament Fabrication (FFF) or Selective Laser Sintering (SLS) [4–7]. These two methods can produce geometrically complex parts and non-standard elements characterized by relatively good operational properties. Their

* Corresponding author. Tel.: +48 261 837 899.
E-mail address: janusz.torzewski@wat.edu.pl

© 2022 Janusz Torzewski.
F916G0011
Peer-review under responsibility of the Kaunas University of Technology, Panevėžys Faculty of Technologies and Business.

production is relatively cheap in the case of the small-lot output [8–10]. Among the most commonly used classes of PA material, which are used in FFF and SLS technologies, we can distinguish PA6, PA11 and PA12 [11–13]. In the FFF technology, the material is applied in the form of extruded lines, while in the SLS technology; the PA elements are in the form of sintered particles. The connection between the powder particles and the extruded lines is in the form of adhesive joints [14, 15]; hence the semi-crystalline nature of PA polymers [16] is better exposed in parts obtained employing the FFF technology.

Hygroscopicity is an essential property of PA materials that can affect the properties of the AM part. Polyamide with lower moisture content becomes brittle, its impact strength worsens, and its tensile strength increases. On the other hand, with growing humidity, the flexibility and impact strength increase, but at the same time, the tensile strength decreases significantly. In practice, when the fibre absorbs water (which may constitute approximately 10 % of its mass), it affects the adhesion of the detail to the carrier plate and the adhesion between the layers, ultimately increasing the roughness of the contour surface of the AM part shells.

Additionally, such a phenomenon may favour nozzle clogging or the "bubble effect" caused by overheating the filament volume's moisture [17]. Another critical issue related to PA-based materials is their susceptibility to warping and deformation and a worse possibility of obtaining suitable quality shapes than other available polymers dedicated to AM. Characteristics AM technology based on layer-by-layer production [18, 19] causes asynchronous volumetric contraction, with additional regularity of molecular chains, which in turn worsens the squeeze of the AM part [20]. With the latest trends in PA technology, the production of material for AM weakens the crystallization ability and hinders the regular arrangement of particle shapes [21]. A noticeable trend in research on elements made of PA is the search for opportunities to improve selected properties of materials [22, 23].

The authors [23] showed that adding 10 % carbon fibres to the PA12 matrix could show a noticeable increase in flexural strength. The positive effect of using fibres as an additive to PA-based materials was demonstrated also by Chacón et al. [22]. Three-point bending tests recorded an incredible impact of glass fibers in PA composite samples. The available literature provides results for specific PA materials or PA-based composites [24–26].

There is also a kind of approach based on comparing different PA materials and AM technology. Interesting results are found in the work of Türk et al. [27], where the authors characterized the mechanical properties of the obtained samples (Young's modulus, yield strength under tensile strength and modulus of elasticity and creep). In the publications reviewed, there is little data on the effect of each additive on material properties that would assist in properly describing the effect of an exact additive compared to a pure base material. Hence, the study investigated the effect of the addition of glass microspheres in the PA-based material on the strength properties in tensile tests. To broaden the scope of the tests, samples for each material were tested in three different printing directions.

2. Materials and methods

For the research, the PA6 GK10 material was used which was provided by the "Spectrum Filaments Ltd. Company". The PA6 GK10 is a glass-microbead-doped (10 % of the total volume of the material) composite. This reinforcement enhances temperature resistance and thermal insulation and lowers the influence of humidity on mechanical properties [28].

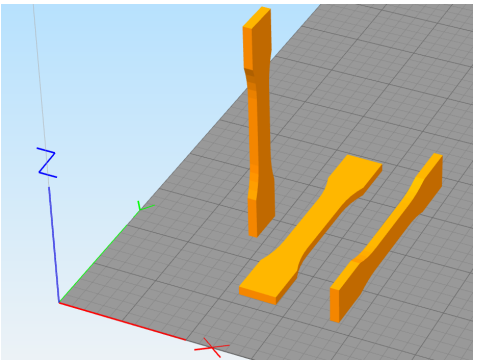
To reach desirable elements properties it had been designed the following process parameters:

- hotend temperature – 300 °C;
- heatbed temperature – 120 °C;
- chamber temperature – 60 °C;
- layer thickness – 0.2 mm;
- outline shell thickness –2 mm;
- infill – 100 %;
- part cooling intensity – 40 %;
- printing speed – 50 mm/s;
- nozzle diameter – 0.4 mm.

The test samples were made using the "Intamsys Funmat HT" 3D printer, which made it possible to obtain the appropriate printing conditions. Thanks to the heated print chamber, high-temperature head and a heated plate up to 160 °C, it was possible to prepare samples without thermal stresses properly. In addition to testing the effect of the dopant on the PA6 material, the influence of the orientation of the samples on the tensile strength during the AM process was also taken into account. Strength tests were performed for five samples in each direction: *X*, *Y* and *Z* (see Fig. 1).

Based on the provisions of the ASTM D638 "*Standard Method for Testing the Tensile Strength of Plastics*" standard, dog bone-shaped specimens were prepared to determine the mechanical properties. Three identical samples were prepared for each test to ensure the reliability of the mechanical property results as well as the ability to measure strain using the standard method and digital image correlation (DIC). The geometry of designed sample is shown in Figure 1.

a) b)



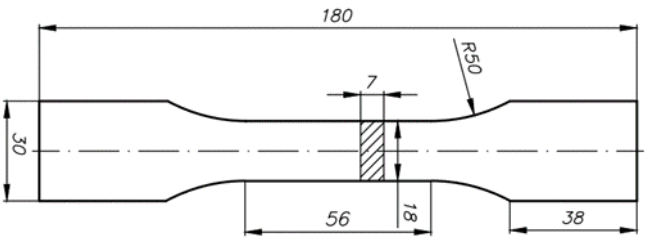


Fig. 1. Illustrative presentation of the orientation of samples: (a) in relation to the axis of the system and dimensions of investigated tensile specimens; (b) based on ASTM D638 (dimensions in mm)

Tensile tests were carried out at room temperature and a constant displacement rate of 4 mm × min^{-1} using servo-hydraulic testing machine "Instron" type 8802 (Instron, Norwood, MA, USA), with a load capacity of 250 kN and equipped with an "Instron" 8800 controller. The uniaxial extensometer "Instron" 2630-112 with a gauge length of 50 mm (axial travel +50 %) has been adopted to measure the axial strain during tensile tests. At the same time, a digital image correlation (DIC) (non-contact, optical method) was used to measure three-dimensional (3D) deformations from "Dantec Dynamics" (Dantec, Ulm, Germany).

3. Tensile test – results, and discussion

Table 1 summarizes the tensile strength test results of PA6 GK10 for each manufacturing directions. The table contains the results of Ultimate Tensile Strength (UTS), Yield Strength (YS) and Strain at break. The standard deviation of the values of the obtained results has been entered in the table as numerical values enclosed in brackets.

Table 1. Mechanical properties of samples tested

Type of property	**Value for *X*-orientation**	**Value for *Y*-orientation**	**Value for *Z*-orientation**
Ultimate tensile strength (MPa)	80.1 (±4.36)	55.8 (±4.02)	18.1 (±3.18)
Yield strength (MPa)	72.0 (±1.98)	-	-
Strain at break (%)	3.1 (±0.22)	48.3 (±6.62)	2.1 (±0.21)

From the analysis of the tensile test results for PA6 GK10 samples (see Table 1), it can be concluded that the direction of sample production dramatically influences the strength properties. The highest UTS values of about 80 MPa were obtained for the *X*-orientation and were over four times higher than for the samples with the *Z*-orientation. As well as, intermediate values were obtained for the samples made by the *Y*-orientation. These differences are most evident in the comparative graph (see Fig. 2) of selected samples from each orientation. The yield strength was determined only for samples with the *X*-orientation, and it was impossible to determine the yield point in the case of the *Y*- and *Z*-orientations.

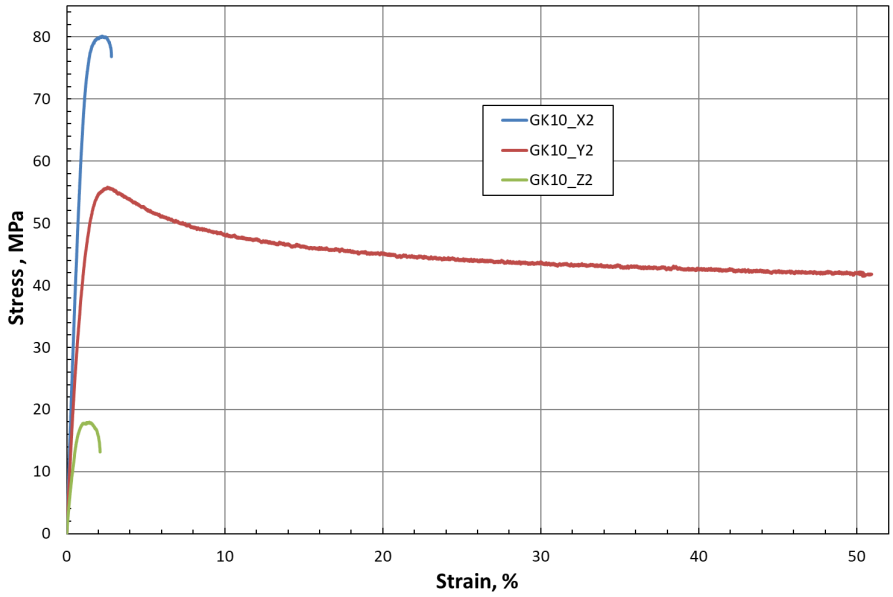


Fig. 2. Representative stress-strain curves for selected samples from each orientation

The strain at break also showed considerable discrepancies depending on the orientation of the samples (see Table 1 and Fig. 2). The highest values, up to 50 %, were obtained for the pieces with the *Y*-orientation, while the samples with the *X*- and *Z*-orientations presented over ten times lower value in comparison to the greatest deformation. This confirms the observations contained in the works on similar materials [29].

4. Digital image correlation – results, and discussion

The deformation behaviour of the PA GK10 samples during the tensile test was monitored by DIC. The deformation maps obtained for the three manufacturing directions are shown in Figures 3–5 for the *X*, *Y* and *Z* directions, respectively. Figures 3, 4, and 5 show the deformation maps for the four loading phases of the samples.

Initial stage – sample unloaded ("Reference").

The second phase – sample load causing strain corresponding to the yield strength (0.2 % strain).

Phase three – sample loading corresponding to the ultimate tensile strength ("UTS").

Final step – sample destroyed ("After").

Such a compilation of deformation maps enables qualitative analysis of samples produced in different directions. The results clearly showed that the strain was almost homogeneously distributed in the specimens, mainly due to the even distribution of glass hollow spheres reinforcements in the material tested. Only for the *Z* direction, the layered direction of the maximum deformations on the sample surface was clearly observed (see Fig. 5), resulting from the method of manufacturing the element.

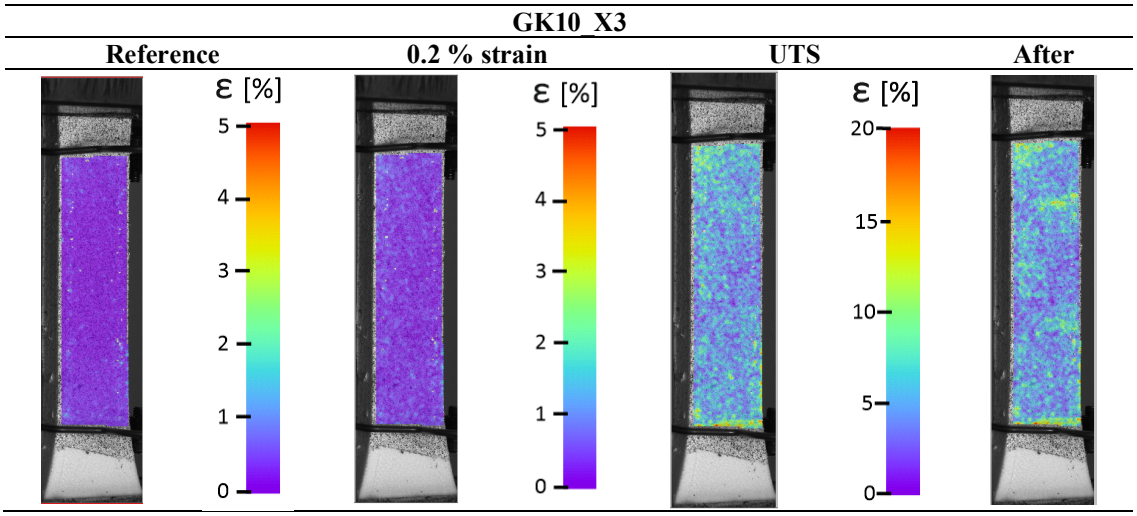


Fig. 3. Representative DIC results for specimens made in the *X* direction

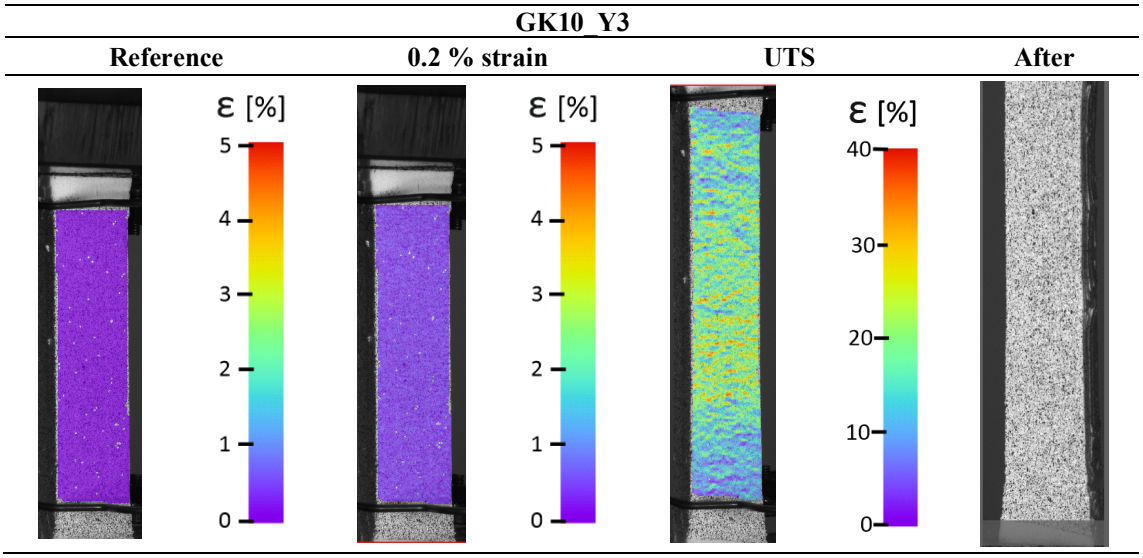


Fig. 4. Representative DIC results for specimens made in the *Y* direction

In the initial loading period (0.2 % strain), all samples showed a similar strain level on the entire surfaces of the analysed measuring area. The most significant deformations were observed for the GK10_Y3 sample, which is consistent with the results shown in the curve in Figure 2. For samples made under the *X* and *Z* directions, a similar level of maximum deformations was observed.

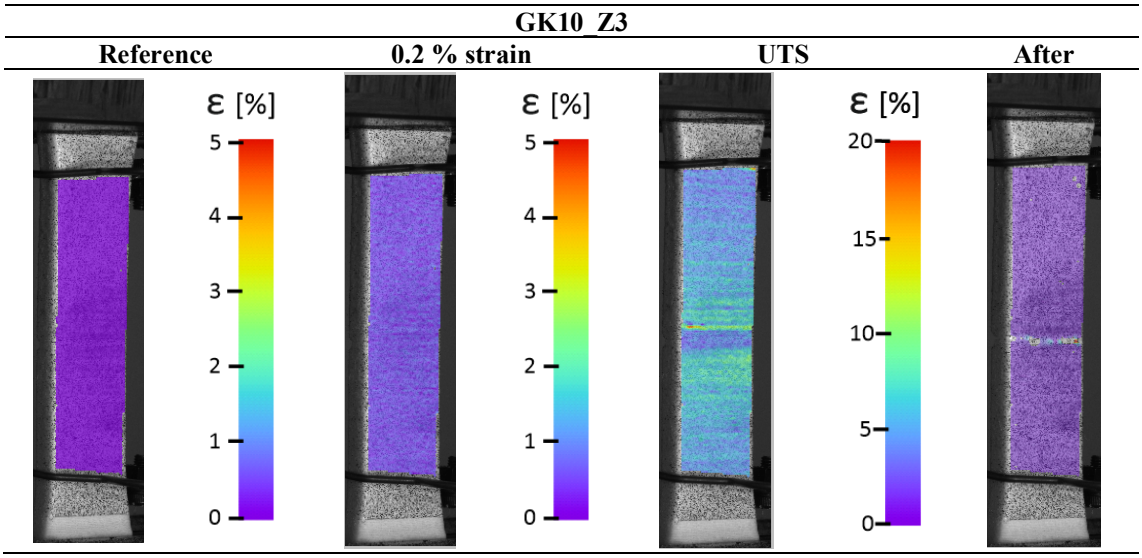


Fig. 5. Representative DIC results for specimens made in the *Z* direction

Still, it is worth noting that the maximum strain was obtained at diametrically different load levels.

5. Conclusions

Based on the research carried out and the analysis of the obtained results, the following conclusions can be drawn:

1. Elements produced in the FFF technology made of PA GK10 material are characterized by high sensitivity to the direction of their production.
2. The highest strength properties are shown in elements made in the *X*-orientation and the most significant deformations in the *Y* direction.
3. Measurements made by the DIC method showed that the most remarkable differences in the deformation course occurred in the case of the samples made in the *Z* direction.

References

[1] Hamidi, F., Aslani, F. Additive Manufacturing of cementitious composites: Materials, methods, potentials, and challenges. *Construction and Building Materials*, 2019, 218, 582–609.

[2] Ngo, T. D., Kashani, A., Imbalzano, G., Nguyen, K. T. Q., Hui, D. Additive Manufacturing (3D printing): A review of materials, methods, applications and challenges. *Composites Part B: Engineering*, 2018, 143, 172–196.

[3] Praveena, B. A., Lokesh, N., Buradi, A., Santhosh, N., Praveena, B. L., Vignesh, R. A comprehensive review of emerging Additive Manufacturing (3D printing technology): Methods, materials, applications, challenges, trends and future potential. *Materials Today: Proceedings*, 2022, 52, 1309–1313.

[4] Dul, S., Fambri, L., Pegoretti, A. Fused deposition modelling with ABS-graphene nanocomposites. *Composites Part A Applied Science and Manufacturing*, 2016, 85, 181–191.

[5] Małek, M., Grzelak, K., Łasica, W., Jackowski, M., Kluczyński, J., Szachogłuchowicz, I., Torzewski, J., Łuszczek, J. Cement-glass composite bricks (CGCB) with interior 3D printed PET-G scaffolding [Internet]. *Journal of Building Engineering*, 2022, 52, 104429. Available from: https://doi.org/https://doi.org/10.1016/j.jobe.2022.104429 (accessed on 19-07-2022).

[6] Grzelak, K., Łaszcz, J., Polkowski, J., Mastalski, P., Kluczyński, J., Łuszczek, J., Torzewski, J., Szachogłuchowicz, I., Szymaniuk, R. Additive Manufacturing of plastics used for protection against COVID-19 – The influence of chemical disinfection by alcohol on the properties of ABS and PETG polymers [Internet]. *Materials* (Basel), 2021, 14. Available from: doi:10.3390/ma14174823 (accessed on 19-07-2022).

[7] Sanatgar, R. H., Campagne, C., Nierstrasz, V. Investigation of the adhesion properties of direct 3D printing of polymers and nanocomposites on textiles: Effect of FDM printing process parameters. *Applied Surface Science*, 2017, 403, 551–563.
[8] Syrlybayev, D., Zharylkassyn, B., Seisekulova, A., Akhmetov, M., Perveen, A., Talamona, D. Optimisation of strength properties of FDM printed parts – A critical review. *Polymers*, 2021, 13, 1587.
[9] Szachogłuchowicz, I., Fikus, B., Grzelak, K., Kluczyński, J., Torzewski, J., Łuszczek, J. Selective laser melted M300 maraging steel – Material behaviour during ballistic testing [Internet]. *Materials* (Basel), 2021, 14. Available from: doi:10.3390/ma14102681 (accessed on 19-07-2022).
[10] Vyavahare, S., Teraiya, S., Panghal, D., Kumar, S. Fused deposition modelling: A review. *Rapid Prototyping Journal*, 2020, 26, 176–201.
[11] Goodridge, R. D., Tuck, C. J., Hague, R. J. M. Laser sintering of polyamides and other polymers. *Progress in Materials Science*, 2012, 57, 229–267.
[12] Salazar, A., Rico, A., Rodríguez, J., Escudero, J. S., Seltzer, R., De La Escalera Cutillas, F. Monotonic loading and fatigue response of a bio-based polyamide PA11 and a petrol-based polyamide PA12 manufactured by selective laser sintering. *European Polymer Journal*, 2014, 59, 36–45.
[13] Olakanmi, E. O., Cochrane, R. F., Dalgarno, K. W. A review on selective laser sintering / melting (SLS/SLM) of aluminium alloy powders: Processing, microstructure, and properties. *Progress in Materials Science*, 2015, 74, 401–477.
[14] Jacques, B., Werth, M., Merdas, I., Thominette, F., Verdu, J. Hydrolytic ageing of polyamide. Hydrolysis kinetics in water. *Polymer*, 2002, 43, 6439–6447.
[15] Gor, M., Soni, H., Wankhede, V., Sahlot, P., Grzelak, K., Szachgluchowicz, I., Kluczyński, J. A Critical review on effect of process parameters on mechanical and microstructural properties of powder-bed fusion Additive Manufacturing of S316l [Internet]. *Materials* (Basel), 2021, 14. Available from: doi:10.3390/ma14216527 (accessed on 19-07-2022).
[16] Tanikella, N. G., Wittbrodt, B., Pearce, J. M. Tensile strength of commercial polymer materials for fused filament fabrication 3D printing. *Additive Manufacturing*, 2017, 15, 40–47.
[17] Costa, S. F., Duarte, F. M., Covas, J. A. Thermal conditions affecting heat transfer in FDM/FFE: A contribution towards the numerical modelling of the process: This paper investigates convection, conduction and radiation phenomena in the filament deposition process. *Virtual and Physical Prototyping*, 2015, 10, 35–46.
[18] Grzelak, K., Kluczyński, J., Szachogłuchowicz, I., Łuszczek, J., Śnieżek, L., Torzewski, J. Modification of structural properties using process parameters and surface treatment of monolithic and thin-walled parts obtained by selective laser melting [Internet]. *Materials* (Basel), 2020, 13, 5662. Available from: doi:10.3390/ma13245662 (accessed on 19-07-2022).
[19] Kluczyński, J., Śniezek, L., Grzelak, K., Oziebło, A., Perkowski, K., Torzewski, J., Szachogłuchowicz, I., Gocman, K., Wachowski, M., Kania, B. Comparison of different heat treatment processes of selective laser melted 316L steel based on analysis of mechanical properties [Internet]. *Materials* (Basel), 2020, 13. Available from: doi:10.3390/ma1317380 (accessed on 19-07-2022).
[20] Abdullah, A., Rahim, T., Hamad, W., Mohamad, D., Akil, H., Rajion, Z. Mechanical and cytotoxicity properties of hybrid ceramics filled polyamide 12 filament feedstock for craniofacial bone reconstruction via fused deposition modelling. *Dental Materials*, 2018, 34, e309–e316.
[21] Kumar, R., Singh, R., Ahuja, I. P. S., Karn, K. N. processing of melt flow compatible thermoplastic composites for solid state welding applications. *Materials Today: Proceedings*, 2019, 18, 3167–3173.
[22] Chacón, J. M., Caminero, M. A., Núñez, P. J., García-Plaza, E., García-Moreno, I., Reverte, J. M. Additive Manufacturing of continuous fibre reinforced thermoplastic composites using fused deposition modelling: Effect of process parameters on mechanical properties. *Composites Science and Technology*, 2019, 181.
[23] Salmoria, G. V., Leite, J. L., Ahrens, C. H., Lago, A., Pires, A. T. N. Rapid manufacturing of PA/HDPE blend specimens by selectivelaser sintering: Microstructural characterization. *Polymer Testing*, 2007, 26, 361–368.
[24] Salmoria, G. V., Leite, J. L., Vieira, L. F., Pires, A. T. N., Roesler, C. R. M. Mechanical properties of PA6/PA12 blend specimens prepared by selective laser sintering. *Polymer Testing*, 2012, 31, 411–416.
[25] Mazurkiewicz, M., Kluczyńnski, J., Jasik, K., Sarzyński, B., Szachogłuchowicz, I., Łuszczek, J., Torzewski, J., Snieżek, L., Grzelak, K., Małek, M. bending strength of polyamide-based composites obtained during the Fused Filament Fabrication (FFF) process [Internet]. *Materials* (Basel), 2022, 15, 5079. Available from: https://doi.org/ 10.3390/ma15145079 (accessed on 19-07-2022).
[26] Liu, Y., Zhu, L., Zhou, L., Li, Y. Microstructure and mechanical properties of reinforced polyamide 12 composites prepared by laser Additive Manufacturing. *Rapid Prototyping Journal*, 2019, 25, 1127–113.
[27] Türk, D. A., Brenni, F., Zogg, M., Meboldt, M. Mechanical characterization of 3D printed polymers for fiber reinforced polymers processing. *Dental Materials*, 2017, 118, 256–265.
[28] *Spectrumfilaments. PA6 GK10* [Internet]. Available from: https://spectrumfilaments.com/filament/pa6-gk10/ (accessed on 19-07-2022).
[29] Jia, Y., He, H., Peng, X., Meng, S., Chen, J., Geng, Y. Preparation of a new filament based on polyamide-6 for three-dimensional printing. *Polymer Engineering and Science*, 2017, 12, 1322–1328.

Author Index

Aviža D., 3

Bartnicki A., 35

Česnulevičius A., 27

Grzelak K., 9, 51

Hutsaylyuk V., 61, 69

Jukna A., 19

Kaupienė J., 27
Klimek A., 35
Kluczyński J., 43

Łukasiak D., 61, 69
Łuszczek J., 51

Śnieżek L., 51
Szachogluchowicz I., 79

Torzewski J., 87

Zacharovienė E., 3
Ziółkowski J., 61, 69